2010-07-12

Multidisciplinary Assessment and Documentation of Past and Present Human Impacts on the Neotropical Forests of Petén, Guatemala

Christopher Stephen Balzotti
Brigham Young University - Provo

Multidisciplinary Assessment and Documentation of Past and Present Human Impacts on the Neotropical Forest of Petén, Guatemala

Christopher S. Balzotti

A thesis submitted to the faculty of
Brigham Young University
in partial fulfillment of the requirements for the degree of

Master of Science

Steven L. Petersen, Chair
Richard E. Terry
Loreen Allphin

Department of Plant and Wildlife Sciences

Brigham Young University

August 2010

ABSTRACT

Multidisciplinary Assessment and Documentation of Past and Present Human

Impacts on the Neotropical Forest of Petén, Guatemala

Christopher S. Balzotti

Department of Plant and Wildlife Sciences

Master of Science

Tropical forests provide important habitat for a tremendous diversity of plant and animal species. However, limitations in measuring and monitoring the structure and function of tropical forests has caused these systems to remain poorly understood. Remote-sensing technology has provided a powerful tool for quantification of structural patterns and associating these with resource use. Satellite and aerial platforms can be used to collect remotely sensed images of tropical forests that can be applied to ecological research and management. Chapter 1 of this article highlights the resources available for tropical forest remote sensing and presents a case-study that demonstrates its application to a neotropical forest located in the Petén region of northern Guatemala. The ancient polity of Tikal has been extensively studied by archaeologists and soil scientists, but little is known about the subsistence and ancient farming techniques that sustained its inhabitants. The objective of chapter 2 was to create predictive models for ancient maize *(Zea mays* L.) agriculture in the Tikal National Park, Petén, Guatemala, improving our understanding of settlement patterns and the ecological potentials surrounding the site in a cost effective manner. Ancient maize agriculture was described in this study as carbon (C) isotopic signatures left in the soil humin fraction. Probability models predicting C isotopic enrichment and carbonate C were used to outline areas of potential long term maize agriculture. It was found that the Tikal area not only supports a great variety of potential food production systems but the models suggest multiple maize agricultural practices were used.

Keywords: Tikal, Guatemala, Classic Maya, Stable Carbon Isotopes; AIRSAR, Landsat, Ancient Agriculture, Hyperniche, Non-Parametric Multiplicative Regression, Model, Modeling, Predictive Modeling

ACKNOWLEDGEMENTS

I would like to thank Dr. Petersen, my advisor, for his guidance throughout this project. I am grateful to Dr. Terry for giving me the opportunity to work in Guatemala and for his years of mentoring and support. I would also like to acknowledge Dr. Allphin. I would like to thank the Sierra del Lacandon project, specifically Charles Golden and Andrew Scherer, and all the local workers associated with the project as well as the support from the Defensores de la Naturaleza. The Re-evaluation of the Earthworks at Tikal, Guatemala project was funded by the National Science Foundation (Grant BCS-0443280) and by Brigham Young University. The Instituto de Antropología e Historia, the Consejo Nacional de Areas Protegidas, and the Parque Nacional Tikal of Guatemala granted permission for this research to take place. Thanks to all those who assisted with the collection, preparation, and analysis of the soil samples. I am grateful to the hard working Guatemalans who helped with sample collection, those involved with the Tikal Earthworks Project, namely David Webster, Tim Murtha, Jay Silverstein, Kirk Straight, Walter Alvarado, and the many others. Special thanks to the Sierra Del Lacandon Project. I am also grateful to Brigham Young University for funding and support. Thanks go to the mentored undergraduates who assisted with soil analyses. Last but not least, thanks to the loving support of my family, specifically Marie Balzotti.

Brigham Young University

SIGNATURE PAGE

of a thesis submitted by

Christopher S. Balzotti

The thesis of Christopher S. Balzotti is acceptable in its final form including (1) its format, citations, and bibliographical style are consistent and acceptable and fulfill university and department style requirements; (2) its illustrative materials including figures, tables, and charts are in place; and (3) the final manuscript is satisfactory and ready for submission.

Date	Steven L. Petersen Chair, Graduate Committee
Date	Richard E. Terry,
Date	Loreen Allphin
Date	Loreen Allphin Graduate Coordinator
Date	Rodney J. Brown Dean, College of Life Sciences

TABLE OF CONTENTS

CHAPTER 1

REMOTE SENSING AS A TOOL FOR TROPICAL ECOLOGY

Chris S. Balzotti[1], Steven L. Petersen[1], Richard E. Terry[1], Andrew K. Scherer[2] and Charles Golden[3]

[1]Department of Plant and Wildlife Sciences, Brigham Young University

[2]Department of Anthropology, Forensic Science, and Archaeology, Baylor University

[3]Department of Anthropology, Brandeis University

A manuscript in press at Geography Compass

REMOTE SENSING AS A TOOL FOR TROPICAL ECOLOGY

ABSTRACT

Tropical forests provide important habitat for a tremendous diversity of plant and animal species. However, limitations in measuring and monitoring the structure and function of tropical forests has caused these systems to remain poorly understood. Remote sensing technology has provided a powerful tool for quantification of structural patterns and associating these with resource use. Satellite and aerial platforms can be used to collect remotely sensed images of tropical forests that can be applied to ecological research and management. The purpose of this article is to highlight the resources available for tropical forest remote sensing and to present a case-study that demonstrates its application to a neotropical forest located in the Petén region of northern Guatemala.

Tropical Forest Ecology and Classification

The term "tropical rain forest" was coined by the French botanist Andreas Franz Wilhelm Schimper during the late 1800's (Richards 1996). Since this time, a variety of tropical forest studies have contributed to our understanding of this important biome. Nonetheless, the biological composition and ecological dynamics of these forests still remains poorly understood (Skole and Tucker 1993; Achard et al. 2002; Carr 2004; Mayaux et al. 2005). This lack of information can be attributed in part to the complexity of these forest ecosystems as well as the difficulties in accessing many of the regions where they occur. Furthermore, Pimm et al. (2001) suggest that the greatest limitation is our inability to synthesize the existing information that has been collected. The objectives of this article are four-fold: first, to provide an introduction to tropical forests, their global importance and research-related challenges; second, to provide a

brief history of remote sensing and its applicability to tropical ecology; third, to look at the actual process of tropical ecology research using remote sensing; and fourth, to present a case-study demonstrating the use of remote sensing to assess land change in a neotropical forest in northern Guatemala.

Compared to temperate climate zones, the tropics are home to a greater diversity of landscapes, more complex forest canopies, and higher species richness (Nagendra 2001). In 1971, Holdridge et al. developed a tropical classification system that gave rise to the three dimensional Holdridge Life Zone System which uses simplified climatic data to predict tropical ecological zones. Although this system has been used extensively, there remains a need for a universally accepted tropical classification system that ensures the consistent classification of multiple ecological/regional identifiers. For example, the neotropical forests of Tikal National Park in Petén, Guatemala were studied by Schulze and Whitacre for forest structure using field collected data in 1999. They found that using Holdridge's classification system, Tikal was classified as a subtropical moist forest. However, when Schulze and Whitacre used an alternate method developed in 1968 by Pennington and Sarukhan, the forest was classified as tropical semi-deciduous. Subsequently, efforts are currently being made to improve tropical forest classification accuracy. In North America, the U.S. Federal Geographic Data Committee (FGDC) was created in 1994 to a federal geospatial vegetation classification standard for the U.S. The Food and Agricultural Organization (FAO) is currently implementing a universal land cover classification system (LCCS). However, this system is in its infancy and global acceptance is necessary for this system to be successful. These differences need to be resolved if tropical forest classification and documentation with remote sensing is to be fully utilized.

Tropical Deforestation

Tropical deforestation has long been of concern among the scientific community, with the first proposed inventory of the world's forests in 1945 (Holmgren and Persson 2002). Despite interest, the first estimations of tropical forest deforestation were not done until much later (Myers 1980). Of the 3.9 billion hectares of forests worldwide, 56% were classified in 2000 as tropical or subtropical by the FAO. Although less than 10% of the earth's surface is comprised of tropical forests, , they are home to 50% of all plant species (Mayaux 2005). The tropics also contribute to global carbon sequestration (Foody & Curran 1994, Malhi & Grace 2000, Schimel et al. 2001) and influence climatic precipitation and temperature patterns. Clearing of tropics leads to a regional precipitation decrease as well as a loss of net radiation and evaporation. This change affects the regional atmospheric circulation, decreases total regional precipitation, and changes the surface climate (McGuffie et al. 1995).

With increasing human influences, including an ever growing global population and economy, tropical forests and their ecological diversity are disappearing at an alarming rate. This loss is influenced by multiple factors including corporation and government mining and logging, local displacement of ranchers and farmers, and accelerated population growth (Pimm et al. 2001, Geist and Lambin 2002, Carr 2004). In the early 1990's, estimates for the previous 50 years identified an alarming nine hundred million hectares of tropical humid forests that had been lost or degraded (Myers 1992). The FAO (2001) reported an annual decrease of approximately 15.2 million hectares of tropical forests worldwide between 1990 and 2000. In contrast, all other forest types combined had annual losses of only 0.9 million hectares . However, Achard et al. (2002) found that FAO overestimated tropical humid forest extent by 23%. Regardless, this estimation represents a global loss of over 3 million hectares between 1990

and 1997. With research unable to keep up with these rapid losses, newer tools such as remote sensing and GIS are crucial to the documentation and investigation of the world's species-rich tropical forests (Kerr and Ostrovsky 2003, Carr 2004).

Remote Sensing

It could be argued that early naturalists such as Alfred Russel Wallace, Charles Darwin and Alexander von Humboldt, who produced detailed drawings and paintings of tropical forests, were practicing remote sensing. Humboldt pushed for accurate paintings of tropical landscapes combining the science of reporting patterns and the art of accurate painting (Bunkse 1981).Over time, remote sensing has expanded with technological developments that have helped establish a new generation of tropical ecologists.

Early aerial photography gained widespread use in forest inventories during the 1940s (Lu 2006). The modern era of remote sensing became widely established in the early 1970's with the addition of remote sensing satellites and improved platforms. In 1960, the Television and Infrared Observation Satellite (TIROS-1) was the first to successfully use a television camera to view limited portions of the planet. Although TIROS-1 only operated for 78 days, it demonstrated the utility of satellites as effective remote sensing platforms, leading to subsequent missions (JPL 2009). The launch of Earth Resource and Technology Satellite (ERTS-1), later renamed Landsat-1 in 1972, was the awakening of current world-wide imaging spectrometry (Goetz 2009). The drive to build Landsat-1 began in the early 1960's. However, permission from federal organizations to begin construction did not occur until 1970. Once permission was granted, construction was complete and the satellite was ready for launch only two years later (JPL 2009). Since that time, six additional Landsat satellites have been placed into orbit, losing

only Landsat-6 before reaching orbit in 1993. Landsat 7, a versatile sensor launched in 1999, has the ability to record data at resolutions of 28.5m at visible and near infra-red (VNIR) wavelengths (4 bands) and short wavelength infrared (SWIR) (2 bands), at 14.25m in a panchromatic band (one very broad band displayed in black and white) and at 60m in the thermal band (Markham et al. 2004). An eighth satellite is scheduled to launch in 2012 under the name Landsat Data Continuity Mission (LDCM) (Goetz 2007).

The quest to better understand weather patterns provided tropical remote sensing with a valuable sensor, the Advanced Very High Resolution Radiometer (AVHRR). Originating in 1979, AVHRR became an important part of a generation of satellites that collect global climate and environmental data. With a revisit time of every 14.5 days and a resolution of 1.1 km, this satellite continues to provide tropical researchers with up-to-date coarse resolution landscape information. In 1981, nearly a decade after the launch of the first Landsat satellite, hyperspectral sensing began with the launch of the Shuttle Multispectral Infrared Radiometer (SMIRR) (Goetz 2009). Hyperspectral imaging is a term that came from a technique of imaging spectrometry defined in Goetz et al. (1985) as "the acquisition of images in hundreds of contiguous, registered, spectral bands such that for each pixel a radiance spectrum can be derived".

Around the same time, active sensors began to be used for remote sensing. Active sensors (Figure 1) use a self generated illumination, eliminating the reliance on the sun needed by passive sensors such as Landsat (Figure 2). Active sensors penetrate cloud cover that passive sensors cannot, proving to be an advantage in tropical areas that have cloud cover much of the year. The first experimental spaceborn imaging radar, Seasat, was developed in 1978 by NASA's Jet Propulsion Laboratory (JPL) (Elachi 1980). Although Seasat's focus was the ocean and only transmitted data for 106 days, it was a key to future imaging radar (JPL 2009). After the success

of Seasat, many Synthetic Aperture Radar (SAR) systems were created across the globe. By 1995, there were at least 12 SAR's ranging from aircraft-mounted systems such as the Airborne Synthetic Aperture Radar (AIRSAR) (developed by NASA's JPL in 1987 to test new radar technology for the purpose of ecological studies) (Pope et al. 1994) to spaceborn systems (ALMAZ-1 Russia, ERS-1 Europe, JERS-1, Japan RADARSAT Canada) (Birk et al. 1995).

A significant step for remote sensing came in 1999 with the launch of IKONOS , the world's first privately owned sub-meter satellite. The resolution of IKONOS at nadir (the point directly below the sensor) is 0.83 meters in the panchromatic band and 3.2 meters in the multispectral bands (i.e. near infrared, red, green and blue). IKONOS resolution without nadir is 1 meter panchromatic and 4 meters multispectral (GeoEye 2009). The finer resolution private satellites have opened up a new market in remote sensing. New sensor systems are rapidly being created by governments and private companies, creating a much needed niche for remote sensing tropical research.

Compatibility of Remote Sensing and Tropical Ecology

The remote sensing process is made up of several components: data acquisition, pre-processing, pattern analysis, ground referencing processes and accuracy assessment. Air and spaceborn remote sensing can provide valuable data at multiple spacial and temporal scales within tropical ecosystems, sometimes referred to as tropical landscape ecology. The term "landscape ecology" was coined in 1939, and further defined in 1950 by Carl Troll (Troll 1950; Turner 2005). Turner (2005), after reviewing multiple definitions, found the commonality between these definitions to be a focus on the reciprocal interaction among spatial heterogeneity and ecological processes (Risser et al. 1984, Urban et al. 1987, Turner 1989, Pickett &

Cadenasso 1995, Turner et al. 2001). The discipline began to gain popularity in the 1980's as aerial photography became available to a wider audience (Turner 2005). As remote sensing has rapidly advanced over the past decades, it has become more closely associated with modern landscape ecology.

Although relatively little is known or efficiently shared about the tropics, early remote sensing of forest changes focused primarily on tropical forest loss (Iverson et al. 1989). Since that time, remote sensing has been shown to be a powerful tool in assessing and modeling biodiversity in the tropics including LAI, NPP and others (Fuller et al. 1998, Kerr & Ostrovsky 2003, Turner et al. 2003, Nagendra & Rocchini 2008), monitoring of deforestation and land use change (Nelson and Holben 1986, Tucker et al. 1984, Malingreau and Tucker 1988, Sader & Joyce 1988, Green & Sussman 1990, Skole & Tucker 1993, Hansen et al. 2000, Sader et al. 2001, Achard et al. 2002, Mayaux et al. 2005, Chowdhury 2006, Harper et al. 2007, Hansen et al. 2008, Lindquist et al. 2008, Reddy et al. 2009) and in predicting carbon stocks and biomass (Zhang et al. 2002, Thenkabail et al. 2004, Lu 2005, Lu 2006, Sanchez-Azofeifa et al. 2009). Some active sensors such as Lidar are able to produce digital terrain models (DTMs) and digital canopy models (DCMs) (Clark et al. 2004), giving researchers crucial terrain and forest structure information that would otherwise be practically unobtainable for tropical areas.

It is important not to over-sell remote sensing as inaccuracies can arise and the applicability is not relevant to every ecological study. Satellites and other sensors are subject to imagery errors that are often difficult to detect without careful evaluation (Kerr & Ostrovsky 2003). Pimm et al. (1991) found that most ecological studies are done on small plots of only a few hectares in size over a short period of time. This limitation in size (spatial resolution) and duration (temporal resolution) makes correlation of field-based data to remote sensing data

challenging. Additionally, recent concerns are future availability, continuity, and global coverage of satellite imagery, which have opened a dialog among researchers. Loarie et al. (2007) brought to attention first, the lack of global coverage with higher-resolution sensors such as IKONOS and QuickBird, second, a potential gap in Landsat data collection (if the current Landsat satellites fail before the LDCM is operational), and third, the cost and availability of replacement sensors for researchers. Since Landsat has a history of providing the longest and most inclusive continual global dataset, this potential gap would be significant (Williams et al. 2006). In response to Loarie et al., Kark et al. (2008) and Loveland et al. (2008) explained that the growing world satellite community has the ability to fill the potential gap with current sensors if collaboration can be accomplished. The responses, however, did not address the high-resolution availability deficit (Loarie et al. 2008). What the authors did agree on is the need for better coordination and funding for future remotely sensed image collection and distribution (Loarie et al. 2007, Loarie et al. 2008 Kark et al. 2008, Loveland et al. 2008). With much of the worlds tropics located in countries with limited resources, this is a concern for all tropical researchers.

Data Acquisition

The rapid advancement of remote sensing technology over the past thirty years has increased data availability, opening doors to researchers worldwide (Kark et al. 2008). Nevertheless, the availability and accessibility of imagery is not evenly represented across the globe. Subsequently, many tropical areas have limited imagery available (Kark et al. 2008). Due to limited availability of tropical imagery, costs to acquire new data greatly contribute to the overall expense of any tropical ecology research project. Even though remote sensing has been shown to be a cost-effective tool in tropical studies (Mumby et al. 1999, Roller 2000, Mayaux et al. 2005, Loarie et al. 2007, Reddy et al. 2009), it is still expensive. Ten years ago, 42 of 60

tropical coast managers interviewed by Mumby et al. (1999), stated that cost was the greatest deterrent to their use of remote sensing data.

The outcome of any study involving how pattern relates to process is influenced by the scale set by the observer. Scale in this context includes both spatial and temporal. Discussion on the appropriate scale for tropical ecology studies remains open and is beyond the scope of this article. However, some ideas on how to address scale are worth mentioning. Levin (1992) emphasized that there is no single scale universal to every natural ecological study. An understanding of the processes involved is crucial in justifying a scale to work at. If data is available, multiple spatial and temporal scales should be used. Platform selection(s) for any remote sensing project is dependent on the project's temporal and spatial scales. Sensors range from high resolution, large scale photography, often flown by small aircraft, to small scale data produced by hyperspectral sensors stationed on satellites. Lists of the available sensors, their uses and specifications can be found in publications reported by Turner et al. (2003), Kerr and Ostrovsky (2003), Boyd and Danson (2005), Jensen (2005), Nagendra and Rocchini (2008) and Goetz (2009) (hyperspectral). Future sensors currently in the planning stages were reported by Kark et al. (2008). Coarse resolution sensors such as AVHRR have been used and accepted for globally-scaled land change projects. However, they have fallen short for local land managers and more localized research, such as biodiversity studies (Mayaux et al. 2005). For example, if a study was only concerned about land change comparing forested versus cleared land, Landsat 30m resolution imagery would be sufficient for the study (Figure 3). If the study involved land conversions of a smaller area, such as forest to pasture, bare ground or crop land, a finer resolution image, such as 4m resolution IKONOS imagery (Figure 4) or 1m resolution aerial photography (Figure 5) would be more appropriate.

One disadvantage to finer resolution sensors is expense, with the exception of the recently available Landsat imagery at little to no cost. Use of multiple sensors at varying resolution may be a viable solution in response to cost issues associated with larger area studies. Multiple sensors may be necessary for most projects because no individual sensor meets all requirements of a comprehensive tropical forest study (Malingreau et al. 1992). Hansen et al. (2008) suggested that for global or large scale (ecologically-speaking) humid tropical forest estimations, moderate resolution sensors such as MODIS can be used to find areas of likely forest cover loss. The selected areas can then be assessed using finer resolution imagery such as Landsat.

Pre Processing

Prior to analyzing patterns of tropical forest structure, preprocessing is required to eliminate data registration errors that occur during image acquisition. The type of preprocessing required depends on the characteristics of the remote sensing platform and typically involves raw image data. The four main types of preprocessing techniques include geometric correction, radiometric correction and calibration, noise removal, and georeferencing. Geometric correction accounts for variations in the altitude, attitude, and velocity of the sensor as well as irregularities in the earth's rotation, curvature, relief, and atmospheric refraction. Radiometric correction and calibration take into consideration atmospheric conditions, earth-sun distance, sun elevation, and haze. Noise removal eliminates unwanted disturbances in the data such as sensor drift or malfunction, electronic interference, or problems that occur during signal digitization and data recording. Georeferencing specifies the location of the acquired imagery in relation to the earth's surface, containing information on spatial location and pixel size. For example, if AVHRR images are used with higher resolution SPOT XS or Landsat data for a multi-sensor area-change

study, an error of only plus or minus 1 pixel in AVHRR transfers to a 50 pixel error in SPOT XS (Van et al. 2008)

Analysis

Interpreting patterns in tropical systems can be confounded by their high spatio-temporal variability and a lack of available field-based information on ecosystem structure and function. Furthermore, remote sensing methods found to work in tropical moist or dry systems may not work in nearby tropical wet forests. During the early Landsat era, researchers were selected by NASA in the 1970's to investigate the multispectral images obtained from Landsat-1. Using the full resources of the JPL, ground-referenced data observed by the researchers did not explain all the patterns seen in the 4 bands of the early satellite imagery (Goetz 2009). Alexander Goetz, one of the lead researchers of the project said, "It became clear that subtle color variations on the images were difficult to identify in the field and spectral reflectance measurements of undisturbed, *in situ* surface samples would be necessary to interpret the image colors properly." (2008).

Classification of remote sensed images can be done both supervised with training data provided by the user as well as unsupervised allowing the software program to select the best fit for a defined number of classes. Caution should be used when classifying and quantifying data from unknown tropical areas. If preprocessing has been performed correctly, quantifiable change and vegetation assessment can be done using vegetation indices such as NDVI. However, sensor degradation needs to be accounted for in tropical forest research. Kogan and Zhu (2001) tested corrections that were implemented for long term NDVI estimations using AVHRR between 1985 and 1999. They found that although the corrections worked for temperate areas, it did not work

as accurately for deserts and tropical forests. The errors associated with tropical forests were thought to be caused by a sharp increase in stratospheric aerosols over tropical areas. This is of real concern because many satellites are operating beyond their expected life spans. There are a variety of software programs available to assist in statistical analysis and sensor correction of tropical remote sensed data (Table 1).

Ground Referencing (*in situ*) and Accuracy Assessment

Accuracy assessment is the means to verify the quality of the information derived from remote sensed data. Accuracy assessment can be based on ground referenced data. Ground referencing, often incorrectly referred to as ground truthing, is a critical aspect in the development of remote sensing products. Jensen (2005) stated "it is a misnomer to refer to *in situ* data as *ground truth data*. Instead, we should refer to it simply as *in situ ground reference data*, and acknowledge that it also contains error." Beyond the semantics of the term used, there are real questions that the remote sensing of tropical ecosystem community needs to ask. Key questions are discussed below.

How accurate are the ground reference data?

Seefeldt and Booth (2006), working with remote sensing in sagebrush, submitted that there were no cover measurements with established accuracy. In a pilot study comparing three *in situ* methods of tree density estimations in the neotropical forests of Petén, Guatemala, large variation was found between the methods (Balzotti et al. in preparation).

Is a standard needed for how much ground data needs to be collected?

Ground data can be collected at the same time the imagery is collected to geo-rectify an image. Ground reference data can also be used in accuracy assessments to verify classifications and, in fine resolution studies, for species spectral identification. Mumby et al. (1999), working in the Turks and Caicos islands with Landsat TM imagery, found that the more field sites used, the greater the accuracy of the supervised classifications. In many cases, previously collected ground cover data or finer resolution imagery is available, but in the tropics, lack of these kinds of data makes remote sensing accuracy assessment difficult. Sader et al. (2001), who assessed land use change in Petén, Guatemala, used multi-date color composite comparisons to deal with the lack of ground data. Oftentimes, the ground referencing method is not clearly stated. There is a wide range of methods used for field verifications, from visual assessment to plot-based methods. Many of the land change papers reviewed did not conduct in-field tests or did not outline the method used. There may be no other aspects of remote sensing and tropical ecology that are more varied in how they are done and what is acceptable error than ground referencing and accuracy assessment.

CASE STUDY-TROPICAL FOREST ASSESSMENT IN NORTHERN PETÉN, GUATEMALA

Introduction and Background Information

From 1966 to 1994, Guatemala's tropical forests decreased by an alarming 38%, which occurred primarily in the northern Petén region of Guatemala (Figure 6) (Bilsborrow and Carr, 2001). As the population of Petén continues to rise (from 600,000 in 1999 to an expected one million by 2020), increased deforestation rates are predicted to continue (Grandia, 2000). Sader and Joyce found 90% of deforestation in Petén occurred within 2 km of roads. (1994). With this sharp increase in population, the need to document and manage the existing forests of Petén, Guatemala is of the utmost importance, not only for the people of the Petén region but also for the global population.

The Petén region of Guatemala is home to the largest lowland tropical forest in Central America (Carr, 2005). The region makes up about one-third of Guatemala's total surface, roughly thirty-six thousand square kilometers in size (Schwartz, 1990). In the late eighties and early nineties, heightened awareness arose over the rapid deforestation of the Petén region and brought about the creation of the Maya Biosphere Reserve (MBR). The MBR was officially created in 1990 with the help of donations from multiple agencies: the United States Agency for International Development (USAID), Nature Conservancy, Conservation International, and CARE International, as well as many private donors in cooperation with the Guatemalan government branch known as the National Council of Protected Areas (CONAP) (Nations, 2006). The MBR is the most extensive tropical rain forest to remain "intact" north of South America (Kaiser, 2001; Carr, 2005). The MBR follows the United Nations Educational,

Scientific, and Cultural Organization (UNESCO) action plan for reserves (Sundberg, 1998). The action plan for a biosphere calls for nuclear zones where no human habitation or use is permitted, a multi-use zone that allows limited resource use (i.e. selective harvesting of forest products such as chicle and Xate palm leaves) and a buffer zone that allows sustainable human use and occupation on a much larger scale (Nations, 2006; UNESCO, 1984). The Guatemalan MBR is made up of 1.6 million hectares of tropical lowland forest consisting of subtropical moist forests, subtropical rain forests, wetlands and savannas (Sundberg, 1998). The MBR is a "protected" home to high biodiversity and unique forests as well as a rich Maya history of cultivation, making it incomparable to any other tropical forest (Gomez-Pompa et al., 1987). The MBR is also home to numerous endangered plants, at least four known endangered insects, two endangered reptiles and several endangered mammals such as the howler monkey (*Alouatta pigra*), Chiapan climbing-rat (*Tylomys bullaris*), and Tumbala climbing-rat (*Tylomys tumbalensis*). The MBR also provides one of the largest refuges for the jaguar (*Panthera onca*), ocelot (*Leopardus pardalis*), white lipped peccary (*Tayassu pecari*), spider monkey (*Ateles* spp.), scarlet macaw (*Ara macao*), harpy eagle (*Harpia harpyja*) and Monelet's crocodile (*Crocodylus moreletii*) (Nations, 2006). The MBR is currently under extreme environmental stress with rapid human migration into the region and in many instances, directly into the nuclear zones. Grunberg and Ramos (1998) found that after the regulations creating the MBR were put into effect in 1990, the MBR was home to approximately 78,000 people. Twenty-two percent of those inhabitants lived in the multi-use zone and 23% lived in the nuclear zone. Many of the people living within the MBR were residents before it was officially created, further complicating regulation of the forests. The preservation and management of the MBR is a daunting task due to its size and the need for constant land inspections. These inspections are necessary in order to make educated

decisions regarding tropical forest conservation and preservation. In 1992, satellite images of deforestation on a grand scale between Guatemala and Mexico's borders were published by National Geographic (Stuart, 1992). Carr observed, "Our understanding of the processes of deforestation remains inchoate; indeed, even estimates of current tropical forest cover remains notoriously unreliable." Carr included the need for modern inter-disciplinary views into deforestation and conservation, referring to remote sensing and GIS studies as possibilities in understanding current deforestation rates in the MBR (2004).

Study Area

The study area was situated in the Sierra del Lacandon National Park (SLNP), one of the 6 nuclear zones of the MBR (Figure 7). The SLNP is the second largest protected area in Guatemala covering 202,865 ha. (Herrera & Paiz 1999). This area was chosen because of present availability of remote sensing data (Landsat, aerial photography, AIRSAR, limited IKONOS and others). More importantly, this region is under severe threat of deforestation by illegal groups living in the park. The dangers posed by these groups make full ecological ground reconnaissance oftentimes untenable. Thus, remote sensing stands as our most powerful tool for tracking changes in the park.

Image Acquisition and Uses

Landsat images were obtained at no cost from the U.S Geological Survey (USGS). The highest resolution data from Landsat 7 is from the panchromatic band at 15 meters. This band was used for visual interpretation. The 30-meter resolution bands were used for computer-based classification, limiting the size of detectible forest clearance to 30 square meters or greater. Furthermore, Landsat 7 has not been fully functional since May, 2003. Despite these limitations,

Landsat data was valuable to this project for large-area long-term information. The imagery for the SLNP was obtained for multiple years and analyzed for overall vegetation cover and change. Aerial photography was obtained from the Defensores de la Naturaleza. The images produced sub-meter resolution, which were then used for accuracy assessment of supervised classification of Landsat data. The aerial photography was limited temporally because it was only a snapshot in 2006. The other limitation of note was its limited spectral range with only 3 bands. AIRSAR 10-meter resolution digital elevation models (DEMs) were used. AIRSAR was flown over the study area in March (the dry season) of 2004 by the JPL. These DEMs were created using the C-band (0.057 meter wavelength). The use of the C-band allows an assessment of general landscape topography based on the canopy height and serves as a means to identify gaps in the canopy from naturally fallen trees as well as legal and illegal felling of forest trees. DEM's were obtained from the Alaska Satellite Facility at no cost. The 10-meter resolution DEM was used to visualize the topographic position of the forest clearing.

Preprocessing and Analysis

Much of the preprocessing was done prior to obtaining the data. The images, despite having been previously georeferenced were further referenced to each other using the commercial software package, ENVI. All Landsat images were accurate to each other with an error no greater than a half-pixel and with root mean square (rms) error values lower than .005 for all years. Training sites were created for the following three vegetation types: cleared, burned and forest. These training sites were used for supervised classification on Landsat imagery. The accuracy of the classification was checked against the aerial photography with a 91% overall Kappa statistic (a conservative estimation of accuracy by comparing the agreement to that which is expected by

chance (Cohen 1960)). Each year's change was mapped and statistics were generated (Figure 8 and Figure 9).

Results and Discussion

Between the years 1988 and 2009, it was found that 49.8% of the study area had been altered by fire or land clearance. After the creation of the SLNP in 1990, it appeared that conservation was possible. However, by 2006, 238 new hectares had been cleared and 2,917 burned. By 2009, there was a further increase of 1,494 newly cleared hectares. Fire data for 2009 has not yet been generated. The cleared areas are of high concern indicating migration and occupation of lands within the park.

The land change tracking methods utilized in this study will allow the park officials more complete up-to-date information on the human-influenced forest changes. This also will support future ecological studies. Tracking these changes will assist in vegetative succession studies by providing baseline data of cleared areas. Permanent plots are planned in the near future to monitor carbon sequestration as well as other ecological functions that can then be compared to remote sensed models. Furthermore, the information gleaned from this and related studies will support upcoming projects as the park seeks monetary support and legal aid in improved maintenance and protection of the park.

CONCLUSION

Despite the difficulty in conducting tropical forest research, the ecological importance of these forests cannot be neglected. Therefore, effective and efficient methods for collecting and synthesizing data are needed for conserving these forests that are currently in rapid decline. Remote sensing can be an effective tool for assessing and monitoring tropical forests, in

particular when good judgment is used in selecting appropriate sensors and in understanding their limitations. Continual data acquisition using cost effective technologies is necessary for the future of monitoring tropical forests. To keep up with the rapid technological advancements in remote sensing platforms, new ground-based methods covering larger areas over longer periods of time are needed and old methods need to be assessed for compatibility. If remote sensing is to be fully utilized as a tool in tropical ecology, education is needed to bridge the gap between research and management, targeting a diverse group of potential users.

References

Achard, F. et al. (2002) Determination of Deforestation Rates of the Worlds's Humid Tropical Forests. *Science* 297, pp. 999- 1002.

Birk, R., Valenti, C., Valenti, E. and McCandless, W. (1995) Synthetic Aperture Radar Imaging Systems. *IEEE AES Systems Magazine* 10(11), pp. 15-23.

Bilsborrow, R.E. and Carr, D.L. (2001) Population, agricultural land use, and the environment in the developing world. In tradeoffs or synergies? Agricultural intensification, economic development and the environment, CAB International. Wallingford, UK. p. 35-55.

Boyd, D.S. and Danson, F.M (2005) Satellite remote sensing of forest resource: three decades of research development. *Progress in Physical Geography* 29(1), pp. 1-26.

Bunkse, E. (1981) Humboldt and an Aesthetic Tradition in Geography. *Geographical Review* 71(2), pp. 127-146.

Carr, D.L. (2005) Forest clearing among farm households in the Maya Biosphere Reserve. *The Professional Geographer* 57:157-168.

---. (2004) Tropical deforestation. In D. Janelle & K. Hansen (Eds.), Geographical Perspectives on 100 Problems. London: Kluwer Academic Publishers. pp. 293-298

Chowdhury, R.R. (2006) Driving forces of tropical deforestation: The role of remote sensing and spatial models. *Singapore Journal of Tropical Geography* 27, pp. 82-101.

Clark, M. L., Clark, D.B. and Roberts, D.A. (2004) Small-footprint lidar estimation of sub-canopy elevation and tree height in tropical rainforest landscape. *Remote Sensing of Environment* 91(1), pp. 68-89.Cohen, J. (1960). A coefficient of agreement for nominal scales. *Educational and PsychologicalMeasurement* 20, pp. 37-46

Elachi, C. (1980) Spaceborne Imaging Radar: Geologic and Oceanographic Applications. *Science* 209(4461), pp. 1073-1082.

Federal Geographic Data Committee (FGDC) (2008). Vegetation Classification Standard, FGDC-STD-005, v2. Washington, D.C., USA.

Food and Agricultural Organization (FOA) (2001). Global Forest Resources Assessment 2000 Main Report: Rome. [Online]. Retrieved August 30 2009 from: http://www.fao.org/docrep/003/Y0900E/y0900e00.htm.

Foody, G.M., Curran, P.J. (1994) Estimation of Tropical Forest Extent and Regenerative Stages Using Remotely Sensed Data. *Journal of Biogeography* 21(3), pp. 223-244.

Fuller, R.M., et al. (1998) The integration of field survey and remote sensing for biodiversity assessment: a case study in the tropical forests and wetlands of Sango Bay, Uganda. *Biological Conservation* 86, pp. 379-391.

GeoEye (2009) GeoEye Constellation fact sheet. [Online]. Retrieved July 15 2009 from:

http://www.geoeye.com/CorpSite/assets/docs/brochures/GeoEyeSatellites2007_v1.pdf

Geist, H.J. and Lambin, E.F. (2002) Proximate causes and underlying driving forces of tropical deforestation. *BioScience* 52(2), 143-150.

Goetz, A.F.H., Vane, G., Solomon, J. and Rock, B. N. (1985) Imaging spectrometry for Earth remote sensing. *Science* 228, pp. 1147-1153.

Goetz, A. F. H. (2009) Three decades of hyperspectral remote sensing of the Earth: A personal view. *Remote Sensing of Environment* 113, pp. S5-S16.

Goetz, S. (2007) Crisis in Earth Observation. *Science* 315, pp. 1767.

Gomez Pompa, A., Flores, A. S. and Sosa, V. (1987) The "Pet Kot": A Man-made Topical Forest of the Maya. *Interciencia* 12, pp. 10-15.

Grandia, L. (2000) Cuántas personas quiera Ud. que vivan en Petén? In Nuevas Perspectivas de Desarrollo Sostenible en Petén. Ed. J. Grunberg, Guatemala City, Facultad Latinoamericana de Ciencias Sociales (FLACSO): 137-151.

Green, M. and Sussman, R.W. (1990) Deforestation History of the Eastern Rain Forest of Madagascar from Satellite Images. *Science* 248(4952), pp. 212-215.

Grunberg,G., and Ramos, V.H. (1998) Base de datos sobre poblacion,tierras y medido ambiente de la Reserva de la Biosfera Maya. Database. Guatemala Guatemala:CONAP.

Hansen, M. C., Defries, R. S., Townshend J. R. G., and Sohlberg, R. (2000) Global land cover classification at 1 km spatial resolution using a classification tree approach. *Int. J. Rem. Sens.* 21(6) pp. 1331-1364.

Hansen, M.C. (2008) Humid tropical forest clearing from 2000 to 2005 quantified by using multitemporal and multiresolution remote sensed data. *PNAS* 105(27), pp. 9439-9444.

Harper, G.J. (2007) Fifty years of deforestation and forest fragmentation in Madagascar. *Environmental conservation* 34(4), pp. 325-333.

Herrera, R. and Paiz, M. (1999) Plan Maestro 199-2003 Parque National Sierra del Lacandon Consejo Nacional de Areas Protegidas. The Nature Conservancy (TNC), Centro Maya y CARE, Guatemala. pp. 45.

Holmgren, P., Persson, R., 2002. Evolution and prospects of global forest assessments. Unasylva 53(210), pp. 3–9.

Iverson, L.R., Graham, R.L. and Cook, E.A. (1989) Application of satellite remote sensing to forested ecosystems. *Landscape Ecology* 3(2), pp. 131-143.

Jensen, J.R. (2005) *Introductory Digital Image Processing*: *A remote Sensing Perspective.* 3rd ed. Upper Saddle River, NJ: Prentice Hall.

Jet propulsion Laboratory (JPL) (2009) Missions: Earth. [Online] retrieved 15 August 2009 from: http://www.jpl.nasa.gov/missions/index.cfm?type=&destination=Earth.

Kaiser, J., (2001) Bold Corridor Project Confronts Political Reality. *Science* 293, pp. 2196-2199.

Kark, S., Levin, N. and Phinn, S. (2008) Global environmental priorities: making sense of remote sensing: Reply to TREE Letter: Satellites miss environmental priorities by Loarie et al. (2007). *Trends in Ecology and Evolution* 23(4), pp. 181-182.

Kerr, J. t., Ostrovsky, M. (2003) From space to species: ecological applications for remote sensing. *Trends in Ecology and Evolution* 18(6), pp. 299-305.

Kogan, F.N. and Zhu, X. (2001) Evolution of Long-Term Errors In NDVI Time Series: 1985-1999. *ADV. Space Res.* 28(1), pp. 149-153.

Levin, S. (1992) The Problem of Pattern and Scale in Ecology. *Ecology* 73(6), pp. 1943-1967

Lindquist, E.J., Hansen, M.C., Roy, D.P. and Justice, C.O. (2008) The suitability of decadal image data sets for mapping tropical forest cover change in the Democratic Republic of Congo: implications for the global land survey. *Int. J. Rem. Sens.* 29(24) pp. 7269-7275.

Loarie, S. R., Joppa, N. and Pimm S. L. (2007) Satellites miss environmental priorities. *Trends in Ecology and Evolution* 22(12), pp. 630-632.

---. (2008) Satellites miss environmental priorities Response to Loveland et al. and Kark et al.:. *Int. J. Rem. Sens.* 23(4), pp. 183.

Loveland, T.R., Cochrane, M.A. and Henebry, G.M. (2008) Landsat still contributing to environmental research. *Trends in Ecology and Evolution* 23(4), pp. 183-184.

Lu, D. (2005) Aboveground biomass estimation using landsat TM data in the Brazilian Amazon Basin. *Int. J. Rem. Sens.* 26, pp. 2509-2525.

---. (2006) The potential and challenges of remote sensing-based biomass estimation. *Int. J. Rem. Sens*. 27(7), pp. 1297-1328.

Malhi, Y., Grace, J. (2000) Tropical forests and atmospheric carbon dioxide. *TREE* 15(8),pp.332-337.

Malingreau, J.P. and Tucker, C.J. (1988) Large-scale deforestation in the southeastern Amazon basin of Brazil. *Ambio* 17, pp. 49-55.

Malingreau, J. P., Verstraete, M. M., and Achard, F. (1992) Monitoring global deforestation: a challenge for remote sensing. In Mather, P. editor, TERRA-1: understanding the terrestrial environment. London: Taylor and Francis, pp. 203-209.

Markham, B. L., Storey, J. c., Williams, D. L. and Irons, J. R. (2004) Landsat Sensor Performance: History and Current Status. *IEEE Transactions on Geoscience and Remote Sensing* 42(12), pp. 2691-2694.

Mayaux, P. et al. (2005) Tropical forest cover in the 1990s and options for future monitoring. *Phil. Trans. R. Soc. B* 360, pp. 373-384.

McGuffie, K. et al. (1995) Global climate sensitivity to tropical deforestation. *Global and Planetary Change* 10, pp. 97-128.

Mumby, P. J., Green E. P., Edwards A. J. and Clark C. D. (1999) The cost-effectiveness of remote sensing for tropical costal resources assessment and management. *Journal of EnvironmentalManagement* 55, pp. 157-166.

Myers, N. (1980) Conservation of tropical moist forests. In National Academy of Sciences Washington, DC: National Academy of Science.

---. (1992) *The Primary Source: Tropical Forests and Our Future*. New York: Norton.

Nagendra, H. and Rocchini, D. (2008) High resolution satellite imagery for tropical biodiversitystudies: the devil is in the detail. *Biodivers Conserv* 17, pp. 3431-3442.

Nagendra, H. (2001) Using remote sensing to assess biodiversity. *Int. J. Rem. Sens.* 22, pp. 2377-2400.

Nations, J.D. (2006) *The Maya Tropical Forests: People, Parks and Ancient Cities.* University of Texas Press, Austin, Texas.

Nelson, R. and Holben, B. (1986) Identifying deforestation in Brazil using multiresolution satellite data. *Int. J. Rem. Sens.* 7, pp. 429-448.

Pickett S.T.A., Cadenasso M.L. (1995) Landscape ecology: spatial heterogeneity in ecological systems. *Science* 269, pp. 331-334.

Pennington, T. D. and Sarukhán K. J. 1968. Manual para la identificación de campo de los principales árboles tropicales de México. Mexico: INIF-FAO-SAG.

Pimm, S. L. et al. (2001) Can We Defy Nature's End? *Science* 293, pp. 2207-2208.

---. (1991) *The Balance of Nature*?: Ecological Issues in the Conservation of Species and Communities. University Chicago press, Chicago.

Pope, K.O., Rey-Benayas, J.M. and Paris, J.F. (1994) Radar remote sensing of wetland and forest ecosystems in Central American tropics. *Remote Sensing of Environment* 48, pp. 205-219.

Reddy C.S., Roa K.R.M., Pattanaik, C. and Joshi P.K. (2009) Assessment of large-scale deforestation of Nawarangpur district, Orissa India: remote sensing based study. *Environ. Monit. Assess.* 154, pp. 325-335.

Richards, P. W. (1996) *The Tropical Rainforest an Ecological Study*. 2nd ed. Cambridge: University Press.

Risser, P.G., Karr, J.R. and Forman, R.T. (1984) Landscape ecology: directions and approaches. Spec. Publ. No. 2, Ill. Nat. Hist. Surv., Champaign, Ill.

Roller, N. (2000) Intermediate multispectral satellite sensors. *Journal of Forestry* 98, pp. 32-35.

Sader, S. A. and Joyce, A.T. (1988) Deforestation rates and trends in Costa Rica, 1940 to 1983. *Biotropica* 20, pp. 11-19.

---. (1994) Forest change estimates for the northern Petén region of Guatemala--1986 to 1990. *Human Ecology* 22(3), pp. 317-322.

Sader, S. A., Hayes, D.J., Hepinstall, J. A., Coan, M., and Soza, C. (2001) Forest change monitoring of a remote biosphere reserve. *Int. J. Rem. Sens.* 22(10), pp. 1937-1950.

Sanchez-Azofeifa, G.A., Castro-Esau, K.L., Kurz, W.A. and Joyce, A. (2009) Monitoring carbon stocks in the tropics and remote sensing operational limitations: from local to regional projects. *Ecological Society of America* 19(2), pp. 480-494.

Schulze, M. D. and Whitacre, D.F. (1999). *A classification and ordination of the tree community of Tikal National Park, Petén, Guatemala*. Bulletin of the Florida Museum of Natural History 41 (3):169-297.

Schimel, D.S, et al. (2001) Recent patterns and mechanisms of carbon exchange by terrestrial ecosystems. *Nature* 414(8), pp. 169-172.

Schwartz, N. B. 1990. *Forest Society: A social history of Petén, Guatemala*. Philadelphia: University of Pennsylvania Press.

Seefeldt, S. S. and Booth D. T. (2006) Measuring Plant Cover in Sagebrush Steppe Rangelands:

A Comparison of Methods. *Environmental Management* 37(5), pp. 703-711.

Skole, D. and Tucker, C. (1993) Tropical Deforestation and Habitat Fragmentation in the Amazon: Satellite Data from 1978-1988. *Science* 260(5116), pp. 1905-1910.

Stuart, G. 1992. Maya heartland under siege. *National Geographic* 182(5), pp. 94-107.

Sundberg, J. (1998) NGO landscapes in the Maya Biosphere Reserve, Guatemala. *The Geographical Review* 88(3), pp. 388-412.

Thenkabail, P.S., et al. (2004) Biomass estimations and carbon stock calculations in the oil palm plantations of Africa derived savannas using IKONOS data. *Int. J. Rem. Sens.* 25, pp. 5447-5472.

Troll, C. (1950) Die geographisched Landscahaft und ihre Erforschung. *Studium Generale* 3, pp. 163-181.

Tucker, C.J., Holben, B. and Goff, T.E. (1984) Intensive forest clearing in Rondonia, Brazil, as detected by satellite remote sensing. *Remote Sensing the Environment* 15, pp. 225-261.

Turner, M.G., Gardner, R.H., O'Neill R.V. (2001) *Landscape Ecology in Theory and Practice*. New York: Springer-Verlag.

Turner, M. G. (1989) Landscape ecology: the effect of pattern on process. *Ann. Rev. Ecol. Syst.* 20 pp. 171-197.

---. (2005) Landscape Ecology: What Is the State of the Science?. *Ann. Rev. Ecol. Evol*. Syst. 36, pp. 319-344.

Turner, W., et al. (2003) Remote sensing for biodiversity science and conservation. *Trends in*

Ecology and Evolution 18(6), pp. 306-314.

United Nations Educational, Scientific and Cultural Organization (UNESCO) (1984) Action plan for biosphere reserves. *Nature and Resources* 20, pp. 11-22.

Urban, D.L., O'Neill, R.V., Shugart, H.H. (1987) Landscape ecology. *Bioscience* 37, pp. 119-127.

Van, A.N., Nakazawa, M., AOKI, Y. (2008) Highly Accurate Geometric Correction for NOAA AVHRR Data Considering Elevation Effect and Coastline Features. *IEICE TRANS. COMMUN*. E91-b (9), pp.2956-2963.

Williams, D.L. et al. (2006) Landsat: yesterday, today, and tomorrow. Photogramm. *Eng. Rem. Sens.* 72, pp. 1171-1178.

Zhang, Q., Justice, C.O., Densanker, P. V. (2002) Impacts of simulated shifting cultivation on deforestation and the carbon stocks of the forest of central. *Agriculture, Ecosystems and Environment* 90, pp. 203-209.

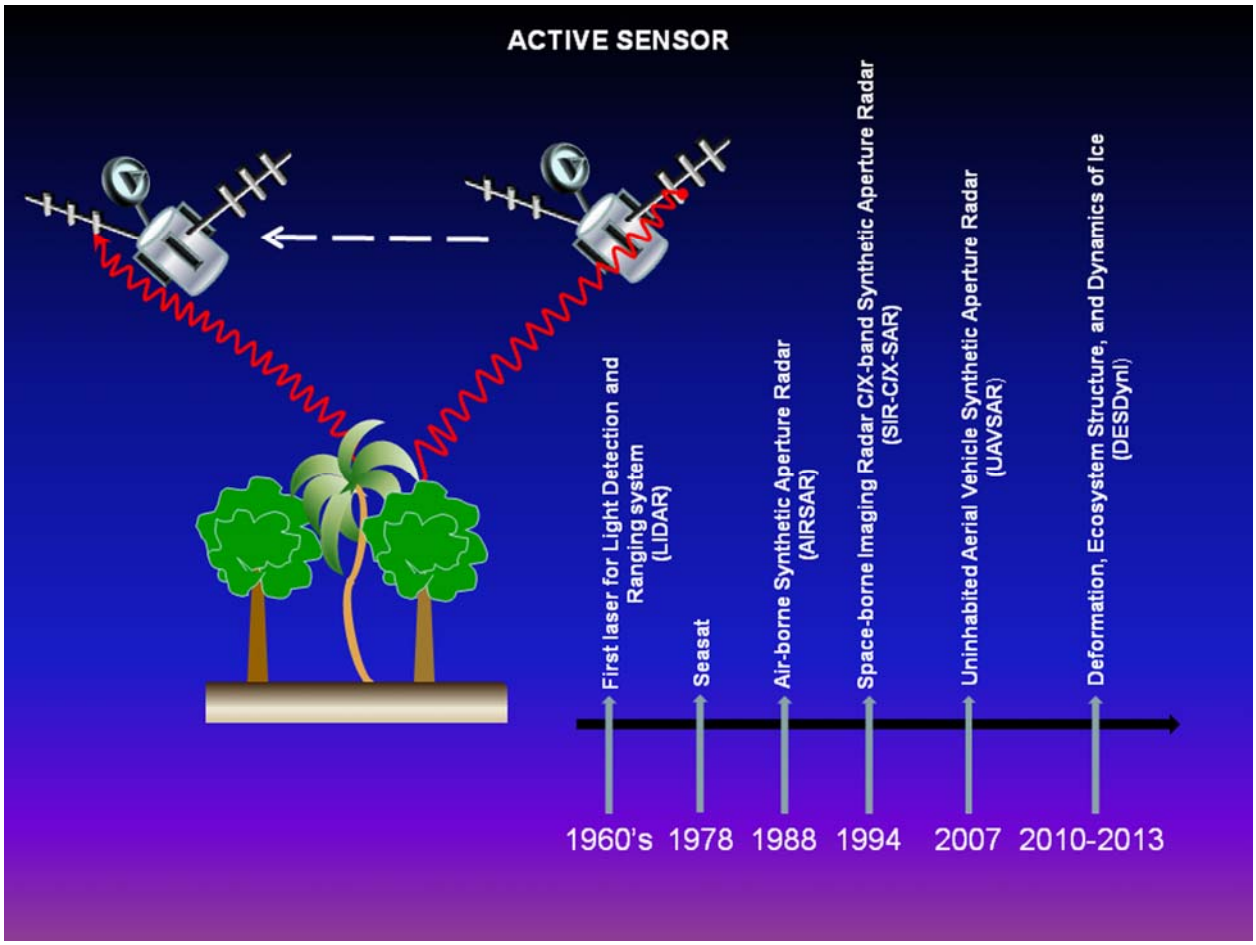

(Figure 1) Active sensors use a self generated illumination. The ability to self generate illumination allows active sensors to work in conditions that passive sensors cannot. The timeline listed above is an abbreviated timeline containing a few key sensors and dates.

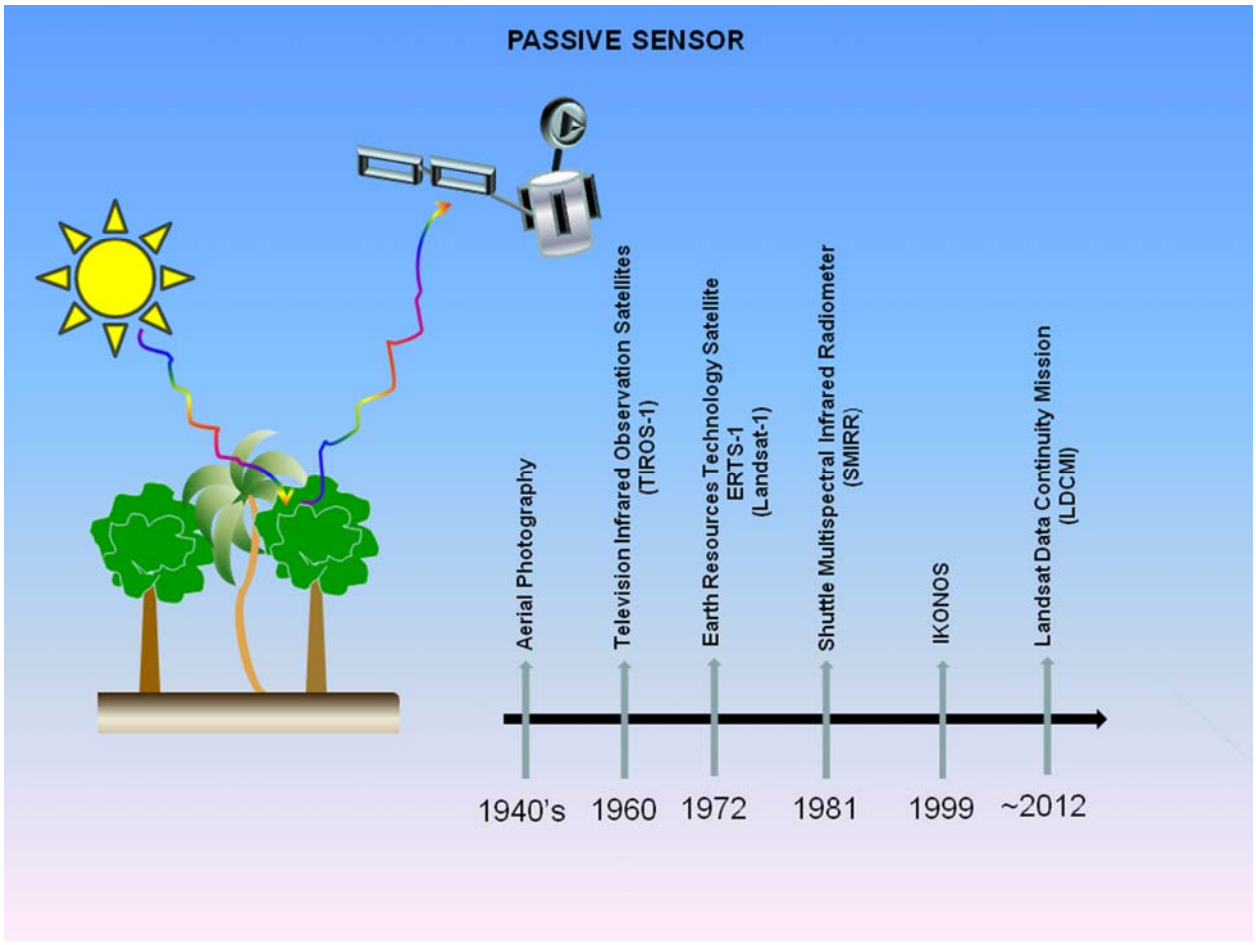

(Figure 2) Passive sensors use illumination generated by the sun. Cloud cover and other atmospheric interference can distort or block image acquisition. The timeline listed above is an abbreviated timeline containing a few key sensors and dates.

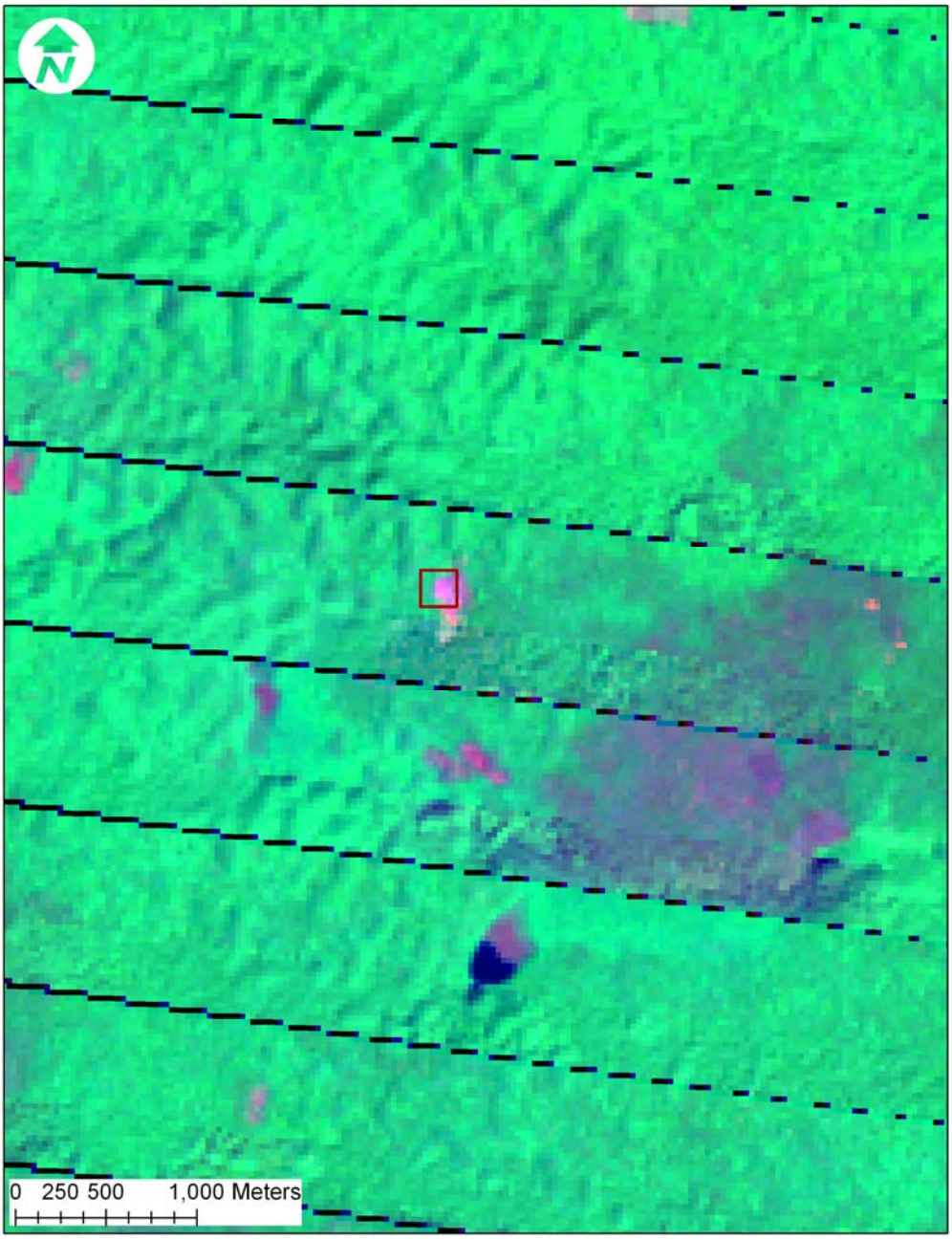

(Figure 3) Landsat land cover imagery, nuclear zone Sierra de Lacandon National Park Guatemala RGB/ 742 (742 was chosen to better show forest versus cleared areas) captured 04/10/2005. The area of the red box is 200 square meters. Figure resolution is 1:25,43. The black lines are a result of scan line problems and an edge between 2 Landsat instantaneous-fields-of views (IFOV).

(Figure 4) Pan sharpened IKONOS RGB/ 321 from 2007. Resolution of the IKONOS at 1:3,749. The area of the red box is 200 square meters. Note the ability to see the structures and variation of the cleared areas.

(Figure 5) Aerial photography (RGB/ 123) from 2007 with a resolution at 1:1,881.The area of the red box is 200 square meters. Note the improved ability to delineate agricultural land from other cleared land, as well as structure identification.

Popular software providers that can assist with statistical analysis of tropical imagery	
ERDAS	http://www.erdas.com/
ESRI	http://www.esri.com/
ENVI	http://www.ittvis.com/
GRASS*	http://grass.osgeo.org/
IDRISI (Taiga)	http://www.clarklabs.org/
Multispec*	http://cobweb.ecn.purdue.edu/~biehl/MultiSpec/
Orfeo toolbox*	http://www.orfeo-toolbox.org/otb/
OSSIM*	http://www.ossim.org/OSSIM/OSSIM_Home.html
PCI	http://www.pcigeomatics.com/
Quantum GIS*	http://www.qgis.org/
* Open source software	

(Table 1) A list of some popular software packages for preprocessing and statistical evaluation of remotely sensed data.

(Figure 6) Map of Guatemala showing the department of Petén in red and the Sierra de Lacandon National Park in Orange.

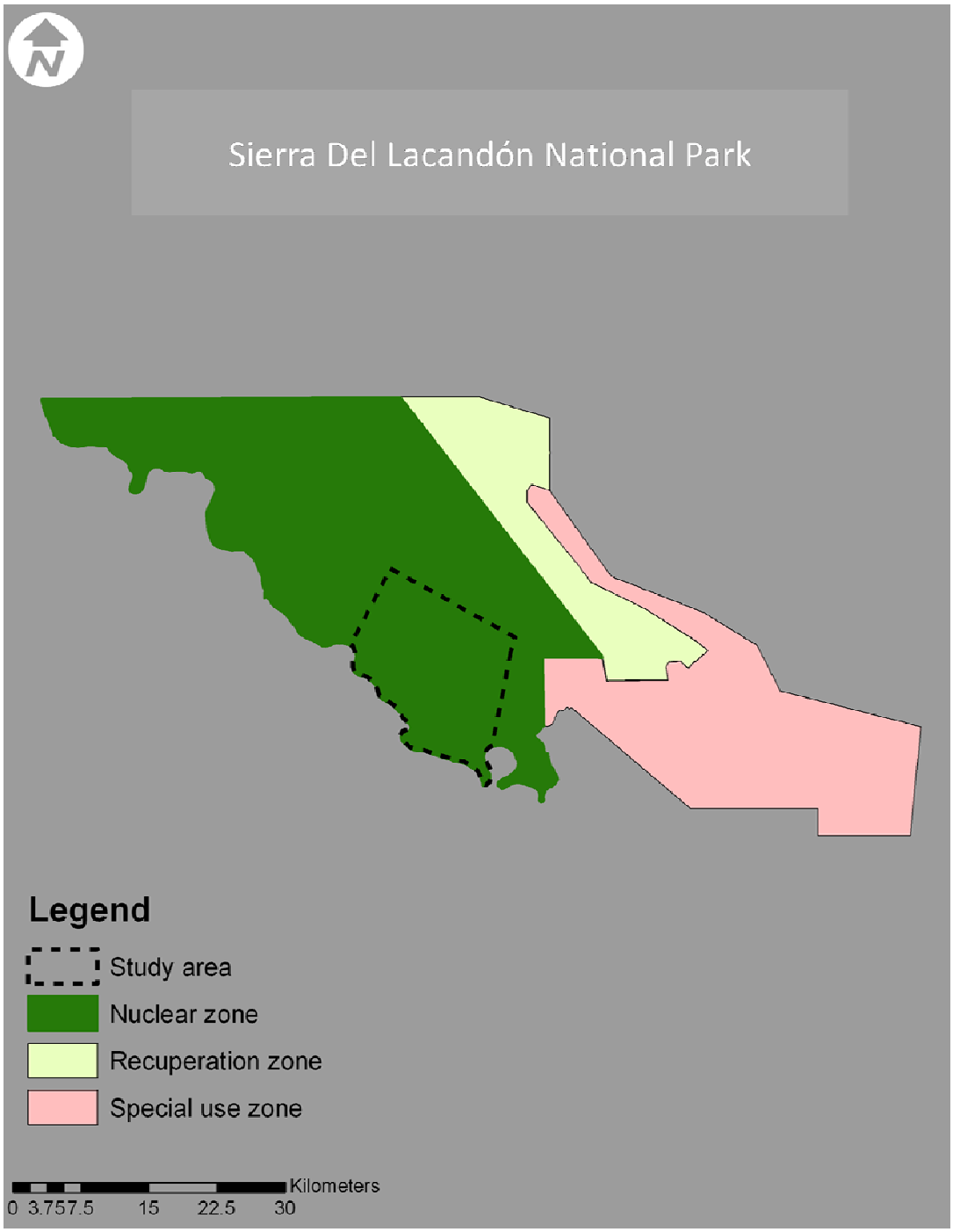

(Figure 7) Map of Sierra Del Lacandón Park, Petén, Guatemala

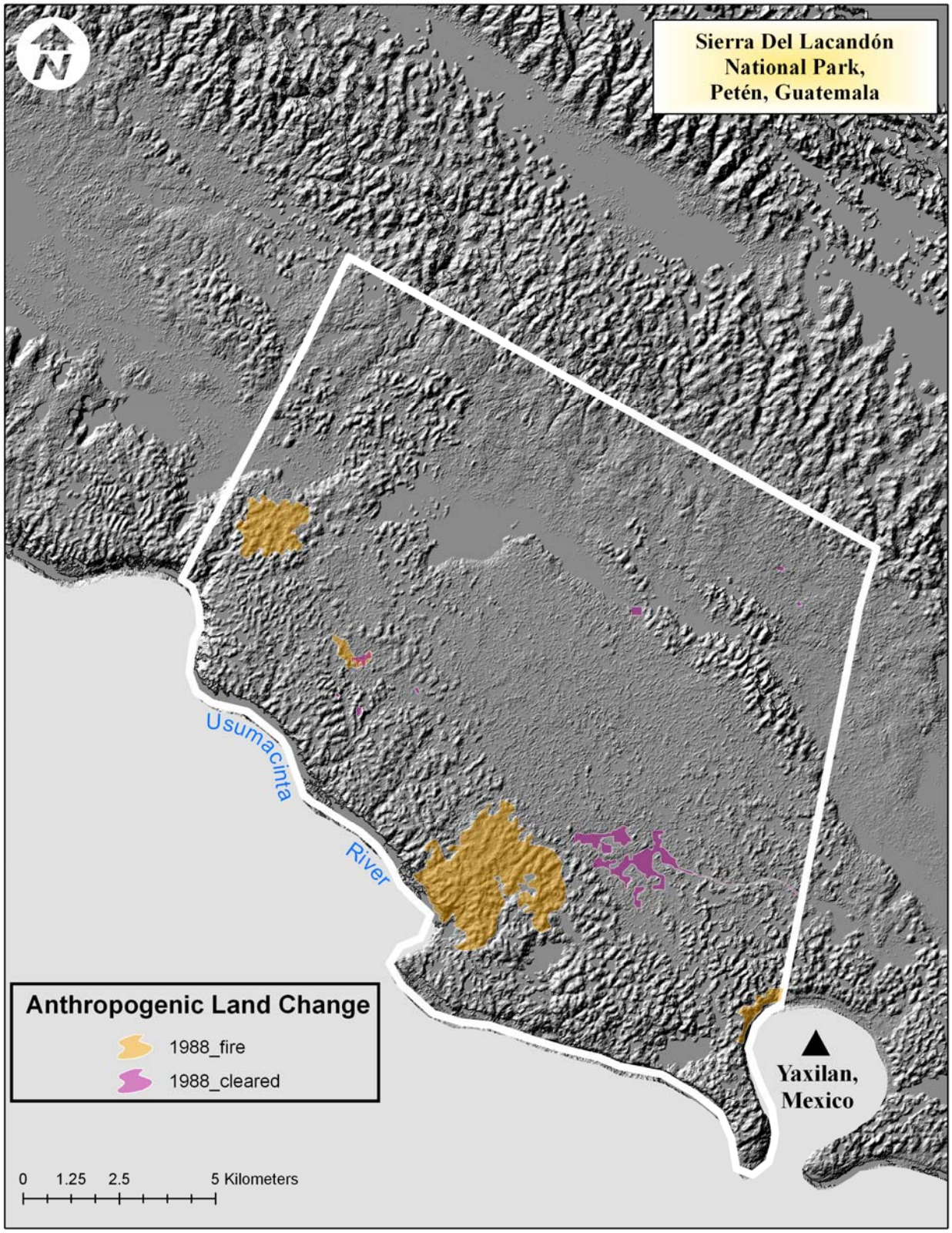

8a

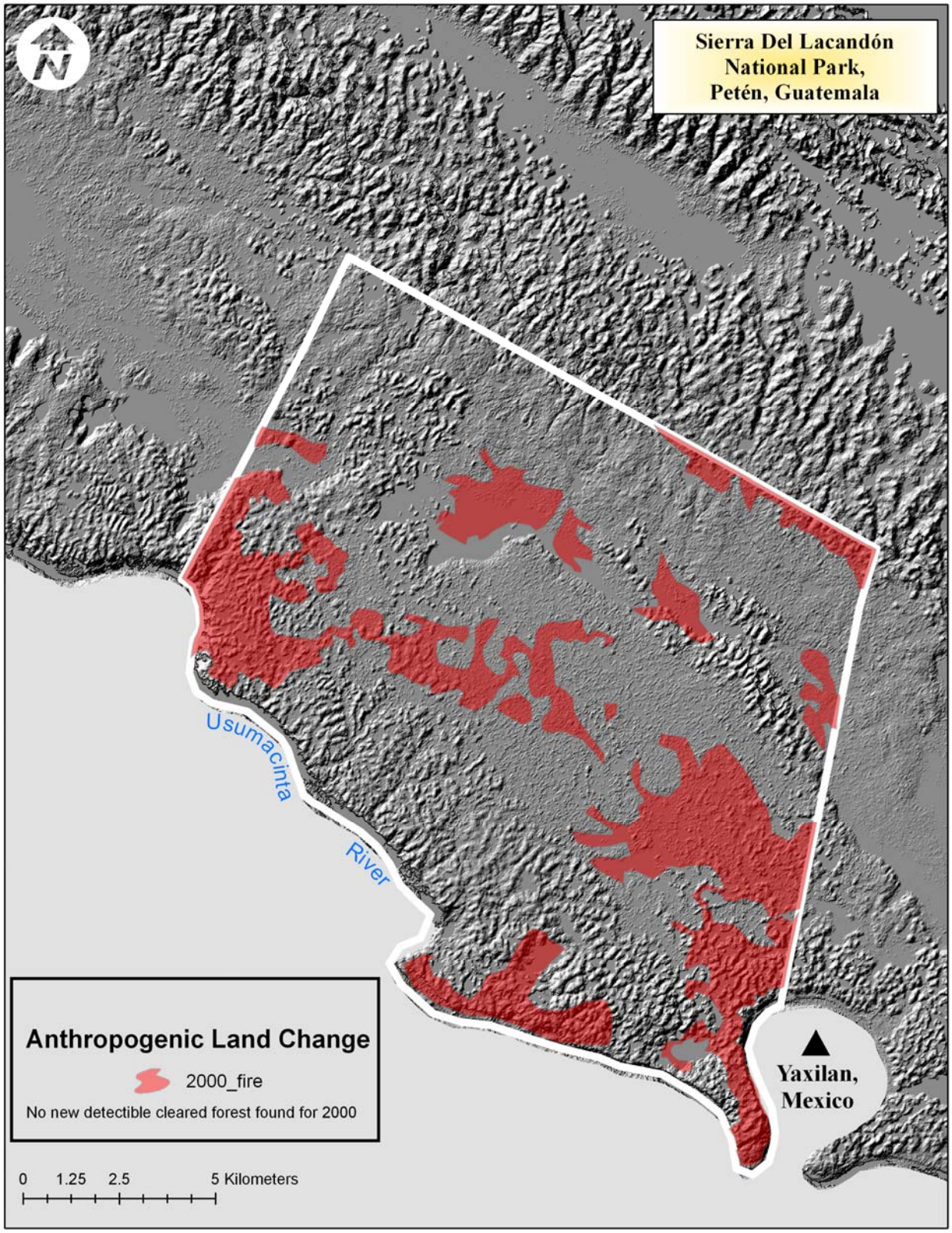

8b

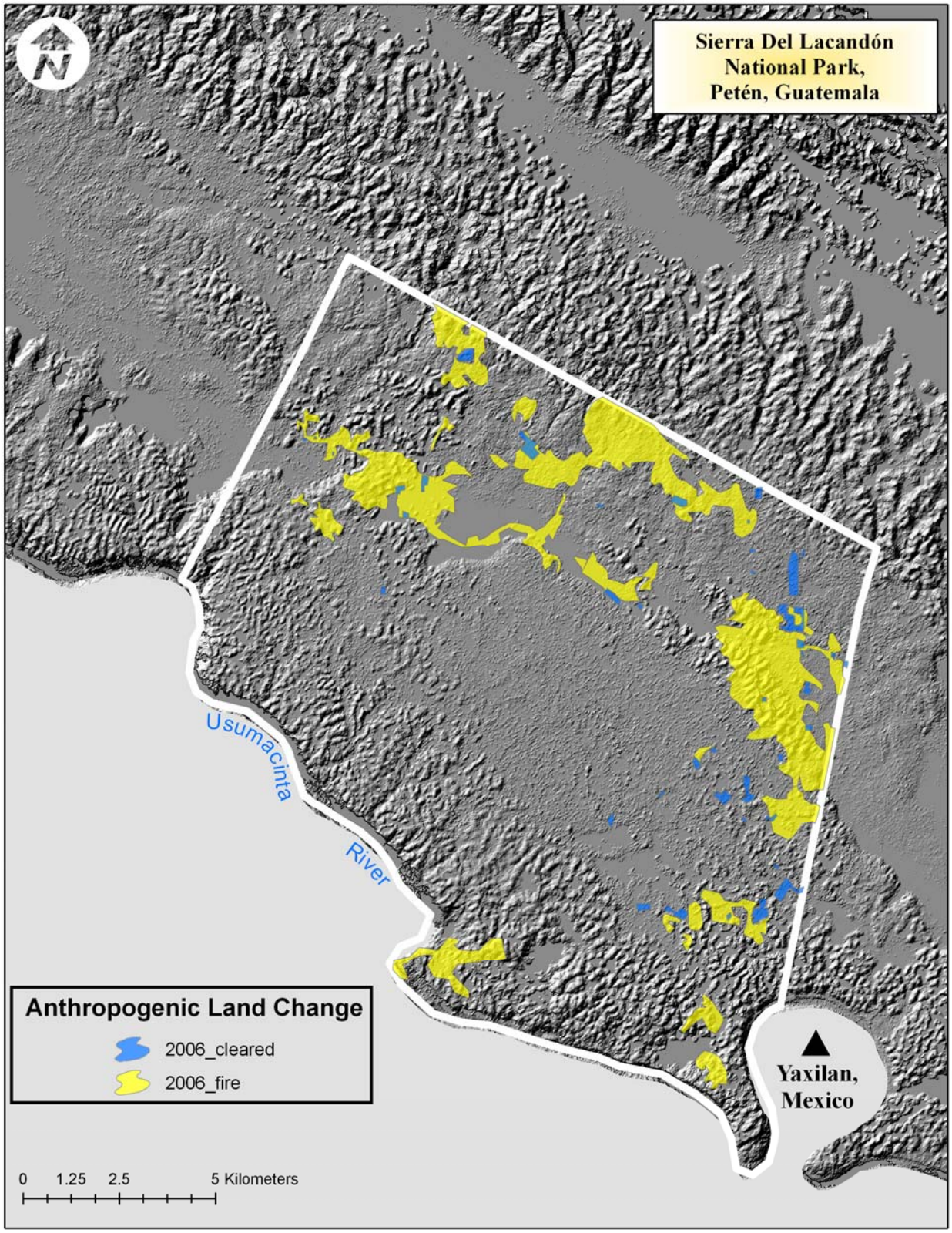

8c

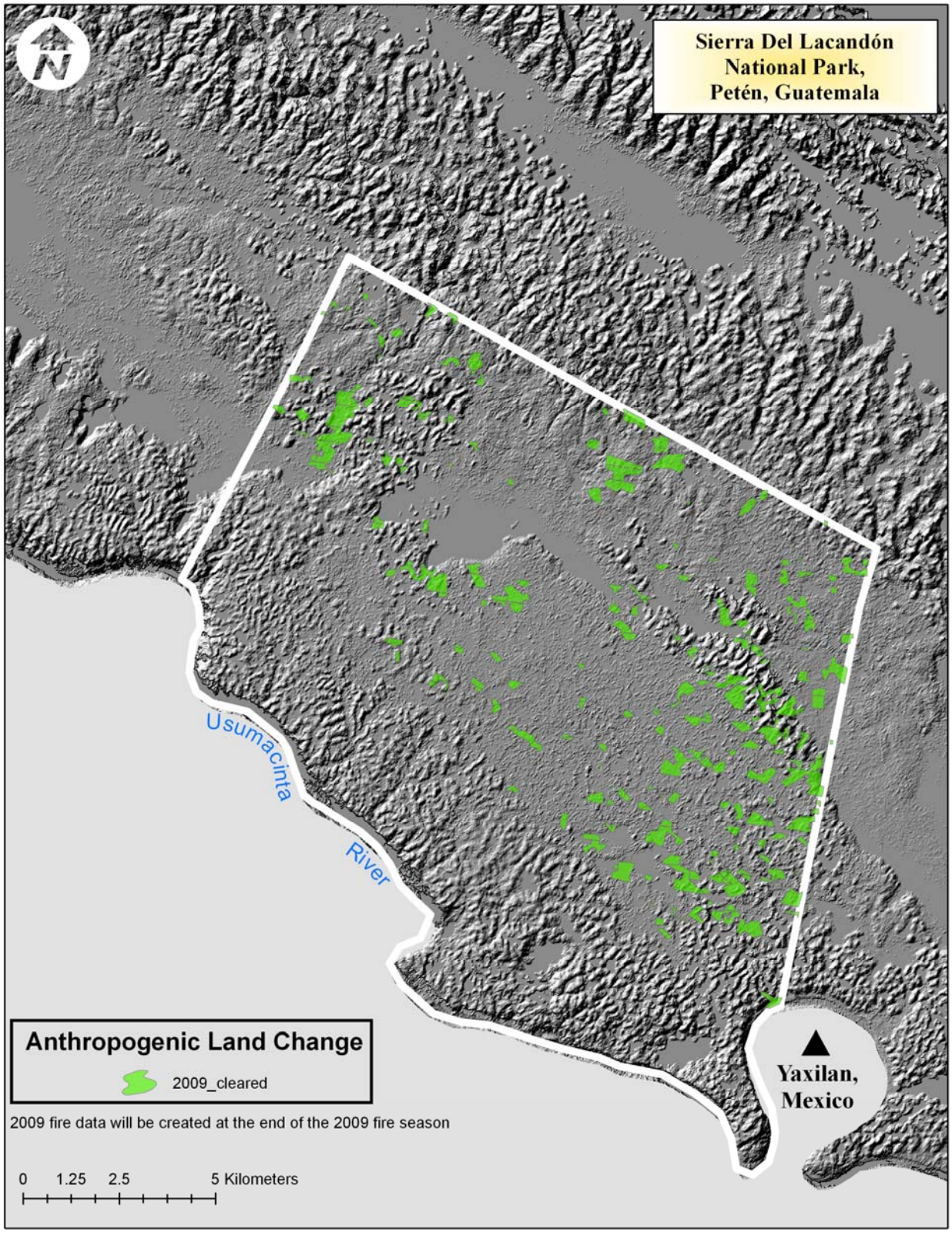

8d

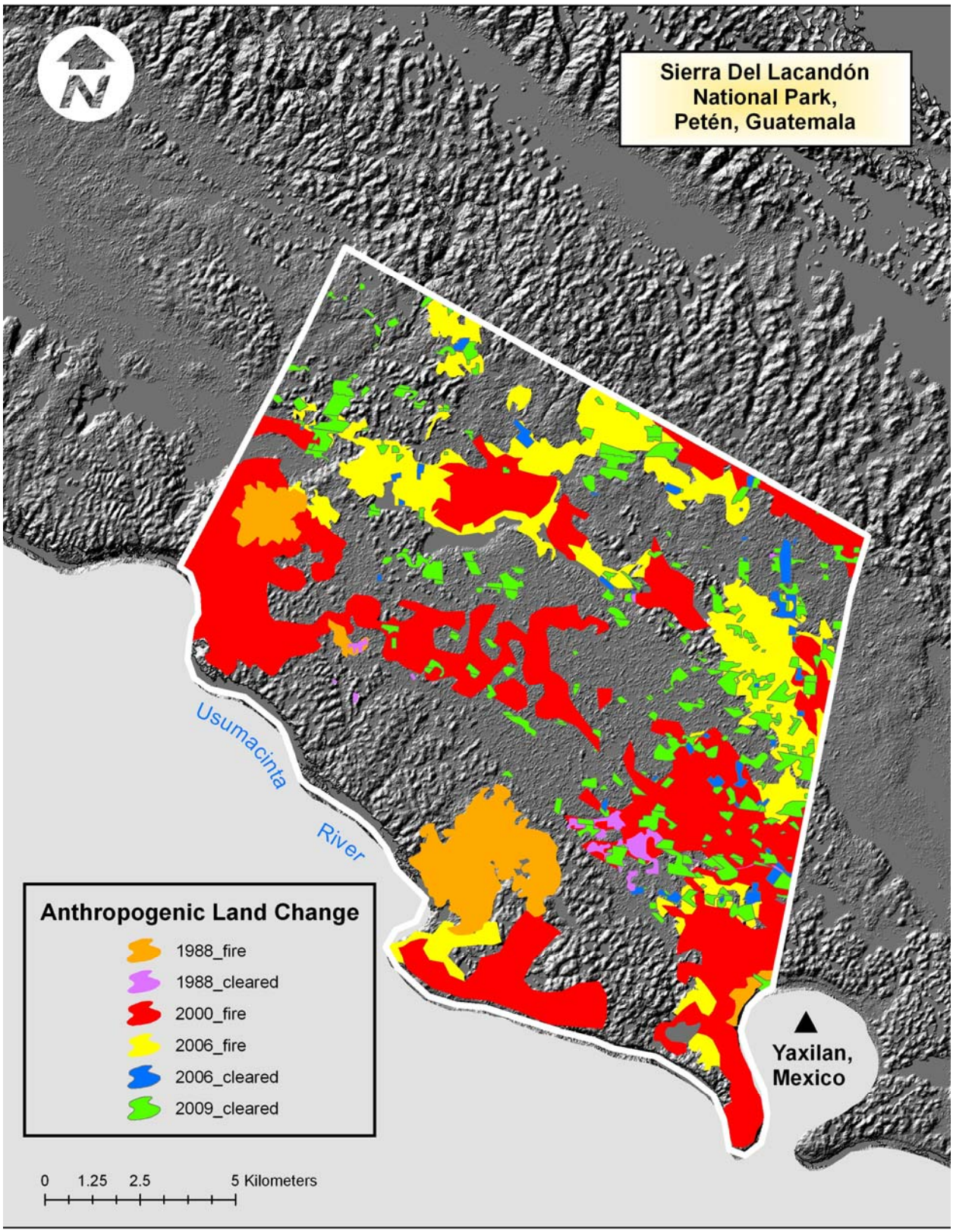

(Figure 8) Land-change maps generated using Landsat imagery draped over an AIRSAR generated digital elevation model. A=1988, B=2000, C=2006, D=2009, E= all years combined.

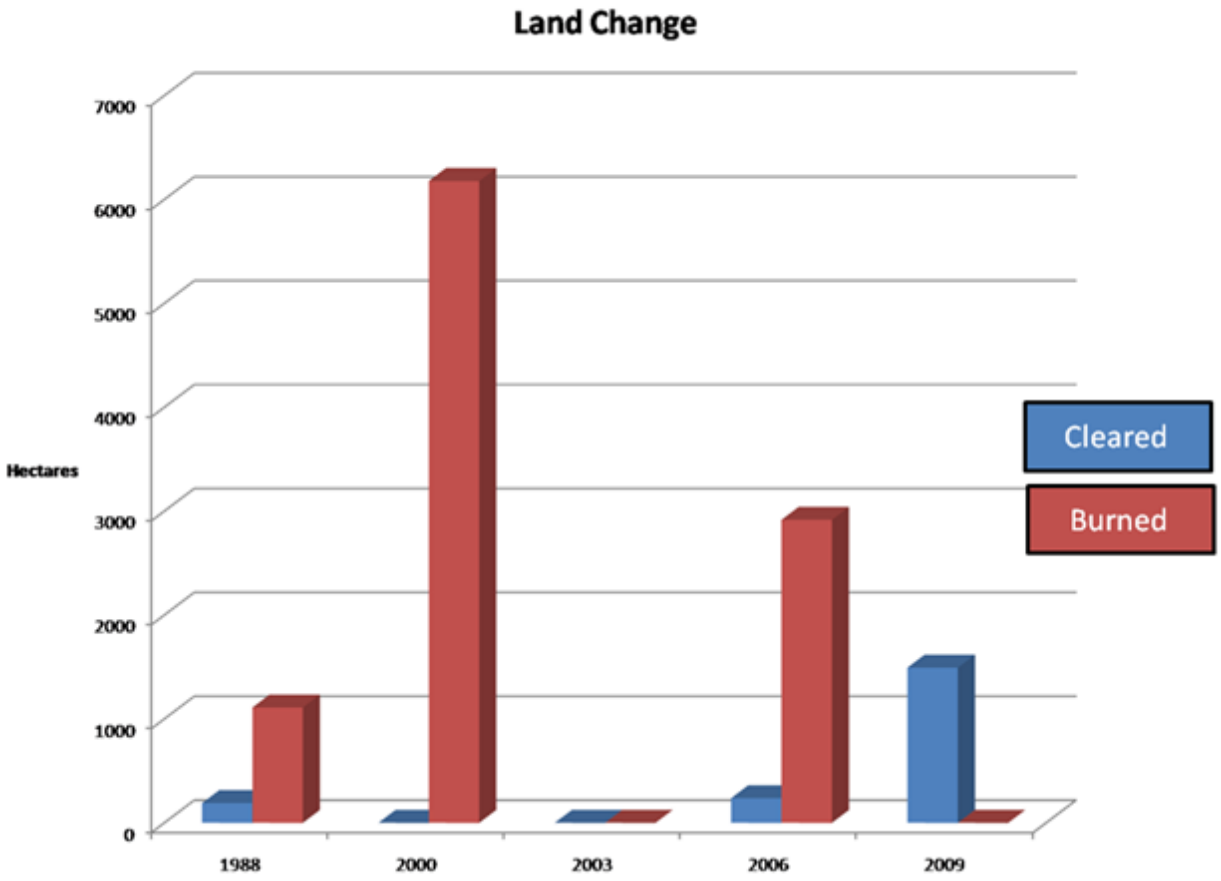

(Figure 9) Statistical summary in hectares of all years burned and cleared within the SLNP.

CHAPTER 2

MODELING THE ANCIENT MAIZE AGRICULTURE POTENTIAL OF LANDFORMS IN TIKAL NATIONAL PARK, GUATEMALA

Chris S. Balzotti, Richard E. Terry, Richard Burnett, Steven L. Petersen, Ryan Jensen

A manuscript to be submitted to Journal of Archaeological Science

MODELING THE ANCIENT MAIZE AGRICULTURE POTENTIAL OF LANDFORMS IN TIKAL NATIONAL PARK, GUATEMALA

ABSTRACT

The ancient polity of Tikal has been extensively studied by archaeologists and soil scientists, but little is known about the subsistence and ancient farming techniques that sustained its inhabitants The objective of this study was to create a predictive model for ancient maize *(Zea mays* L.) agriculture in the Tikal National Park, Petén, Guatemala, improving our understanding of settlement patterns and the ecological potentials surrounding the site in a cost effective manner. Ancient maize agriculture was described in this study by carbon (C) isotopic signatures of C_4 vegetation left in the soil humin fraction. Probability models predicting C isotopic enrichment and carbonate C were used to outline areas of potential long term maize agriculture. It was found that the Tikal area not only supports a great variety of potential food production systems but the models suggest multiple maize agricultural practices were used.

INTRODUCTION

The Maya people have occupied and utilized the Mesoamerican lowlands for millennia (Ford, Clarke and Raines 2009). The ancient Maya were not only able to produce food for survival; they were successful in construction of permanent political centers, implying that food was in sufficient excess to dedicate time and resources to such endeavors. Many of the early permanent settlements were located near lowland depressions in the karst topography (bajos) (Bullard 1960; Dunning et al. 2002). One such notable political center located in Petén, Guatemala surrounded by bajos is Tikal. Estimations of Tikal populations at its peak range from 30,000-35000 (Sanders 1973), 40,000-49,000 (Haviland 1969, 1972, 2003), 62,000 (Culbert et al. 1990), to as high as 69,705-76,699 (Dickson 1980) inhabitants. Even at the lowest estimations, the area would be required to supply copious amounts of food to sustain the people of Tikal. Although Tikal has been extensively studied, very little is known regarding one of the most basic cultural components, food production. Wilken (1971) emphasized the value of finding evidence of farming techniques stating that it would provide clues to the development and organization of the Maya civilization. Multiple hypotheses have been presented on the subject of food production. Some of the early botanists and archaeologists implied ancient Maya use of *Brosimum alicastrum* Sw. (commonly referred to as ramón). Puleston further proposed ramón as the main food source of the ancient Maya supplemented by maize (*Zea mays* L.) (Puleston 1968, 1971, 1976, 1982; Folan et al. 1979). This was later disputed by Lambert and Arnason (1982), Miksicek et al. (1981) and discussed by Peters (1983). Dickson (1980), using a linear model, suggested the Tikal populations used a mixed subsistence strategy that incorporated milpa, intensive farming, ramón cultivation and root cropping. Webster (1981), in support of a more conservative Tikal population and maize as the staple food source, disagreed with Dickson's

maize component of the model. He concluded that the "maize model" (maize as the primary food source) was still feasible and that Dickson underestimated the caloric value of maize. Dickson (1981) rebutted after running his model with Webster's suggested higher maize caloric values and concluded that populations at Tikal would have been even higher with the adjusted caloric values, and that the "maize model" of Maya subsistence "bends to the grave". Studies involving collagen stable carbon isotopes in skeletal remains at Tikal found that maize was a primary food source making up 50% or more of the dietary intake (Tykot 2002; Wright 2005). Despite disagreements on the extent of maize influence on the diets of the ancient Maya, it is generally accepted that the Maya consumed maize to some degree. However, none of the studies mentioned above proposed where maize may have been cultivated and thus, there is a need to locate ancient maize agricultural sites surrounding Tikal.

Ancient Maize Identification Using Stable Carbon Isotopes

Artifactual and structural evidence of ancient agriculture are often difficult to find in the Maya lowlands and have not been reported in the Tikal National Park (Nations and Nigh 1980; Nigh 2008). Stable C isotope studies have been adapted to delineate areas with histories of vegetation change from C_3 forest to C_4 maize agriculture and back to the contemporary C_3 forest. This method has been used extensively throughout the Maya lowlands (Beach et al. 2008; Fernandez et al. 2005; Johnson et al 2007; Johnson,Wright and Terry 2007; Sweetwood et al. 2009; Webb et al. 2004, 2007; Wright, Terry, and Eberl 2009).

The ancient maize agriculture predictive models presented herein were predicated on the results of stable C isotopes contained in the soil organic matter (SOM); therefore a brief explanation of the process of stable C isotope discrimination in plants and microbes is warranted.

Carbon 13 (^{13}C) is a stable isotope, one of two naturally occurring stable isotopes of carbon (Farquhar 1989). Carbon dioxide (CO_2) formed from ^{13}C ($^{13}CO_2$) is chemically identical to CO_2 formed from ^{12}C ($^{12}CO_2$) but is slightly heavier with a mass difference of 2.3% and is much less abundant in the atmosphere, making up roughly 1.1 atom percent (Evens and von Caemmerer 1996; Farquhar, O'Leary and Berry 1982; Farquhar, Ehleringer and Hubick 1989). Plants isotopically discriminate against the already scarce $^{13}CO_2$, making their composition of ^{13}C lower than that of the atmosphere (Farquhar O'Leary and Berry 1982). Plant isotopic discrimination of carbon ($\delta^{13}C$) per mil (‰) is defined here as the ratio of ^{13}C to ^{12}C compared to that of the standard, Pee Dee Belemnite (PDB) (Cerling et al. 1997):

$$(\% \, \delta^{13}C = [(^{13}C/\,^{12}C) \text{ sample}/ (^{13}C/\,^{12}C) \text{ PDB } -1] \text{ X } 1{,}000)$$

PDB is a carbonate of the mollusk *Belemnitella americana* from the Pee Dee formation of South Carolina, USA (Noordwijk et al. 1997). It is important to note that although plants have a positive discrimination against the heavier $^{13}CO_2$, the $\delta^{13}C$ values are negative, because they are a comparison to the PDB standard (Farquhar Ehleringer and Hubick 1989). All plants do not discriminate against $^{13}CO_2$ to the same degree. Plants that utilize the Hatch-Slack pathway (C_4) for carbon reduction, discriminate less than those that use the Calvin Cycle (C_3) (Cerling 1997; Farquhar, O'Leary and Berry 1982; Smith and Epstein 1971). Plants discriminate against atmospheric $^{13}CO_2$ in multiple ways. First, in order to be taken up by the plant, CO_2 must diffuse to the site of carboxylation (the initial C incorporation using a carboxyl group). The heavier $^{13}CO_2$ is slower to diffuse through the stomata openings, lowering the overall concentration of $^{13}CO_2$ within the plant (Evans and von Caemmerer 1996). Secondly, and more substantial is the biochemical discrimination that occurs during the interaction with the catalyst for carboxylation. C_3 plants use ribulose-1, 5-bisphosphate carboxylase oxygenase (rubisco) as a catalyst. Rubisco

has a higher discrimination against the $^{13}CO_2$ than that of the C_4 pathway catalyst, phosphoenolpyruvate carboxylase (PEP carboxylase). Therefore, C_3 plants have an overall $\delta^{13}C$ of -20 to -30‰ with an average of -27‰ compared to that of the C_4 plants with $\delta^{13}C$ values of -10 to -14‰ averaging -12‰ (Bender 1968; Cerling et al. 1997; Ehleringer 1991; Liu, Clapp and Cheng 1997).

$\delta^{13}C$ Signature From the Plant to the Soil

Once ^{13}C is incorporated into the plant, it can then be deposited into the soil as SOM by means of above ground decomposition (Rochette et al. 1999), below ground biomass (Amos and Walters 2006), and rhizodeposition (described below) (Amos and Walters 2006; Kuzyakov and Domanski 2000). The primary source of soil organic C (SOC) is deposition by plants and their residues (Balesdent Wagner and Mariotti 1988; Kuzyakov and Domanski 2000). Plants export roughly 50% of the total C fixed by photosynthesis below ground (Nguyen 2003). Rochette et al. (1999) in Quebec found that maize residue decomposition from above ground biomass contributed to the SOC and increased the overall soil $\delta^{13}C$ by 2 to 7% in a 2 year period, compared to that of bare ground control plots. Bolinder et al. (1999) gives estimates for C incorporated from maize above ground and below ground biomass to the SOC at 7.7 to 20% and 16 to 30%, respectively. Amos and Walters (2006) conducted a literature review on maize below ground biomass and net rhizodeposition of C into the SOC. After reviewing 45 studies spanning the entire life cycle of maize from both the greenhouse and the field, they found that the typical physiologically mature maize plant has a root to shoot ratio of 0.16 with an average root biomass of 13.6g C plant^{-1} with a net root derived below ground C contribution of 29 ± 13% of the shoot biomass. Plant rhizodeposition is the process of organic compounds being released by the root into the environment (Nguyen 2003). Rhizodeposition continually contributes C into the SOC

accounting for 5-21% of all photosynthetically fixed carbon released into the soil (Marschner 1995). Rhizodepositions can be grouped into four major mechanisms of input: 1) lysates (substances released from the cells, such as dead or dying cells), 2) exudates (passive compounds such as low molecular weight compounds that chemically diffuse from cells), 3) secretions (actively released compounds such as enzymes) and 4) gaseous compounds (CO_2, ethane, terpene etc.) (Marschner 1995; Wichern 2007). Border cells function as both lysates and exudates, living a short period of time producing mucilage, independent of the root after being sloughed off the growing root cap. It was found that maize seedlings can have thousands of border cells at any given time with an estimated pulse of 0.1 grams of C into the rhizosphere when the seedlings grow from unsaturated to saturated soil strata conditions (Iijma et al. 2004). Border cells of maize vary, depending on growth conditions and soil medium and can contribute 5-10% of total carbon from the plant deposited into the soil (IIjma Griffiths and Bengough 2000). Carbon secretions and exudates can reach the soil in the form of sugars, organic acids, enzymes and other more complex molecules that sustain and repel the micro flora of the rhizosphere (Jaeger et al. 1999). All these and many other mechanisms move C (^{12}C and ^{13}C) from the plant to the soil, thus depositing the isotopic signature of the dominant vegetation of the region into the SOM.

Once in the soils, the isotopic signature is preserved with minimal change to overall $\delta^{13}C$ values, in most cases less than 2.5‰ (Agren, Bosatta, and Balesdent 1996, Baldesdent and Mariotti 1987, Boutton 1996, Cerling et al. 1997). The amount of time it takes to "create" an isotopic signature in the soil is not fully understood. However, soil composition and environment influence the amount of time needed for an isotopic signature to change. For example, Vittorello et al. (1989) found that twelve years after a forest (C_3 plants) was converted to sugar cane (C_4),

90% of the carbon in the clay fraction still had the forest signature, demonstrating the ability of the clay to "protect" the isotopic signature. It also demonstrates that in the system, twelve years of continual cultivation was not sufficient to replace forest C_3 signature.

Interpretation of Stable C isotope signatures

The SOM $\delta^{13}C$ values can be used to distinguish the type of plant pathway that contributed to the C in the soil (Liu, Clapp and Cheng 1997). This identifiable isotopic discrimination variation is important because maize utilizes the C_4 pathway while the dominant vegetation of the semi dry neotropical forests of the Tikal region use the C_3 pathway. This distinction makes it possible to identify potential ancient maize agricultural sites. Furthermore, of all known plant species, it is estimated that only roughly 1% utilize the C_4 pathway (Edwards and Walker 1983) making a false positive less likely. The soils laboratory at Brigham Young University has tested plant tissue of many of the modern forest species including grasses local to the Tikal region and as of yet, have not found any evidence of C_4 plants in the dominant modern vegetation (Johnson et al. 2007, Wright et al. 2009, Webb et al. 2007, Burnett et al. 2010). Therefore, by means of isotopic signatures from the plant organic matter left in the soils, SOM distinctions can be inferred as to what vegetation was present throughout the soil profile.

Additional lines of evidence for the shift from C_3 forest to mixed C_3/C_4 vegetation associated with Maya agriculture have been reported. Beach et al., (2008a) recently reviewed the literature on the ancient environment, climate, vegetative history, and periods of soil erosion and deposition in the Maya Lowlands. The changes in vegetative history associated with forest clearance and the advances and declines in ancient maize agriculture that correspond to population dynamics are well documented. Sedimentation studies of lakes in the Petén region of

Guatemala (Deevey et al., 1979; Rice, 1996; Rosenmeier et al., 2002; Brenner et al., 2003; Wahl et al., 2006), including lake Las Pozas about 5 km south of Aguateca (Johnston et al., 2001) and lake Tamarindito, approximately 5 km to the north (Dunning et al., 1998) revealed early to middle Holocene, organic-rich sediments with pollen from high forest taxa and low quantities of charcoal. Forest pollen declined and the first maize pollen appeared about 4600 cal yr BP (2600 BC). Charcoal, phosphorus and pollen of economic species are contained within a significant deposition layer of silicate clays that began to accumulate in the preclassic period about 3000 cal yr BP and continued through the classic (1000 cal yr BP).

Non-Parametric Multiplicative Regression

Non-parametric multiplicative regression (NPMR) is a method for statistical analysis that utilizes a local multiplicative smoothing function that applies a leave-one-out cross-validation to estimate a particular response variable (Berryman and McCune 2006). NPMR was used to create statistical models despite its main disadvantage of being a computationally intense multiplicative kernel smoother trial and error method for fit. Additionally, it lacks an equation in the results of the analysis for interpretation relating the response variables to the predictor variables (McCune 2006). However, NPMR offers a solution to representing species response surfaces within a multidimensional niche space, allowing predictors to covary in an intricate manner using multiplicative kernel smoothers, without the need to define the overall response form of the ecological sample space (McCune 2006). Multiplicative regression was chosen in order to better fit the complex interaction of the environmental variables that make up, in part, the ecological niche (as defined by Hutchinson 1957) associated with maize agriculture. The automatic multiplicative combination of the predictors can be used to account for interactions of unacceptable maize conditions that may not be accounted for using additive modeling techniques

(McCune & Mefford 2004; McCune 2006; Grundel & Pavlovic 2007). NPMR uses local model and a kernel function to create a final model form. The local model is used to select the shape of the function that will be used to fit a value in the space defined by the independent variables, for example: local mean, local linear regression or local logistic regression. The kernel (weighting function) is used to specify how the weight around each target point varies based on ecological distance, for example: uniform within a window or Gaussian. Multiplicative kernel smoothing allows all the predictors to interact (McCune 2009). The objective of this chapter is to combine NPMR, stable carbon isotopes, soil properties, and remote sensing data for predictive modeling of ancient maize agricultural areas surrounding Tikal.

MATERIALS AND METHODS

Sample Strategies

The NPMR model study of the Tikal National Park was broken up into two sample areas: northwest (Bajos el Grande, Antonio and Tikal transects West and North) and the southeast (satellite settlements of Ramonal and Chalpate). Ramonal/Chalpate (hereafter referred to as Ramonal) samples were collected using a centric systematic area-sample method (CSS) that had been stratified by archaeologist Timothy Murtha using remotely sensed data layers (Webster 2007, Burnett 2010, Burnett et al. nd a, nd b) (Figure 1). Further sample points were obtained throughout Tikal using spatial toposequence intervals along archeological transects and near structures (Burnett 2010). Systematic sampling was used over the preferred random sampling due to the length of the field season, the problematic nature of obtaining reliable GPS points under the closed canopy, and navigational difficulty due to dense local vegetation. The CSS method allowed for representation of the entire Ramonal area in a gridded fashion. It is assumed

that there is not periodic variation in the collected data allowing the data to be analyzed as random (Milne 1959). Milne (1959) using 50 enumerated (means and variances known) biological populations, found that there was no error introduced from CSS sampling if the data did not have periodic variation, allowing the data to be analyzed as random (Krebs 1999).

***In situ* soil collection and laboratory analysis (Table 1)**

Soil profiles were collected from bucket auger cores, as well as from archaeological test pits throughout the study area. Leaf litter was removed from the soil surface and profile samples were acquired in 15cm increments. The collected samples were sealed in plastic bags until analysis was conducted at the Soils Laboratory, Brigham Young University. Upon arrival at the laboratory, samples were air dried, crushed and sieved to pass a 2mm (10mesh) sieve. The pH was assessed on the A and buried A horizons using a glass electrode with a 1:2 soil water mixture. Phosphorus (P) and potassium (K) levels of all A horizons were based on extraction using the Olsen sodium bicarbonate method (Olsen et al. 1954; Wantanbe and Olsen 1965). Carbonate C content (%) of each horizon was determined by titration as outlined by the United States Salinity Laboratory Staff (1954). Total Carbon and Nitrogen were calculated with an elemental analyzer using dry combustion (Costech EA, Valencia, CA).

Five gram sub-samples were further ground to pass a 250 um (60 mesh) sieve prior to removal of carbonates and humic and fulvic acid fractions as outlined by Webb et al. (2004, 2007, 2010) and Wright et al. (2009). Stable C isotope ratios of the remaining humin fraction were determined using a Thermo Finnigan isotope ratio mass spectrometer (Waltham, MA) coupled with a Costech elemental analyzer (EAIRMS). In order to compare multiple soil profiles, the largest shift in $\delta^{13}C$ between the surface horizon and subsurface horizons within

each profile was reported as the $\delta^{13}C$ enrichment ($\delta^{13}C_{enrichment} = \delta^{13}C_{depth} - \delta^{13}C_{surface}$). Enrichment as defined herein is consistent with $\Delta^{13}C$, reported by Martinelli et al. (1996). However, the Δ symbol is often used in reference to the positive plant discrimination rather than the comparison with the PDB standard (Farquhar, Ehleringer and Hubick 1989). To avoid confusion, it will simply be referred to as $\delta^{13}C$ enrichment. A more in depth review of the soil analysis methods and listings of the data can be found in Burnett (2010) and in Burnett et al. (nd a; nd b).

Remote Sensing and GIS Layers (Table 2)

Remotely sensed (RS) and GIS data correction, extraction, and interpretation were conducted in the Geospatial Habitat Analysis Laboratory, Brigham Young University. All RS and GIS data were projected into WGS 1984 UTM zone 16N before any corrections or combinations were performed. Landsat 7 Enhanced Thematic Mapper Plus (Landsat7) imagery was acquired at no cost from the U.S Geological Survey (USGS) (http://www.usgs.gov/). Dry season (February-May) imagery was used in order to observe the greatest disparity of plant stress as well as to obtain imagery with the lowest percent cloud cover. Landsat7 bands 10-70 (1-7) reflectance values were included in the model and have spatial resolutions of roughly 30m for bands 1-5 and 7, 60m resolution for band 61, and 120m for band 62 (Table 3) (Jensen 2005; JPL 2009; Mladinich 2006). Although Landsat7 imagery was georeferenced and some basic preprocessing had been done by the USGS, further preprocessing was conducted to enhance model performance. To reduce effects of atmospheric distortion, dark object subtraction was implemented using the ©Envi software general utilities (dark subtract tool). To fill in any missing data as well as ensure compatibility of the bands with model output cell size, all bands were resampled to 5m using the nearest neighbor method with ©ESRI ArcMap 9.3 (ArcMap) software

(this resampling does not improve the resolution). After preprocessing was completed, reflectance values were extracted from each band using the ArcMap extraction tool. Relative elevation data was extracted from a 5m resolution Airborne Synthetic Aperture Radar (AIRSAR) derived digital elevation model (DEM). AIRSAR was flown over the study area in March of 2004 by the Jet Propulsion Laboratory (JPL 2009). The DEM was created using the C-band (0.057 meter wavelength) and was obtained from the Alaska Satellite Facility at no cost. Preprocessing of the DEM was conducted using ArcMap and included the filling of missing data and removal of small imperfections using the hydrology tool (fill).The AIRSAR DEM was also used along with the ArcMap extension Benthic Terrain Modeler (BTM) created by NOAA Costal Service Center to create a Topographic Position Index (TPI), as well as a rugosity index (Wright 2005). Rugosity indices and TPIs were generated to separate out valley bottoms such as bajos and flat landforms on hill tops from mid elevation slopes, reducing the influence of the elevation data on the model. The Iverson et al. (1997) Integrated Moisture Index model (IMI) was created using ArcMap to asses topographically influenced moisture availability using the DEM derived layers hillshade, flow accumulation and curvature. The hillshade and the curvature layers were created with the surface analysis tools (hillshade and curvature). The flow accumulation was derived with the hydrology tools (flow direction and flow accumulation). The curvature layer values were inverted and the all layers were normalized and reclassified on a scale of 0-100. The reclassified layers were than combined in a weighted fashion to create an IMI: (IMI= (hillshade x 0.5) + (curvature x 0.15) + (flow accumulation x 0.35) with a 0-100 scale, zero indicating no moisture retention 100 representing the maximum moisture retention (Davis 2009). The AIRSAR DEM was further used to create stand alone layers for slope, aspect, curvature and curvature direction of slope. Slope is a calculation of maximum rate of change in

elevation between the cell and its eight neighbors. Aspect is the direction of the slope. Curvature how the slope flows was used to identify the physical characteristics defining drainage basins often used to understand erosion and runoff processes. Curvature direction of slope is the direction of the maximum slope.

AIRSAR stand alone layers in the model were from the p-band (0.68 m) and included the hh, hhvv and hv polarization combinations (see Table 2). IKONOS imagery was obtained from the Earthworks at Tikal Project. The IKONOS-2 satellite imagery was obtained during the dry season in March of 2001. The bands used were red, green, blue and near-infrared. The resolution was 1m. All IKONOS bands were resized using nearest neighbor to 5 m in ArcMap. Due to the extent of the IKONOS coverage available, it was only used on models specific to the Ramonal area. However, none of the bands were found to be statistically relevant in the models.

Model Analysis

All NPMR modeling was done with ©HyperNiche version 1.12 software (McCune and Mefford 2004). Hyperniche was used because it has built in controls for over-fitting the data. Over-fitting is controlled simultaneously by using cross validation when fitting the model, minimum average neighborhood size for analysis, and parsimony control using previously listed controls along with adjustable improvement criterion and data predictor ratio (McCune 2009). All NPMR models used a local mean model with a Gausian Kernel for the overall model form. Each model created used a single response variable (enrichment or Carbonate C) and multiple predictor variables generated by RS, GIS, and lab data (elevation, reflectance, ph, etc.). Responses varied between quantitative data on a gradient and presence absence data represented as binomial. The models were created using a free search for the best fit model in a stepwise

fashion. Stepwise works by starting with a one variable model, then adding additional variables based on improvement criteria. The newly created models were assessed in a forward and backward manner allowing reassessment of all variables already in the model each time a new variable was added or taken out. The result of the free search was the model with the best subset of predictor variables defined by either a log β (binomial) or an xR^2 (quantitative) value (defined below). For each best fit model, a GIS raster grid representation was created for visual as well as statistical analysis using HyperNiche and ArcMap software packages.

Binomial

Two model types were run using binomial data sets, both of which used enrichment as the response variable and all the GIS/RS layers as predictor variables. One included only the samples collected in the southeast part of the study area (Ramonal Binomial RS (13C Enrich.). The other included all samples (Tikal Total Binomial RS (13C Enrich.). On all models that were based on presence and absence (enrichment value > 2.5), log base 10 of Bayes factor (log β) was used to assess the outcome of the model. The log β uses the Bayseian approach to hypothesis testing developed by Jeffreys (1935,1961). Kass and Reftery (1995) define the Bayes factor as "…a summary of evidence provided by the data in favor of one scientific theory, represented by a statistical model, as opposed to another." The log β here differs from the true Bayes factor in that the model is not an assessment of improvement from model 1 to the previous model 2; it is an assessment of each model over a naïve model. The naïve model in this case is the probability of encountering maize in the study area based on average frequency of maize presence within the *in situ* data (McCune 2006). The scale for log β interpretation that was incorporated in this study was suggested by Jefferys (1961) and outlined as follows by Kass and Reftery (1995):

0 to 0.5 = “not worth more than a bare mention”

0.5 to 1.0 = “Substantial”

1 to 2.0 = “strong”

Greater than 2 = “Decisive”

Once the best fit model for the provided predictor variables was found, a Monte Carlo Test was run. The test was done to evaluate if the variables selected by the NPMR method were a better fit than that of a random selection including the same number of predictor variables from the total available predictors. After the Monte Carlo test, individual predictor variables within the selected model were further assessed as to the relative influence on the model or “importance”. This influence was accomplished using a sensitivity test:

Sensitivity = (mean difference in response/ range in response)/(difference in predictor/ range in predictor)

Sensitivity was used because there were no fixed coefficients or slopes to compare to when using non-parametric regression (McCune 2006). The predictor variables’ values were nudged one at a time by plus or minus five percent. The difference seen in the response variables (mean absolute difference) was used to interpret the effect of the nudge (McCune 2004). The more influence a variable has, the more the nudge affects the overall model outcome. Further assessment was conducted using 2 and 3D response curves created to visualize the correlations of the predictor variables and the response variable, soil enrichment. The overall accuracy of each model was based on the comparison to the naïve model.

Quantitative Response

Four enrichment models: (Ramonal Lab Only (^{13}C Enrich.), Ramonal RS Only (^{13}C Enrich.), Ramonal RS and Lab (^{13}C Enrich.), Tikal Total RS (^{13}C Enrich.) and four carbonate C models: (Ramonal Lab Only ($CO_3^{=}$-C), Ramonal RS Only ($CO_3^{=}$-C), Ramonal RS and lab ($CO_3^{=}$-C), and Tikal Total RS ($CO_3^{=}$-C), were run in a quantitative manner. The enrichment data were run both quantitatively and binomially. However, the carbonate C model was only run quantitatively. Models were evaluated using a cross R^2 value (xR^2), defined as the size of the residual sum of squares in relationship to the total sum of squares (Antoine and McCune 2004). xR^2 produces a more conservative estimate from that of the traditional R^2 because xR^2 excludes each data point from the basis for the estimate of the response at that given point. With this method, weak models can have residual sum of squares that can exceed the total sum of squares, producing an overall negative xR^2 (poor fit) to an xR^2 of 1 (perfect fit). Coefficients in a fixed equation are not used in NPMR; the standard deviations from the Gaussuan smoothers (tolerances) are used instead (Berryman and McCune 2006, McCune 2009).

RESULTS AND DISCUSSION

^{13}C Enrichment Binomial RS Model

The best fit model for ^{13}C enrichment within soil profiles using the Tikal Total Binomial RS (^{13}C Enrich.) data had a log β value of 7.18 (Table 4) (Figure 5) and is considered a decisive model (see scale above). The results from the Monte Carlo test produced no randomly created models that were equal to or better than the best fit with a p-value of < 0.05. Of the 20 predictor variables, 5 were considered statistically relevant in the best fit model. The sensitivity test was used to create the final predictor variable order based on relative influence after more than 300 nudges. The predictor variable order is as follows (sensitivity values and tolerances listed in

parenthesis respectively): elevation (1.26, 3.58), curvature direction of slope (0.300, 2.79), Landsat band 50 (0.25, 3.8), Landsat band 40 (0.10, 5.25) and aspect (0.05, 249.77). The model's overall accuracy was an improvement of 72.7% over the naïve model.

The best fit model for C isotope enrichment using the Ramonal Binomial RS (^{13}C Enrich.) data had a log β of 4.36 and is also considered decisive. However, with less data points (due to the smaller sampling area) used in the model, the outcome not only differed in the log β value from that of the model listed above but it also differed in predictor variable relevance despite the fact that the same predictor variables were used. The Monte Carlo test revealed no randomly generated models equal to or better than the best fit model with a p value < 0.05. Only 3 of the 20 variables were considered statistically relevant: elevation (0.89, 4.23), slope (0.60, 2.41), and curvature direction of slope (0.26, 2.72). The models overall accuracy was an improvement of 73.3% over the naïve model.

Quantitative Models of δ^{13}C Enrichment

The best fit model for δ^{13}C enrichment within soil profiles using only soils laboratory data (Ramonal Lab Only (^{13}C Enrich.)) (Table 4) (Figure 3) was restricted to the southeast sample area (98 profiles at Ramonal) and had an xR^2 of 0.583 with four of seven predictor variables statistically relevant. A Monte Carlo test was unable to determine any randomly generated models equal to or better than the best fit model with a p value < 0.05. Sensitivity analysis revealed the following order of the laboratory data predictor variables: phosphorus content (0.76, 0.67), profile depth (0.39, 16.35), carbonate C (0.07, 4.67), and pH (0.03, 1.14). Although this model is fairly strong statistically, it is only slightly more cost effective than field collected data, eliminating only the final steps of the laboratory procedure, to obtain actual δ^{13}C

values. All samples still must be collected in the field. In contrast, the model for the Ramonal area using only RS derived data (Ramonal RS Only (^{13}C Enrich.)) (Figure 4) had a statistically weaker xR^2 of 0.215 and a Monte Carlo test that found of the 100 runs, 20 produced randomly generated models equal to or better than the best fit model. However, all the predictor variables were obtained or generated from RS platforms. The total number of relevant predictor variables for the RS model was 6 of 25: elevation (1.16, 2.59), curvature direction of slope (0.28, 2.59), AIRSAR P band vv (0.15, .03), aspect (0.04, 226.61), Landsat band 4 (0.02, 8.25), and TPI fine scale (0.01, 358.5). The best fit for the isotopic enrichment data using both lab and RS predictors (Ramonal RS and Lab (13C Enrich.)) had an xR^2 of 0.592, improving slightly the model over the laboratory only model. There were 6 of 32 predictor variables that were statistically relevant in the Ramonal lab data model: phosphorus (0.72, 0.67), profile depth (0.43, 17.44), carbonate C (0.06, 4.96), AIRSAR p band hhvv (0.03, 187.04), pH (0.03, 1.44), and rugged index (0.02, 0.05). The laboratory data predictors far outweigh the RS predictor variables in statistical significance.

The final quantitative model for isotopic enrichment included all 169 profiles covering both the southeast and northwest profiles (Tikal Total RS (13C Enrich.). This model only used RS predictor variables. The xR^2 value was 0.305 with an improvement over Ramonal RS Only (^{13}C Enrich.) xR^2 by 0.09 with 5 relevant predictor variables: elevation (1.35, 2.86) Landsat band 50 (0.36, 2.47), TPI fine scale (0.13, 76.44), AIRSAR p band hv (0.04, 0.03), and curvature direction of slope (0.01, 13.19). A Monte Carlo test was unable to find any randomly generated models equal to or better than the best fit model with a p value < 0.05. Both the Ramonal RS Only (13C Enrich.) and the Tikal Total RS (13C Enrich.) models had elevation as the most significant variable. In addition, they both included TPI fine scale and curvature direction of

slope. However, they differed in that the Landsat band was included in the model as well as the AIRSAR band. In the Ramonal RS Only (13C Enrich.) model, the fifth predictor variable was Landsat band 40 (near-infrared) and the AIRSAR P band vv (vertical sent vertical received) was the third. In the Tikal Total RS (13C Enrich.), the second variable was Landsat band 50 (Mid-infrared) and the AIRSAR band PHV (horizontal sent vertical received) was fourth. Both Landsat bands are sensitive to vegetation health and are present in the binomial model. More points need to be taken to elucidate better the most relevant Landsat and AIRSAR bands to the model.

Carbonate C

The best fit model for carbonate C content using only soils lab data (Ramonal lab only ($CO3^{=}$- C)) was restricted to the southeast sample area (98 profiles) and had an xR^2 of 0.76 with 4 predictor variables statistically relevant out of 6. A Monte Carlo test was unable to find any randomly generated models equal to or better than the best fit model with a p value < 0.05. Sensitivity analysis revealed the following order of the predictor variables: pH (1.50, 0.13). ppm phosphorus (0.34, 1.33), % organic C (0.15, 4.21), and % total nitrogen (N) (0.03, 0.71). As with the enrichment laboratory model (Ramonal Lab Only (^{13}C Enrich.)), although the predictions are strong they are restricted to only lab collected data and therefore, actual carbonate C values can be determined directly. The model for the same area using only RS derived data (Ramonal RS Only ($CO3^{=}$- C)) had a statistically weaker xR^2 of 0.387. However, all the predictor variables were obtained or generated from RS platforms and the model is an improvement over the enrichment RS model with a Monte Carlo test unable to find any randomly generated models equal to or better than the best fit model with a p value < 0.05. The total number of relevant predictor variables was 5 of 25: elevation (1.48, 2.59), Landsat band 1 (0.38, 1.80), curvature

direction of slope (0.30, 2.59), Landsat band 7 (0.04, 4.50), and TPI broad scale (0.03, 257.95). Similar to the enrichment models, combination of the lab and the RS layers led to little or no improvement. The Ramonal RS and lab ($CO3^{=}$- C) model with an xR^2 value of 0.747 did not improve over the Ramonal lab only ($CO3^{=}$- C) model. The total number of relevant predictor variables for the Ramonal RS and lab ($CO3^{=}$- C) model was 7 of 31: pH (1.36, 0.13), elevation (0.24, 10.37) curvature (0.08, 4.60), Iverson Moisture Index (0.29, 22.79) AIRSAR P band phh (0.25, 0.09), % organic C (0.22, 11.58) and curvature direction of slope (0.01, 8.41). A Monte Carlo test was unable to find any randomly generated models equal to or better than the best fit model with a p value < 0.05. Unlike the enrichment models, the Ramonal RS and lab ($CO3^{=}$- C) model predictor variables were not dominated by the laboratory variables and were made up of 5 RS variables and only 2 laboratory variables. The total study area model for % carbonate C had xR^2 of 0.335 and used only RS derived layers (Tikal Total RS ($CO3^{=}$- C). This model included the most predictor variables in the final model with 10 of the 20 used: elevation (1.20, 3.58) curvature direction of slope (.41, 2.79), Landsat band 4 (0.12, 4.50), Landsat band 61 (0.12, 1.25), Landsat band 2 (0.12, 3.00), aspect (0.11, 160.56), Landsat band 3(0.06, 4.20), AIRSAR P band phv (0.05, 0.03), slope (0.05, 15.21), and Landsat band 1 (0.05, 6.00). Of all the % carbonate C models Tikal Total RS ($CO3^{=}$- C) has the most potential in both predicting poor maize presence and possible human structure location.

Estimation of Long Term Maize Agricultural Potential by Scale

Using the AIRSAR data frame available, the maize potential can be classified and quantified for food production and sustainability studies. Due to the difficulty of defining the political boundaries of the Tikal sustaining area, maize agricultural potential was calculated for the available AIRSAR data frame and for concentric circles at 1 km-radius intervals out to 4 km,

centered on Temple 1 (Figure 8 and Table 5). Calculations only included the areas that were modeled by the Tikal Total Binomial RS (^{13}C Enrich.) model (Table 5). Within 1 and 2km radii, the model predicted less than 3% and 9%, respectively, of the area as medium to high potential for long term maize agriculture. Within 3 and 4km radii, the model predicted approximately 20% and 21%, respectively, of the area as medium to high potential for long term maize agriculture. For the total AIRSAR data frame (Figure 5), the model predicted less than 31% of the area as medium to high potential for long term maize agriculture. This means that the area of prime maize agriculture was located beyond 3 km of the site center. And much of this production was on flat, depressions and bajo edges. It is likely that other types of agriculture took place on the shallow backslopes and shaded areas beneath the forest canopy closer to the site center.

Conclusions

The use of RS layers will prove more valuable in predicting carbonate C which has an inverse relationship to potential maize locations. This also may be valuable in predicting architectural structures located beneath the canopy. The models presented here suggest that many areas were left forested or cleared for short periods of time. However, they also show areas with very high enrichment near the bajo edges and around some of the structures, suggesting long term maize agricultural practices existed where they could be sustained, such as house gardens and or highly favorable soil close to surface water.

An alternative hypothesis could be that deposition of eroded upland soils carried isotopic signatures of ancient C_4 vegetation to the bajo edges. Burnett et al. (2010) reported evidence of deposition of the "Maya clay" and of buried A horizons in some Tikal soil profiles. Beach et al. (2006; Beach 1998) reported a significant deposition layer of approximately 50 cm of "Maya

clay" across the bajos of the Petexbatun region of Guatemala and of northern Belize that resulted from preclassic and classic maya agriculture and soil erosion in the uplands. However, Johnson et al. (2007) examined profiles from both perennial and seasonal wetlands at the foot of the Aguateca escarpment in the Petexbatun region. Three soil profiles exhibited approximately 40-cm thick layers of "Maya clay" above buried A horizons. Carbon isotopic evidence of ancient C_4 plants including maize agriculture was only found in the seasonal wetland soil that was sufficiently drained in the dry season for maize production. Profiles affected by Maya clay in the perennial wetland did not exhibit evidence of ancient C_4 plant growth. The permanently flooded perennial wetland profiles would not have been conducive to maize growth. Johnson et al. (2007) suggested that the C isotope signatures of ancient C_4 vegetation was the product of in place C_4 plant growth and rhizodeposition and not the result of deposition of eroded soils.

Indirect evidence for maize agriculture at the site of Ramonal can be found in the presence of *Orbigyna cohune* (Mart), Dahlgren ex Standl (cohune palm) in the deep foot and toeslope soils. The presence of this palm is often used by local farmers as an indicator of well drained nutrient soil for maize agriculture. Indirect and direct food potential in the forests and large areas not showing medium to high C_4 $\delta^{13}C$ enrichment (C_3 forest and strong C_4 $\delta^{13}C$ signatures of maize are mutually exclusive) suggest that an assortment of food production methods were used ranging from silviculture to long and short term maize agriculture. The findings here support that the Tikal Maya created mosaics (Ford 2008) and utilized diverse methods of food production (Ford, Clarke, and Raines 2009; Whitmore and Turner 2001).

REFERENCES

Amos, B., and Walters, D.T. (2006) Maize Root Biomass and Net Rhizodeposited Carbon: An Analysis of the Literature. *Soil Sci. Soc. Am. J.* 70, pp. 1489-1503

Antoine, M. E., and McCune (2004) Contrasting fundamental and realized ecological niches with epiphytic lichen transplants in an old-growth *pseudotsuga* forest. *Bryologist* 107 pp. 163-173

Agren,G.I., Bosatta, E., and Balesdent, J. (1996) Isotope discrimination during decomposition of organic matter. A theoretical analysis. *Soil Sci. Soc. Am. J.* 60 pp.1121–1126.

Balesdent, J., Wagner, G. H., and Mariotti, A., (1988) Soil Organic Matter Turnover in Long-term Field experiments as Revealed by Carbon-13 Natural Abundance. *Soil Sci. Soc. Am. J.* 52, pp. 118-124

Beach, T, Luzzadder-Beach, S., Dunning, N., and Cook, D. (2008) Human and Natural impacts on fluvial and karst depressions of the Maya Lowlands. *Geomorphology* 101:308-331.

Bender, M. M. (1968) Mass spectrometric studies of carbon-13 variations in corn and other grasses. *Radiocarbon* 10, pp. 468-472.

Berryman, S. & B. McCune. (2006). Estimating epiphytic macrolichen biomass from topography, stand structure and lichen community data. *Journal of Vegetation Science.* 17, pp. 157-170

Bolinder, M.A., Angers, D.A., Giroux, M., and Laverdiere, M. R. (1999) Estimating C inputs retatined as soil organic matter from corn (*Zea Mays* L.). *Plant and Soil.* 215(1), pp. 85-91

Boutton, T.W.(1996) Stable carbon isotope ratios of soil organic matter and their use as indicators of vegetation and climate change. In: Boutton, T.W., Yamasaki, S,I (Eds.), Mass Spectrometry of Soils. Marcel Dekker, New York, pp. 47-82

Brenner, M., Hodell, D., Curtis, J.H., Rosenmeier, M., Anselmetti, F.,Ariztegui, D. (2003) Paleolimnological approaches for inferringpast climate in the Maya region: recent advances and methodological limitations. In: Go´mez-Pompa, A., Allen, M., Fedick, S.L. Jime´nez-Osornio, J.J. (Eds.), Lowland Maya Area: Three Millennia at the Human-Wildland Interface. Haworth Press, Binghamton, NY, pp. 45– 76.

Bullard, W. R., Jr. 1960. Maya settlement pattern in northeastern Petén, Guatemala. *American Antiquity* 25:355-372.

Burnett, R. L., Terry, R. E., Alvarez, M., Balzotti, C., Murtha, T., Webster, D., and Silverstein, J. (N.D.) The ancient agricultural landscape of the satellite settlement of ramonal near Tikal, Guatemala. *Quaternary International* In Review.

Burnett, R. L., Terry, R. E., Sweetwood, R. V., Murtha, T., Webster, D., and Silverstein, J. (N.D.) Upland and lowland soil resources of the ancient Maya at Tikal, Guatemala. *Soil Science Society of America Journal* In review.

Culbert, T. Patrick, Kosakowsky, L. J., Fry, R. E., and Haviland, W. A., (1990). The population of Tikal, Guatemala. In *Precolumbian Population History in the Maya Lowlands*, edited by T. P. Culbert and D. S. Rice. Albuquerque: University of New Mexico Press.

Cerling, T. E., Harris J.M., MacFadden, B.J., Leakey M.G., Quade, j., Eisenmann, V.E., and Ehleringer, J. R. (1997) Global vegetation change through the Milocene/Pliocene boundry. *Nature* 389, pp. 153-158

Deevey, E.S., Rice, D. S., Rice, P. M., Vaughan, H. H., Brenner, M., and Flannery M.S. (1979) Mayan Urbanism: Impact on a Tropical Karst Environment. *Science*. 206, pp. 298-306

Dickson, D. B. (1980). Ancient agriculture and population at Tikal, Guatemala: An application of linear programming to the simulation of an archaeological problem. *American Antiquity* 45 (4), pp. 697-712.

Dickson, D. B. (1981). Further Simulation of Ancient agriculture and population at Tikal, Guatemala. *American Antiquity.* 46 (4), pp.922-926.

Dunning, N. P., Luzzadder-Beach, S., Beach, T., Jones, J. G., Scarborough, V., and Culbert, T. P., (2002) Arising from the bajos: The evolution of a neotropical landscape and the rise of Maya civilization. *Annals of the Association of American Geographers* 92 (2):267-283.

Dunning, N.P., Rue, D.J., Beach, T., Covich, A., and Traverse, A. (1998) Human-Environmental Interactions in a Tropical Watershed: The Paleoecology of Laguna Tamarindito, El Peten, Guatemala. *Journal of Field Archaeology* 25, pp.139-151

Edwards, G. E., and Walker, D. (1983) *C_3, C_4: Mechanisms and Cellular and Environmental Regulations of Photosynthesis*. University of California Press, Berkeley

Ehleringer, J. R. (1991) 13C/12C fractionation and its utility in terrestrial plant studies. *In Carbon Isotope Techniques*, edited by D. C. Coleman and B. Fry. San Diego: Academic Press Inc.

Evans, J. R. and von Caemmerer S. (1996) Carbon Dioxide Diffusion inside Leaves. *Plant Physiol.* 110, pp. 339-346

Farquhar, G. D., Hubick, K. T., Condon, A. G., Richards, R. A. (1989) Carbon isotope fractionation and plant water-use efficiency. In PW Rundel, JREhleringer, KA Nagy, eds, Stable Isotopes in Ecological Research. Springer-Verlag, New York, pp 21–40

Farquhar, G. D., Ehleringer, J. R., and Hubick, K. T. (1989) Carbon Isotope Discrimination and Photosynthesis. *Annu. Rev. Plant. Physiol. Mol.* 40 pp. 503-537

Farquhar, G. D., O'Leary, M. H., and Berry, J. A. (1982) On the Relationship between Carbon Isotope Discrimination and the Intercellular Carbon Dioxide Concentration in Leaves. *Aust. J. Plant Physiol* 9, pp. 121-137

Fernandez, Fabián G., Kristofer D. Johnson, Richard E. Terry, Sheldon Nelson, and David Webster. (2005) Soil Resources of the Ancient Maya at Piedras Negras, Guatemala. *Soil Science Society of America Journal* 69:2020-2032.

Folan, W. J., Fletcher, L.A., and Kintz, E. R. (1979) Fruit, Fiber, Bark and Resin: Social Organization of a Maya Urban Center. *Science* 204, pp. 697-701

Ford, A., (2008) Dominant Plants of the Maya Forests and Gardens of El Pilar: Implications for Paleoenvironmental Reconstruction. *Journal of Ethnobiology*. 28(2), pp. 179-199

Ford, A., Clarke, K. C., Raines, G. (2009) Modeling Settlement Patterns of the Late Classic Maya Civilization with Bayesian Methods and Geographic Information Systems. *Annals of the Association of American Geographers*. 99(3), pp. 496-520

Grundel, R., and Pavlovic N.B. (2007) Response of bird species densities to habitat structure and fire history along midwestern open-forest gradient. *The Condor* 109, pp. 734-749

Haviland, W. A. (1969). A New Population Estimate for Tikal, Guatemala. *American Antiquity*. 34 (4), pp. 429-433

Haviland, W. A. (1972). Family size, prehistoric population estimates, and the ancient Maya. *American Antiquity*. 37, pp. 135-139

Haviland, W. A. (2003). Settlement, society, and demography at Tikal. In *Tikal: Dynasties, foreigners, & affairs of state*, edited by J. A. Sabloff: School of American Research Press.

Hutchinson, G. E. (1957) Concluding remarks. *Cold Springs Harbor Symposia on Quantitative Biology*. 22(2), pp. 415-427

Iijima, M., Griffiths, B., and Bengough G. (2000) Sloughing of cap cells and carbon exudation from maize seedling in roots in compacted sand. *New Phytol*. 145, pp. 477-482

Iverson, L.R., Dale, M.E., Scott, C.T., and Prasad, A. (1997). A GIS-derived integrated moisture index to predict forest composition and productivity of Ohio forests (USA). *Landscape Ecology*. 12, pp. 331-348.

Jaeger, C.H., Lindow, S.E., Miller, W., Clark, E., & Firestone, M.K. (1999) Mapping of sugar and amino acid availability in soil around roots with bacterial sensors of sucrose and tryptophan. *Appl Environ Microbiol.* 65, pp 2685–2690.

Jeffreys, H. (1961) Theory of Probability (3rd ed.), Oxford, U.K.: Oxford University Press.

Jensen, J.R. (2005) *Introductory Digital Image Processing*: *A remote Sensing Perspective.* 3rd ed. New Jersey: Prentice Hall.

Jet propulsion Laboratory (JPL) (2009) Missions: Earth. [Online] retrieved 15 August 2009 from: http://www.jpl.nasa.gov/missions/index.cfm?type=&destination=Earth.

Johnson, Kristofer D., Richard E. Terry, Mark W. Jackson, and Charles Golden. (2007) Ancient soil resources of the Usumacinta River Region, Guatemala. *Journal of Archaeological Science* 34:1117-1129.

Johnson, Kristofer D., David R. Wright, and Richard E. Terry. 2007. Application of carbon isotope analysis to ancient maize agriculture in the Petexbatún region of Guatemala. *Geoarchaeology: An International Journal* 22:313-336.

Kass R. E., and Raftery A.E. (1995) Bayes Factors. *Journal of the American Statistical Association* 90 (430) pp. 773-795

Kuzyakov, Y., and Domanski, G. (2000) Carbon input by plants into the soil. Review. *Journal of Plant Nutrition and soil Science*. 163 (4) pp. 421-431

Krebs, C., J. (1999) *Ecological Methodology*, 2nd edn. Menlo Park, CA: Longman.

Lambert, J. G., and Arnason, T. (1982) Ramon and Maya Ruins: An Ecological, Not an Economic relation. *Science*. 216 pp. 298-299

Liang, B. C., Wang, X. L., and Ma, B. L., (2002) Maize Root-Induced Change In Soil Organic Carbon Pools. *Soil Sci. Soc. Am. J.* 66, pp. 845-847

Liu, R.,Clapp, C. E., and Cheng, H. H. (1997) Usefulness of the carbon-13 tracer technique for characterizing terrestrial carbon pools. *Nutrient Cycling in Agroecosystems*. 49, pp. 261-266.

Marschner, H. 1995. *Mineral nutrition of higher plants*, 2nd Edn. Academic Press, London, p.889

Martinelli, L.A., Pessenda, L.C.R., Espinoza, E., Camargo, P.B., Telles, E.C., Cerri, C.C., Victoria, R.L., Aravina, R.J., and S. Trumbore. 1996. Carbon-13 variation with depth in soils of Brazil and climate change during the Quaternary. *Oecologia* 106, pp. 376-381.

McCune, B. 2006. Non-parametric habitat models with automatic interactions. Journal of *Vegetation Science* 17, pp. 819-830

McCune, B. 2009. Nonparametric Multiplicative Regression for Habitat Modeling. Accessible online at: <http://www.pcord.com/NPMRintro.pdf>.

Miksicek, C. H., Elsesser, K., Wuebber, I. A., Bruhns, K. O., and Hammond, N. (1981) Rethinking Ramon: Comment on Reina and Hill's Lowland Maya Subsistance. *American Antiquity*. 46 (4), pp. 916-919

Milne, A. (1959) The centric systematic area-sample treated as a random sample. *Biometrics* 15, pp. 270-297

Mladinich, C. S., Bustos, M. R., Stitt, S., Root, R., Brown, K., Anderson, G. L., and Hager, S., (2006) The Use of Landsat 7 Enhanced Thematic Mapper Plus for Mapping Leafy Spurge. *Rangeland Ecol manag.* 56, pp. 500-506

Molina J A E, Clapp C E, Linden D R, Allmaras R R, Layese M R, Dowdy R H and Cheng H H 2001.Modeling the incorporation of corn (Zea mays l.) carbon from roots and rhizodeposition into soil organicmatter. Soil Bio. Biochem. 33, 83-92.

Nguyen C., (2003) Rhizodeposition of organic C by plants: mechanisms and controls. *Agronomie* 23, pp. 375–396.

Noordwijk, M.V., Cerri, C., Woomer, P.L., Nugroho, K., Bernoux, M. (1997) Soil carbon dynamics in the humid tropical forest zone. *Geoderma* 79, pp. 187-225

Olsen, S. R., C. V. Cole, F.S. Wantanabe, and L. A. Dean. (1954) Estimation of available phosphorus in soils by extraction with sodium bicarbonate. *USDA Circular No. 939*.

Peters, C. M, (1983) Observations on Maya Subsistence and the Ecology of a Tropical Tree. *American Antiquity*. 48(3), pp. 610-615

Puleston, D. E. (1971) An Experimental Approach to the Function of Classic Maya Chultuns. *American Antiquity* 36, pp 322-335

Puleston, D. E. (1982) The Role of Ramon in Maya Subsistence. In Maya Subsistence: Studies in Memory of Dennis E. Puleston, edited by K. Flannery. Academic Press, New York, pp. 349-366

Rice, D.S (1996) Paleolimnological Analysis in the Central Peten Guatemala, In Fredick, S. (Eds), The Managed Mosaic Ancient Maya Agriculture and Resource Use. University of Utah press, Salt Lake City, pp. 91-105

Rochette, P., Angers, D. A., and Flanagan, L. B., (1999) Maize Residue Decomposition Measurement Using Soil Surface Carbon Dioxide Fluxes and Natural Abundance Carbon-13. *Soil Sci. Soc. Am. J.* 63, pp. 1385-1396

Rosenmeier, M.F., Hodell, D.A., Brenner, M., Curtis, J.H., Guilderson, T.P. (2002) A 4000-year lacustrine record of environmental change in thesouthern Maya lowlands, Peten. *Quaternary Research* 57, pp. 183–190

Sanders, W. T. (1973). The cultural ecology of the Lowland Maya: a re-evaluation . In *The Classic Maya Collapse*, edited by T. Patrick Culbert, pp. 325-365.University of New Mexico Press, Albuquerque

Smith, B. N., Epstein S. (1971) Two Categories of 13C/12C Ratios for Higher Plants. *Plant Physiology*. 47 (3), pp. 380-384

Sweetwood, Ryan V., Richard E. Terry, Timothy Beach, Bruce H. Dahlin, and David Hixson. (2009) The Maya footprint: Soil resources of Chunchucmil, Yucatan, Mexico. *Soil Science Society of America Journal* 73 (4):1209-1220.

Tykot, R. H. (2002). Contribution of Stable Isotope Analysis to Understanding Dietary Variation among the Maya. *Archaeological Chemistry*. Washington, DC, American Chemical Society pp. 214-230.

United States Salinity Laboratory Staff. (1954). *Agricultural Handbook No. 60: Diagnosis and Improvement of Saline and Alkali Soils.* Edited by L. A. Richards. Riverside: United States Department of Agriculture.

Vittorello,V.A., Cerri, C.C., Andreux, F., Feller, C. & Victoria, R. L. (1989) Organic matter and natural carbon-13 distribution in forested and cultivated oxisols. *Soil Sci. Soc. Amer. J.* 53, pp.773–778

Wahl, D., Byrne, R., Schreiner, T., and Hansen, R. (2006) Holocene vegetation change in the northern Peten and its implications for Maya prehistory. *Quaternary Research.* 65, pp. 380-389

Wantanabe, F.S., and S. R. Olsen. 1965. Test of an ascorbic acid method for determining phosphorus in water and $NaHCO_3$ extracts from soil. *Soil Science Society of America Proceedings* 29:677-678.

Webb, E. A., Schwarcz, H. P., Jensen, C. T., Terry, R.E, Moriarty, M.D., and Emery, K.F. (2007) Stable carbon isotopes signature of ancient maize agriculture in the soils of Motul de San José, Guatemala. *Geoarchaeology: An International Journal* 22 pp. 291-312.

Webb, E. A., Schwarcz, H. P., and Hely, P.F. (2004) Detection of ancient maize in lowland Maya soils using stable carbon isotopes: evidence from Caracol, Belize. *Journal of Archaeological Science*. 31, pp 1039-1052

Webster, D (1981) Egregious Energetics. *American Antiquity* 46(4), pp. 9l9-922.

Webster, D., Murtha, T., Silverstein, J., Martinez, H., Terry, R., Burnett, R. The Tikal Earthworks Revisited. *Journal of Field Archaeology* 32 (1) pp. 41-64

Wichern, F. (2007) Estimating C and N Rhizodeposition of Peas and Oats, Kassel University Press, Kassel, Germany 148pp.

Wilken, G. C. (1971) Food-Producing Systems Available to the Ancient Maya. *American Antiquity*. 36 (4), pp. 432-448

Wright, D. J., E. R. Lundblad, E. M. Larkin, R. W. Rinehart, J. Murphy, L. Cary-Kothera, and K. Draganov. (2005). ArcGIS Benthic Terrain Modeler, Corvallis, Oregon, Oregon State

University, Davey Jones Locker Seafloor Mapping/Marine GIS Laboratory and NOAA Coastal Services Center. Accessible online at: http://www.csc.noaa.gov/products/btm/

Wright, D. R., Terry, R. E., and Eberl, M. (2009). Soil properties and stable carbon isotope analysis of landscape features in the Petexbatún region of Guatemala. *Geoarchaeology: An International Journal* 24 (4):466-491.

Wright, L. E. (2005) Identifying immigrants to Tikal, Guatemala: Defining local variability in strontium isotope ratios of human tooth enamel. *Journal of Archaeological Science*. 32, pp. 555-566

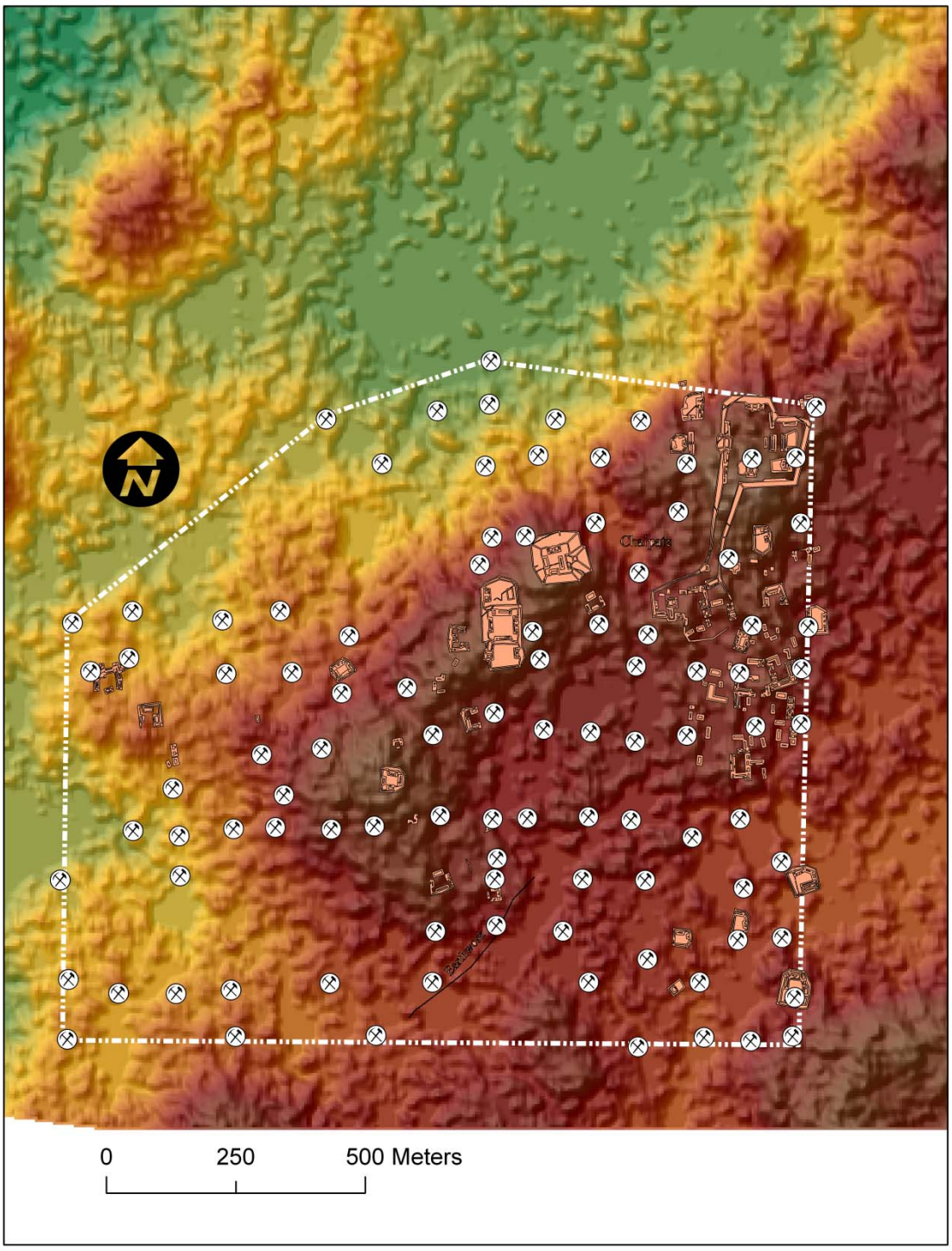

(Figure 1)Ramonal sample points based on a centric systematic area-sample method (CSS) that had been stratified by archaeologist Timothy Murtha using remotely sensed data layers.

Lab Predictor variables	Description
Depth cm	Soil depth to marl or bedrock layer or a maximum of 1 m.
pH	Assessed on the A and buried A horizons using a glass electrode with a 1:2 soil water mixture
Phosphorus, mg/kg	Run on all A horizons, based on the Olsen bicarbonate extraction.
Potassium, mg/kg	Run on all A horizons, based on the Olsen bicarbonate extraction.
Carbonate C, Percent	Calcium carbonate equivalent determined by titration (United States Salinity Laboratory Staff, 1954) and converted to percent carbonate C
Total Nitrogen, Percent	Calculated with an elemental analyzer using dry combustion.
Organic C, Percent	Calculated with an elemental analyzer using dry combustion.

(Table 1)Predictor variables generated in the laboratory used in model creation. All laboratory data came from the Soils Analysis Laboratory Brigham Young University.

Remote Sensing & GIS Predictor Variables	Description	Sensor data was Derived from	Resolution Before Resized to 5 m
Relative Elevation	Digital elevation model (DEM) derived with the C band with Z values representing elevations.	AIRSAR	5 m
Slope	Slope assessed at 5 m intervals created from the DEM . Slope is a calculation of maximum rate of change in elevation between the cell and its eight neighbors.	AIRSAR	5 m
Aspect	Aspect assessed at 5 m intervals created from the DEM. Aspect is the direction of the slope	AIRSAR	5 m
Landsat band 1	See Landsat7 table.	Landsat7	30m
Landsat band 2	See Landsat7 table.	Landsat7	30m
Landsat band 3	See Landsat7 table.	Landsat7	30m
Landsat band 4	See Landsat7 table.	Landsat7	30m
Landsat band 5	See Landsat7 table.	Landsat7	30m
Landsat band 61	See Landsat7 table.	Landsat7	60m
Landsat band 62	See Landsat7 table.	Landsat7	120m
Landsat band 7	See Landsat7 table.	Landsat7	30m
Ikonos R	red reflectance.	IKONOS-2	1m
Ikonos G	green reflectance.	IKONOS-2	1m
Ikonos B	blue reflectance.	IKONOS-2	1m
Ikonos NIR	Near- infrared reflectance.	IKONOS-2	1m
AIRSAR band P hh	P band antenna radiation polarized and transmitted horizontally and restricted to receive horizontally polarized radiation.	AIRSAR	5m
AIRSAR band P vv	P band antenna radiation polarized and transmitted horizontally and restricted to receive vertically polarized radiation.	AIRSAR	5m
AIRSAR band P hv	P band antenna radiation polarized and transmitted vertically and restricted to receive vertical polarized radiation.	AIRSAR	5m
AIRSAR band P hhvv	P band channel combing HH and VV.	AIRSAR	5m
Rugged Index	The ratio of surface area to planar area derived from a DEM	AIRSAR	5m
Topographic Position Index Broad Scale	Location is compared to overall landscape, for example a hill top vs. a valley bottom (200 m radius) derived from a DEM	AIRSAR	5m
Topographic Position Index Fine Scale	Location is compared to overall landscape, for example a hill top vs. a valley bottom (20 m radius) derived from a DEM	AIRSAR	5m
Curvature	Curvature derived from a DEM was used to identify the physical characteristics defining drainage basins often used to understand erosion and runoff processes.	AIRSAR	5m
Curvature Direction of Slope	The direction of the maximum slope derived from a DEM	AIRSAR	5m
Iverson Moisture Index	Used to asses topographically influenced moisture availability using the DEM derived layers hillshade, flow accumulation and curvature.	AIRSAR	5m

(Table 2) Predictor variables generated in using GIS and remotely sensed data. All remotely sensed data was further preprocessed in the Geospatial Habitat Analysis Laboratory Brigham Young University.

Landsat 7 ETM +			
Band Number	**Spectral Range (μm)**	**Spatial Resolution at Nadir (m)**	**Band Characteristic**
10	0.45-0.52	30 x 30	(Blue-green) Water penetration and vegetation soil discrimination. Highly susceptible to Rayleigh scattering
20	0.52-0.60	30 x 30	(Green) Vegetation discrimination and plant vigor
30	0.63-0.69	30 x 30	(Red) Vegetation type, bare ground and roads. Within the spectra of Chlorophyll absorption
40	0.76-0.90	30 x 30	(Near-infrared) Water bodies , Soil moisture, vegetation biomass and crop identification
50	1.55-1.75	30 x 30	(Mid-infrared) Discriminates roads, bare soil, water bodies and vegetation type and water content. Band 5 is efficient at penetrating atmospheric haze
60 62	10.40-12.56	60 x 60	(Thermal-infrared) Sensitive to infrared radiant energy emitted to obtain temperature from target. Used for thermal mapping plant stress and soil moisture. Band 60 is taken in high gain band 62 is low gain.
70	2.08-2.35	30 x 30	(Mid-infrared) Vegetation cover, soil moisture and mineral and rock type.
80	.520-.900	15 x 15	(Black and White) Panchromatic band for image resolution enhancing. Band 8 was not utilized in this study

(Table 3) Landsat general band characteristics.

Model Name	xR^2	log β	Response Variable	Predictor variables included in final model (sensitivity, tolerance)
Ramonal Lab Only (13C Enrich.)	0.583	-	$\delta^{13}C$ enrichment	ppm phosphorus (0.76, 0.67), depth (0.39, 16.35), % carbonate (0.07, 4.67) and pH (0.03, 1.14)
Ramonal RS Only (13C Enrich.)	0.215	-	$\delta^{13}C$ enrichment	elevation (1.16, 2.59), curvature direction of slope (0.28, 2.59), AIRSAR band P vv (0.15, .03), aspect (0.04, 226.61), Landsat band 4 (0.02, 8.25), and TPI fine scale (0.01, 358.5).
Ramonal RS and Lab (13C Enrich.)	0.592	-	$\delta^{13}C$ enrichment	ppm phosphorus (0.72, 0.67), depth (0.43, 17.44), % carbonate (0.06, 4.96), AIRSAR P band hhvv (0.03, 187.04), pH (0.03, 1.44), and rugged index (0.02, 0.05).
Ramonal Lab Only ($CO_3^=$-C)	0.76	-	$CO_3^=$-C	pH (1.50, 0.13). ppm phosphorus (0.34, 1.33), % organic C (0.15, 4.21), and % total nitrogen (N) (0.03, 0.71)
Ramonal RS Only ($CO_3^=$-C)	0.387	-	$CO_3^=$-C	elevation (1.48, 2.59), Landsat band 1 (0.38, 1.80), curvature direction of slope (0.30, 2.59), Landsat band 7 (0.04, 4.50), and TPI broad scale (0.03, 257.95).
Ramonal RS and lab ($CO_3^=$-C)	0.747	-	$CO_3^=$-C	pH (1.36, 0.13), elevation (0.24, 10.37) curvature (0.08, 4.60), Iverson Moisture Index (0.29, 22.79) AIRSAR P band phh (0.25, 0.09), % organic C (0.22, 11.58) and curvature direction of slope (0.01, 8.41)
Tikal Total RS (13C Enrich.)	0.305	-	$\delta^{13}C$ enrichment	elevation (1.35, 2.86) Landsat band 50 (0.36, 2.47), TPI fine scale (0.13, 76.44), AIRSAR P band hv (0.04, 0.03), and curvature direction of slope (0.01, 13.19)
Tikal Total Binomial RS (13C Enrich.)	-	7.18	$\delta^{13}C$ enrichment	elevation (1.26, 3.58), curvature direction of slope (0.300, 2.79), Landsat band 50 (0.25, 3.8), Landsat band 40 (0.10, 5.25) and aspect (0.05, 249.77)
Ramonal Binomial RS (13C Enrich.)	-	4.359	$\delta^{13}C$ enrichment	elevation (0.89, 4.23), slope (0.60, 2.41), and curvature direction of slope (0.26, 2.72).
Tikal Total RS ($CO_3^=$-C)	0.335	-	$CO_3^=$-C	elevation (1.20, 3.58) curvature direction of slope (.41, 2.79), Landsat band 4 (0.12, 4.50), Landsat band 61 (0.12, 1.25), Landsat band 2 (0.12, 3.00), aspect (0.11, 160.56), Landsat band 3(0.06, 4.20), AIRSAR P band phv (0.05, 0.03), slope (0.05, 15.21),Landsat band 1 (0.05, 6.00)

(Table 4) Model lists with corresponding xR^2 and log β values. The predictor variables are listed in order of statistical relevance with the sensitivity and tolerance values in parentheses.

(Figure 2)Ramonal enrichment values are $\delta^{13}C$ enrichment defined as the largest shift in $\delta^{13}C$ from the surface to depth within the profile. Structure locations are included for reference.

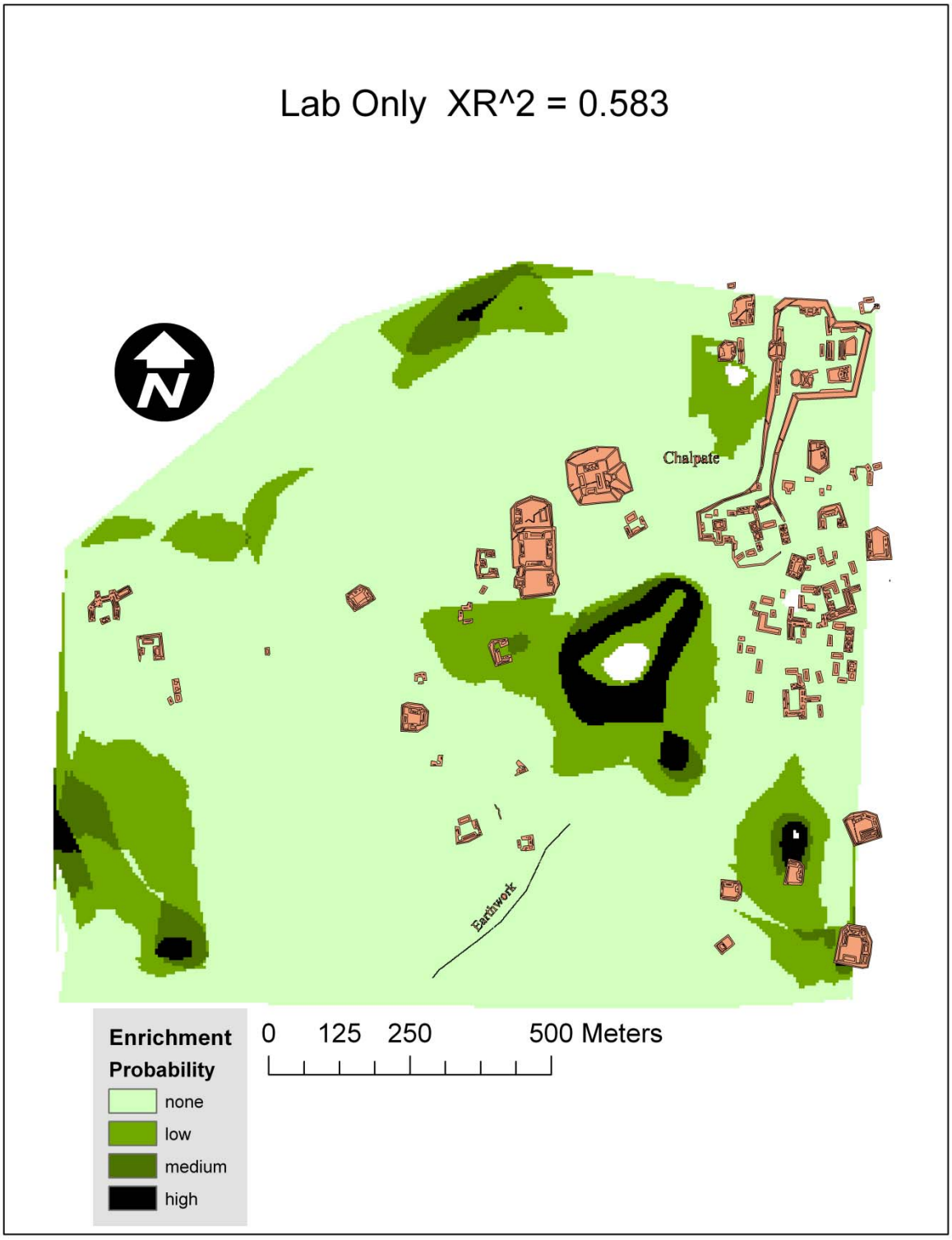

(Figure 3) Ramonal enrichment values are $\delta^{13}C$ enrichment predicted with the Ramonal Lab Only (13C Enrich.) model. Structure locations are included for reference.

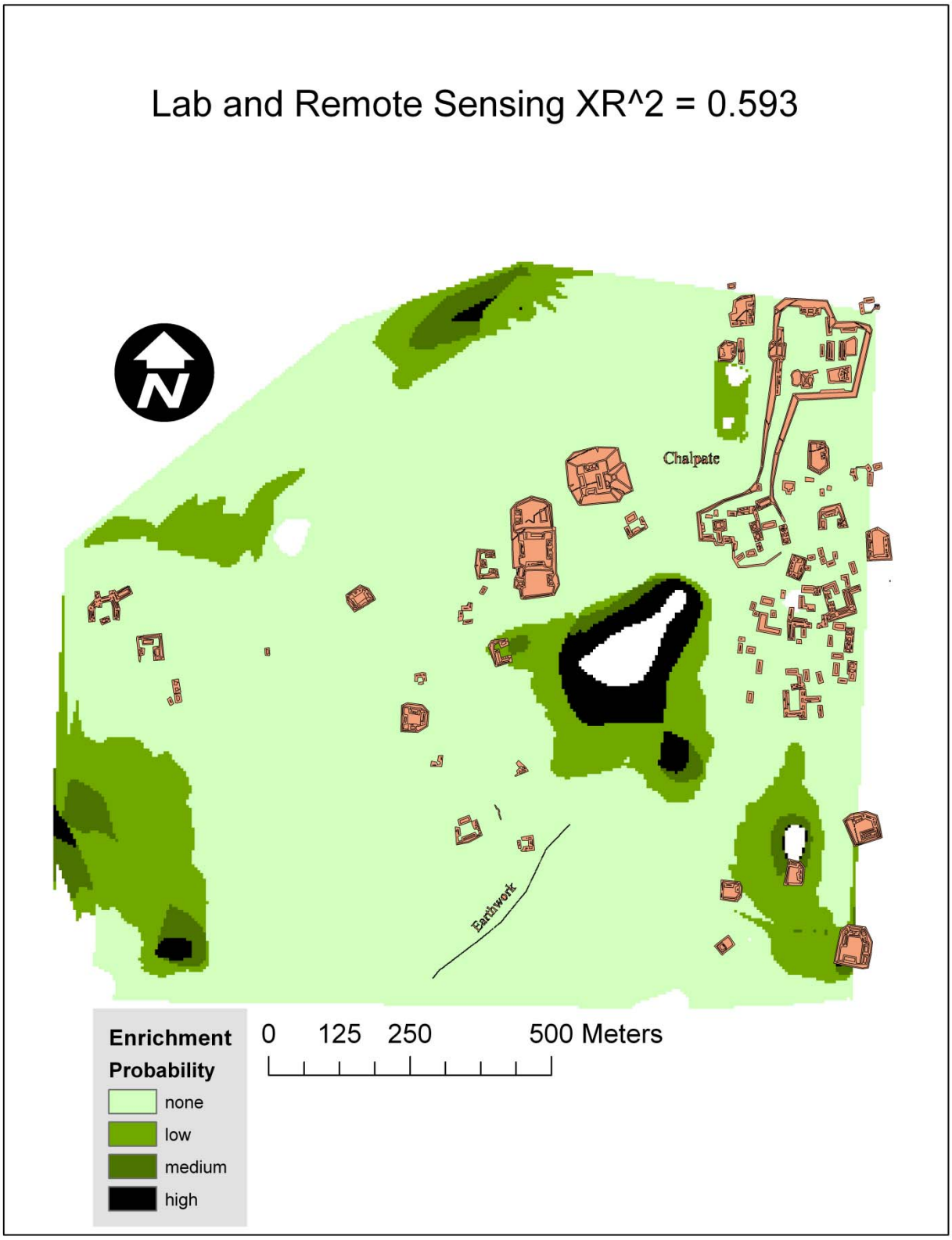

(Figure 4) Ramonal enrichment values are $\delta^{13}C$ enrichment predicted with the Ramonal RS and Lab (13C Enrich.) model. Structure locations are included for reference.

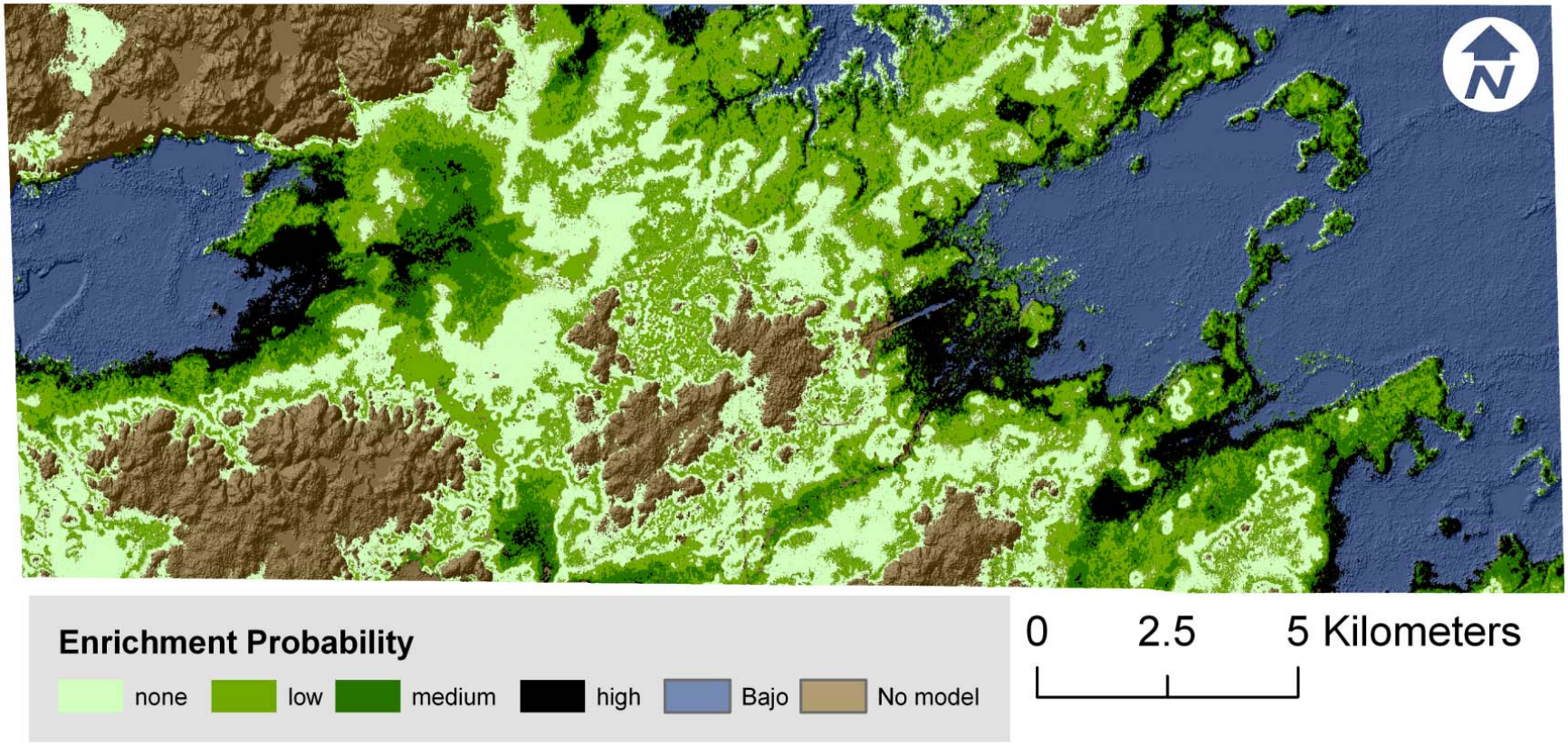

(Figure 5) Tikal Total Binomial RS (13C Enrich.) model with a log β value of 7.18. Areas labeled Bajo and No model have insufficient evidence to predict to avoid over fitting the data. Ramonal is in the south east corner of the map.Ramonal is in the southeast corner Tikal is in the center.

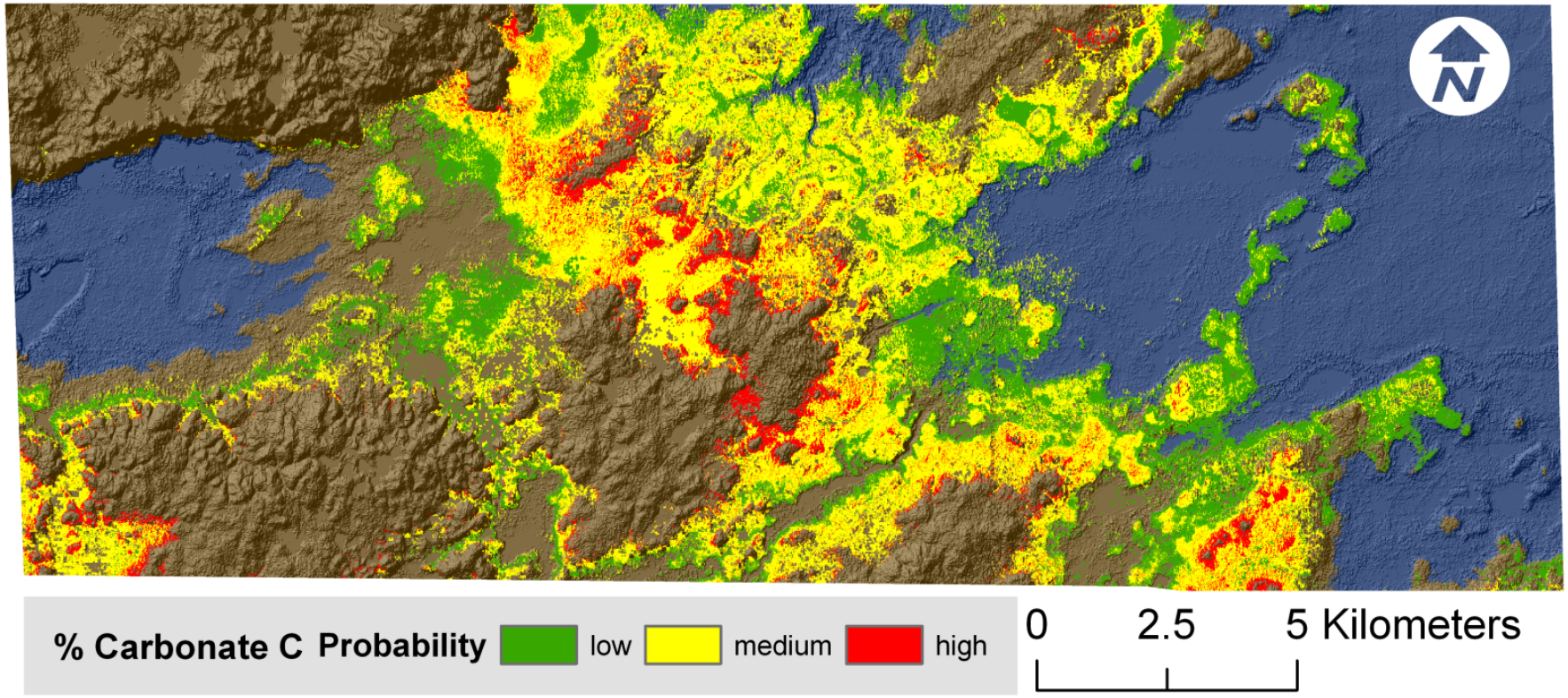

(Figure 6) Tikal Total RS ($CO_3^=$-C) model the brown and dark blue are areas the model was unable to predict due to insuficient information. The dark blue is Bajo, and the brown in the highest elevations. Ramonal is in the south east corner of the map.Ramonal is in the southeast corner Tikal is in the center.

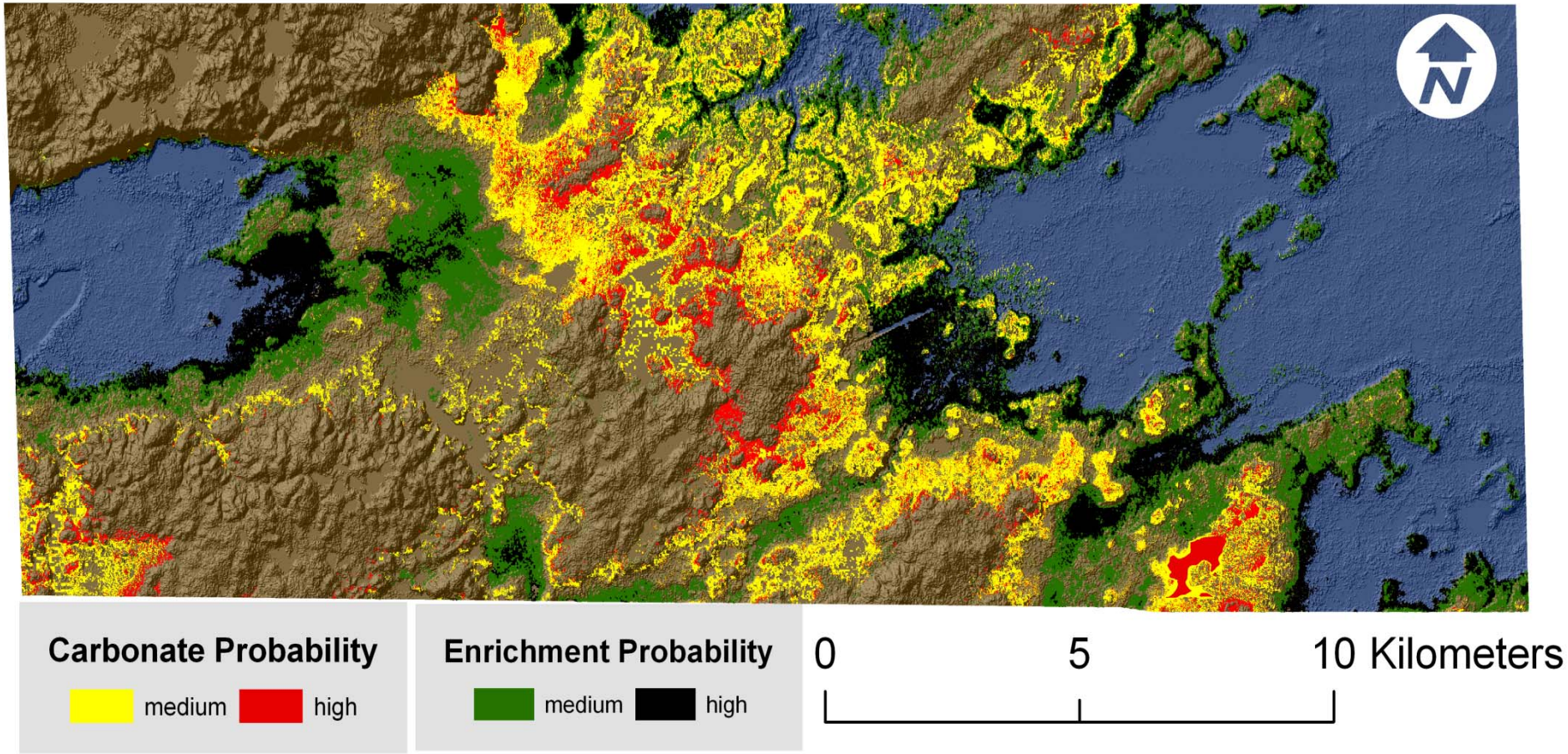

(Figure 7) Combination of Tikal Total RS ($CO_3^{=}$-C) and Tikal Total Binomial RS (13C Enrich.) models showing only the medium and high probabilities of both. The dark blue is Bajo, and the brown in the highest elevations. Ramonal is in the south east corner of the map.Ramonal is in the southeast corner Tikal is in the center.

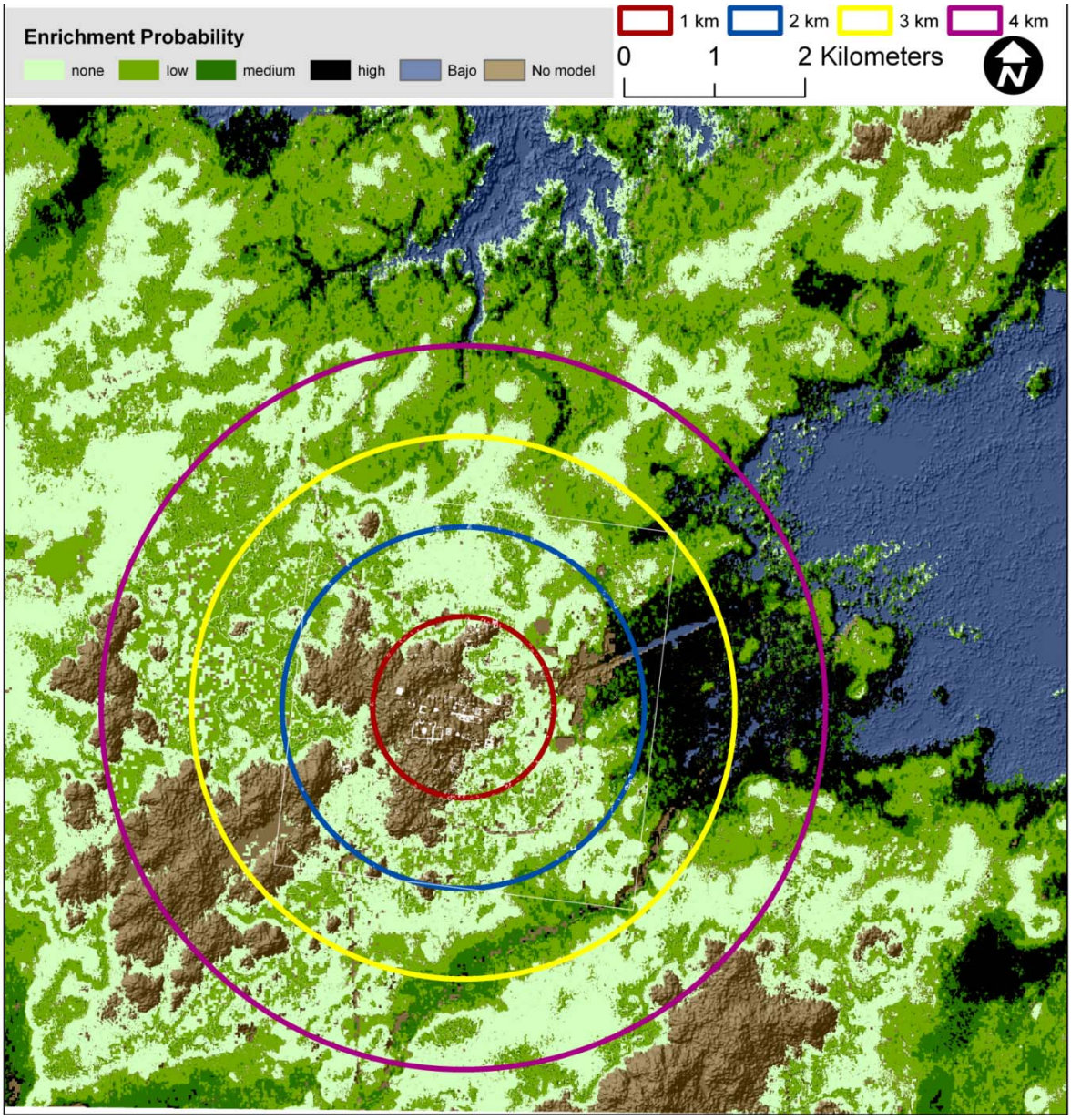

(Figure 8) Tikal site center scale Tikal Total Binomial RS (13C Enrich.) model.

	Percent of Model			
Radius	None	Low	Medium	High
1km	72.38	24.71	2.72	0.19
2km	61.76	29.34	5.93	2.97
3km	46.32	34.67	8.72	10.29
4km	44.05	35.43	9.66	10.87
Total frame	35.87	33.44	18.14	12.54

(Table 5) Percent of area modeled within concentric circles using the Tikal Total Binomial RS (13C Enrich.) model

Appendix Table. The response variables and remotely sensed predictors used in the NPMR models.

Profile	Response variables: Binomial	Response variables: Change in		Predictors: Elevation	Ruggedness: Slope	Ruggedness: Aspect	Ruggedness: Index	Topo postion index: Broad	Topo postion index: Fine	Slope direction: Curvature	Slope direction: Curvature	R	Ikonos Bands: G	Ikonos Bands: B	Ikonos Bands: NDVI	Landsat Bands March 2003: B1	B2	B3	B4	B5	B61	B62	B7	AIRSAR polarized p-Band: phh	phhvv	phv	pvv
Number	^{13}C enrich	δ^{13}C	$CO_3^=$-C	m (msl)	%	degrees																					
		‰	%																								
1	1	3.56	5.35	276.5	9.53	107.65	1.027	91	139	7.744	-6.590	80	84	83	78	99	72	58	79	68	144	72	31	0.018	87.017	0.019	0.040
2	0	1.37	1.19	252.8	0.00	-1.00	1.000	-25	-19	0.000	0.000	175	167	148	177	96	71	57	83	68	143	71	31	0.026	153.209	0.006	0.077
3	0	0.32	4.56	258.6	7.17	312.01	1.009	91	-19	1.310	-0.986	104	112	104	131	96	69	55	76	62	143	69	29	0.037	148.488	0.010	0.028
4	0	0.50	6.67	256.3	3.60	196.12	1.004	91	-19	2.016	-0.134	109	114	108	133	96	69	54	80	63	143	69	31	0.049	300.521	0.006	0.017
5	0	1.31	0.22	253.9	7.19	163.78	1.008	-25	-19	-0.225	-0.228	125	127	119	172	97	71	56	81	64	144	71	31	0.070	179.105	0.019	0.024
6	0	0.80	7.30	259.1	5.33	334.64	1.011	-25	-19	-2.823	1.236	144	154	150	171	96	71	56	79	63	143	71	29	0.050	103.943	0.014	0.042
7	1	2.52	0.87	253.3	8.87	337.12	1.013	-25	-19	-1.009	1.372	133	139	127	184	96	68	56	77	65	143	68	29	0.045	236.691	0.006	0.103
8	0	0.47	8.44	264.2	3.13	267.62	1.004	-25	-19	-3.330	2.961	109	123	102	157	95	70	54	77	64	142	70	31	0.028	111.890	0.012	0.103
9	0	0.60	9.83	260.2	11.59	238.65	1.028	91	139	8.076	-3.678	30	37	34	35	97	69	58	81	67	143	69	31	0.059	312.545	0.009	0.024
10	0	0.60	7.63	268.1	8.49	294.25	1.015	-25	-19	0.031	2.086	137	144	132	187	96	69	57	78	63	143	69	30	0.105	126.819	0.013	0.051
11	0	0.35	7.76	264.0	3.66	54.31	1.009	-25	-19	-5.721	1.976	128	137	130	122	97	70	53	75	63	143	70	29	0.027	178.996	0.003	0.016
12	0	0.88	9.80	277.1	14.71	317.52	1.040	-25	-19	-4.314	3.311	148	153	154	96	99	70	57	75	59	143	70	28	0.040	47.380	0.013	0.075
13	0	0.68	7.66	271.0	17.20	273.49	1.050	-25	-19	-1.393	1.590	125	134	125	150	98	73	56	81	66	145	73	29	0.030	91.530	0.017	0.069
14	0	0.06	9.08	273.7	18.42	350.58	1.064	-25	-19	-5.040	5.947	101	109	108	133	99	71	60	77	66	144	71	32	0.036	157.636	0.010	0.039
15	0	0.98	9.18	270.9	5.93	254.07	1.021	-25	-19	-1.540	4.436	85	96	91	110	99	74	61	76	62	144	74	28	0.006	131.917	0.004	0.007
16	1	3.74	0.10	270.7	0.00	-1.00	1.000	-25	-19	0.000	0.000	80	87	82	107	101	73	58	77	65	144	73	31	0.013	86.705	0.003	0.055
17	0	1.74	0.16	264.5	0.00	-1.00	1.000	-25	-19	0.000	0.000	118	128	110	171	100	72	60	80	67	144	72	32	0.028	165.555	0.004	0.019
18	1	2.46	8.40	271.2	6.57	145.99	1.027	326	299	12.125	-5.298	105	110	101	182	101	71	59	78	65	144	71	30	0.078	304.982	0.015	0.103
19	0	1.59	0.26	266.6	1.55	45.00	1.003	-25	-19	0.000	0.000	123	143	116	203	98	72	59	79	66	145	72	30	0.017	50.673	0.002	0.011
20	0	0.56	8.53	268.6	3.69	263.14	1.013	91	139	4.142	-5.461	12	15	22	26	99	73	58	76	65	144	73	31	0.046	184.377	0.003	0.022
21	1	4.78	0.25	270.4	21.37	199.31	1.080	91	139	6.468	-3.416	30	36	37	104	98	72	57	76	60	143	72	28	0.108	134.987	0.006	0.067
22	0	0.81	8.90	270.7	8.20	83.15	1.013	-25	-19	-1.317	2.332	97	97	99	151	100	73	60	79	72	144	73	35	0.033	206.909	0.008	0.017
23	1	3.05	0.39	266.2	0.00	-1.00	1.000	-25	-19	0.000	0.000	94	102	88	115	99	72	59	76	68	143	72	30	0.027	112.726	0.010	0.025
24	1	5.26	0.22	270.5	0.00	-1.00	1.000	-25	-19	0.000	0.000	84	100	93	145	101	73	57	78	68	144	73	33	0.019	125.532	0.004	0.033
25	1	4.59	0.31	249.8	5.78	264.75	1.008	-25	-19	-1.704	1.208	98	103	96	75	95	68	55	74	63	143	68	31	0.018	304.319	0.015	0.053
26	1	2.44	0.24	248.7	13.37	221.65	1.031	-25	-19	-2.380	0.475	146	141	135	180	96	69	55	79	64	143	69	30	0.132	52.084	0.006	0.027
27	0	2.00	1.67	257.5	6.01	346.93	1.012	91	139	5.265	-3.234	101	115	101	145	93	71	55	75	63	143	71	28	0.042	89.845	0.013	0.029
28	0	1.05	0.18	254.2	6.13	184.54	1.010	-25	-19	-3.412	3.385	44	44	42	79	96	69	55	75	59	143	69	27	0.031	349.663	0.017	0.108
29	0	1.24	7.15	268.0	10.99	270.35	1.021	-25	-19	1.654	-0.885	131	129	125	153	98	71	56	79	65	143	71	29	0.018	30.049	0.005	0.027
30	0	2.23	1.15	251.2	3.28	181.82	1.004	-25	-19	-2.646	2.646	60	71	62	104	96	69	55	78	63	143	69	30	0.015	219.970	0.003	0.009
31	0	1.11	7.68	276.8	10.05	231.30	1.020	-25	-19	-3.160	3.095	104	113	96	112	97	68	56	73	61	143	68	30	0.060	176.706	0.015	0.090
32	0	0.43	6.82	258.0	4.71	306.53	1.007	-25	-19	-3.245	3.015	156	158	158	174	96	71	56	81	65	143	71	29	0.065	24.845	0.016	0.055
33	1	3.96	8.45	277.8	4.02	111.80	1.005	-25	-19	-3.233	2.823	137	139	127	142	100	72	58	83	68	144	72	30	0.053	274.680	0.007	0.012
34	0	2.34	3.63	269.9	6.13	223.72	1.007	91	-19	-1.812	1.182	151	157	141	183	97	71	53	75	61	142	71	27	0.037	231.109	0.005	0.010
35	0	2.28	0.33	266.0	4.94	352.09	1.005	-25	-19	-2.551	0.794	146	155	141	190	96	69	55	81	64	143	69	30	0.058	42.067	0.006	0.053
36	0	0.16	8.63	271.7	13.14	256.07	1.028	-25	-19	1.871	-1.633	43	46	47	56	95	68	55	76	63	143	68	29	0.046	48.510	0.013	0.017
37	0	0.19	8.32	266.0	5.20	102.21	1.007	91	139	4.394	-2.349	141	149	140	199	96	69	55	79	65	142	69	31	0.036	112.026	0.007	0.052
38	0	1.50	7.37	279.4	4.43	45.59	1.006	-25	-19	-0.930	1.607	159	159	156	159	95	71	56	77	63	143	71	31	0.023	194.096	0.004	0.051
39	0	0.27	6.50	268.6	10.67	215.58	1.030	91	139	9.132	-3.324	117	127	114	147	98	70	56	82	68	144	70	32	0.011	77.544	0.005	0.014
40	0	0.29	7.67	285.4	7.04	170.91	1.008	91	-19	1.834	-1.334	76	94	78	161	98	70	57	78	66	144	70	31	0.037	242.714	0.008	0.018
41	1	2.55	8.62	273.0	21.77	182.02	1.082	-143	-19	2.599	-2.105	167	168	158	177	96	72	57	78	67	143	72	32	0.023	94.469	0.011	0.010
42	0	0.94	7.59	282.0	5.72	118.53	1.009	91	-19	0.568	1.429	73	89	69	105	97	70	56	81	67	144	70	31	0.008	307.578	0.006	0.034
43	0	0.59	7.50	272.2	3.64	349.28	1.004	-25	-19	-1.417	1.890	137	133	133	94	98	73	59	81	67	144	73	30	0.014	210.589	0.015	0.018
44	0	1.39	6.00	274.8	6.98	46.22	1.018	208	139	5.816	-2.157	144	150	142	148	98	71	58	80	70	144	71	31	0.092	107.275	0.021	0.047
45	0	0.26	5.98	274.5	19.61	105.91	1.064	-25	-19	-2.862	2.118	92	92	95	85	98	72	58	79	68	143	72	32	0.050	57.527	0.012	0.049
46	1	2.48	0.20	274.9	4.95	337.50	1.006	91	-19	-1.421	-0.180	147	150	135	137	100	73	58	76	63	144	73	33	0.110	40.965	0.042	0.054
47	0	2.14	2.37	275.7	10.38	102.76	1.026	91	139	5.354	-5.110	154	153	148	132	97	72	55	78	69	143	72	32	0.030	61.234	0.002	0.017
48	0	0.95	0.44	272.2	12.92	117.77	1.031	-25	-19	-3.472	0.215	136	137	130	150	100	75	61	81	73	144	75	35	0.016	109.907	0.005	0.007
49	0	1.25	8.83	278.2	4.08	77.96	1.008	-143	-19	-4.903	1.973	150	158	154	167	100	74	60	80	69	144	74	32	0.068	49.075	0.010	0.085
50	0	0.17	9.35	275.5	5.63	203.60	1.008	-25	-19	-1.051	2.292	90	104	96	132	101	73	59	73	59	143	73	29	0.109	278.980	0.005	0.015
51	0	0.70	9.14	284.0	4.75	146.21	1.009	-25	-19	-2.914	2.805	146	155	143	148	98	71	58	75	64	144	71	30	0.013	147.336	0.002	0.013
52	0	1.10	9.33	290.2	12.01	294.44	1.028	208	139	4.473	-3.790	116	129	113	148	98	72	59	75	61	144	72	31	0.056	125.583	0.021	0.022
53	0	1.91	9.40	276.9	12.68	253.00	1.037	-143	-19	-6.064	3.976	105	121	103	168	100	72	58	76	64	144	72	31	0.033	251.784	0.022	0.090
54	0	0.00	9.78	294.0	10.92	341.80	1.021	91	139	2.232	-0.198	90	97	94	89	99	72	58	79	66	143	72	30	0.048	68.149	0.002	0.011
55	0	0.00	9.40	268.9	2.17	35.45	1.004	-25	-19	-2.431	2.400	120	129	100	181	99	72	58	78	65	145	72	32	0.028	292.012	0.005	0.011
56	0	1.92	9.29	285.5	5.49	45.85	1.007	-25	-19	0.936	0.173	98	103	103	55	99	71	57	74	62	144	71	30	0.024	18.470	0.007	0.033
57	0	0.11	9.05	267.6	1.88	30.84	1.005	-25	-19	-1.091	-1.330	41	47	46	89	100	71	59	80	67	142	71	29	0.041	103.228	0.018	0.107
58	0	1.37	8.67	261.2	9.02	14.96	1.016	-25	-19	1.756	-1.916	97	104	103	103	97	73	57	76	64	142	73	30	0.034	125.835	0.022	0.044
59	0	0.71	8.92	277.5	10.63	298.68	1.018	-25	-19	-0.471	0.476	125	133	115	98	100	71	57	74	60	143	71	29	0.044	204.096	0.006	0.088
60	0	0.00	8.22	265.6	19.20	337.08	1.064	91	-19	3.555	0.154	68	79	74	100	98	72	56	76	64	143	72	29	0.030	252.886	0.008	0.040
61	0	0.05	8.22	265.2	16.88	324.05	1.060	-25	-19	-2.995	5.147	83	84	86	43	100	71	56	76	62	143	71	27	0.094	281.622	0.015	0.026
62	1	4.35	6.94	250.4	8.10	355.81	1.018	-25	-19	-0.092	-0.766	131	139	127	155	101	72	59	76	59	143	72	28	0.025	333.137	0.004	0.032
63	0	0.64	8.43	255.2	1.27	8.72	1.002	-25	-19	-1.526	-0.487	95	104	106	90	101	73	56	79	66	143	73	32	0.139	189.825	0.020	0.069

Appendix Table. The response variables and remotely sensed predictors used in the NPMR models.

Response variables				Predictors																								
Profile	Binomial	Change in					Ruggedness	Topo postion index		Slope direction			Ikonos Bands				Landsat Bands March 2003								AIRSAR polarized p-Band			
Number	^{13}C enrich	$\delta^{13}C$	$CO_3^{=}$-C	Elevation	Slope	Aspect	Index	Broad	Fine	Curvature	Curvature	R	G	B	NDVI	B1	B2	B3	B4	B5	B61	B62	B7	phh	phhvv	phv	pvv
		‰	%	m (msl)	%	degrees																						
64	1	2.45	0.47	250.2	11.70	71.93	1.022	91	-19	0.470	0.817	156	156	153	128	98	71	59	77	68	144	71	32	0.023	44.180	0.013	0.051
65	0	0.94	0.95	251.2	8.45	13.92	1.021	208	299	7.619	-2.883	150	151	143	152	98	71	56	80	65	144	71	31	0.074	236.227	0.006	0.038
66	0	0.43	8.44	254.2	4.09	328.22	1.003	-25	-19	-1.637	1.161	109	118	101	85	100	72	58	77	61	144	72	30	0.025	110.561	0.002	0.063
67	0	2.38	0.29	243.9	2.85	16.27	1.002	-25	-19	1.541	-0.334	113	111	110	89	98	73	57	76	67	143	73	32	0.039	250.058	0.015	0.038
68	1	2.86	0.27	241.1	0.00	-1.00	1.000	-25	-19	0.000	0.000	129	127	122	120	101	74	62	77	69	143	74	32	0.079	95.965	0.011	0.044
69	1	4.81	1.33	245.7	8.35	305.21	1.021	-25	-19	3.147	-1.926	114	121	107	156	99	73	58	76	63	143	73	30	0.030	103.006	0.013	0.040
70	0	1.08	9.75	281.4	21.87	130.65	1.090	-25	-19	-1.302	0.136	155	160	151	177	99	76	61	78	76	143	76	38	0.029	274.554	0.005	0.044
71	0	0.63	8.59	279.4	4.35	5.03	1.004	-25	-19	-1.804	1.680	129	140	113	178	99	73	59	79	70	143	73	33	0.034	108.562	0.009	0.029
72	0	0.49	8.82	275.2	8.89	210.33	1.026	-143	-179	-10.044	6.354	76	90	80	101	104	70	57	73	64	143	70	30	0.025	181.547	0.008	0.019
73	0	0.08	7.80	258.3	4.50	300.03	1.006	-25	-19	-4.191	2.732	101	106	98	141	94	68	55	79	62	143	68	29	0.044	111.102	0.012	0.042
74	0	0.99	4.95	265.0	11.60	260.86	1.022	91	-19	-2.174	0.769	143	149	134	176	96	70	54	76	60	143	70	28	0.040	50.600	0.016	0.060
75	1	5.73	0.94	258.1	1.88	337.27	1.002	-25	-19	-0.396	-0.946	158	163	156	197	95	67	54	80	61	144	67	28	0.091	229.971	0.011	0.103
76	0	0.45	8.92	259.4	18.65	163.21	1.069	208	139	5.990	-2.296	122	125	122	124	94	69	55	83	69	143	69	31	0.032	241.101	0.005	0.022
77	0	0.28	0.23	253.6	1.85	212.41	1.002	-25	-19	-0.699	0.699	140	151	145	172	92	65	52	78	61	142	65	29	0.026	186.025	0.003	0.019
78	0	0.00	0.25	258.6	5.23	330.77	1.008	91	139	2.786	-1.519	129	135	126	154	92	65	53	78	61	144	65	29	0.269	192.479	0.031	0.062
79	0	1.27	6.68	267.1	0.00	-1.00	1.000	-25	-19	0.000	0.000	33	41	33	62	102	75	63	78	75	143	75	38	0.010	233.462	0.003	0.033
80	0	0.29	7.26	273.5	10.03	121.67	1.019	-25	-19	-2.341	2.344	134	147	118	174	98	75	59	80	76	143	75	37	0.028	50.096	0.012	0.051
81	0	1.40	5.07	274.1	14.32	54.85	1.034	-25	-19	-0.100	0.922	54	62	54	38	100	73	61	80	73	143	73	34	0.027	47.756	0.016	0.023
82	0	0.23	7.93	279.9	13.91	219.28	1.034	-25	-19	0.408	1.635	89	105	88	107	102	77	61	79	78	143	77	41	0.024	323.545	0.015	0.108
83	1	2.64	8.12	279.1	11.84	123.51	1.031	91	139	4.345	-4.505	115	125	107	152	105	73	60	77	67	143	73	33	0.033	214.046	0.009	0.045
84	0	0.24	8.54	277.4	13.02	144.51	1.030	91	139	4.393	-1.565	128	127	126	157	99	73	61	75	74	143	73	37	0.024	49.261	0.017	0.087
85	0	1.78	0.17	274.6	12.65	38.01	1.026	-25	-19	-2.152	1.406	116	126	111	179	99	71	58	75	70	143	71	35	0.119	320.055	0.006	0.025
86	1	4.45	0.34	273.3	6.53	310.71	1.018	-25	-19	-1.298	-2.163	168	170	160	195	100	73	61	78	65	144	73	33	0.040	143.783	0.013	0.046
87	0	0.75	9.39	285.8	6.61	253.02	1.009	-25	-19	-1.447	1.666	115	126	106	140	97	73	60	80	69	144	73	35	0.041	39.293	0.009	0.034
88	0	0.00	7.69	269.6	5.79	347.49	1.006	-25	-19	1.231	-0.179	125	138	119	133	99	72	55	77	62	143	72	30	0.023	43.503	0.013	0.053
89	0	1.55	6.66	273.7	0.18	225.00	1.000	-25	-19	0.000	0.000	135	133	129	71	98	74	58	77	65	144	74	30	0.010	136.446	0.007	0.013
90	0	2.38	8.35	275.5	9.24	263.24	1.016	-25	-19	0.991	0.029	97	106	96	136	98	72	58	75	68	144	72	33	0.046	269.002	0.028	0.043
91	1	2.63	0.28	273.4	2.72	20.59	1.004	-25	-19	-1.133	1.141	74	76	76	69	98	71	56	77	64	143	71	33	0.085	47.343	0.012	0.076
92	0	0.87	0.36	273.4	4.18	3.92	1.006	-25	-19	-3.265	3.288	106	118	107	169	100	72	59	76	63	144	72	32	0.069	269.931	0.031	0.063
93	0	0.17	7.14	271.6	0.44	151.31	1.001	-25	-19	-0.242	0.798	109	124	106	146	99	72	58	79	68	144	72	31	0.022	57.074	0.002	0.012
94	0	0.00	3.19	267.0	7.97	54.07	1.013	-25	-19	-3.050	2.478	135	139	129	196	98	71	57	79	65	144	71	31	0.039	239.159	0.017	0.029
95	0	1.02	8.21	266.6	3.42	284.51	1.004	-25	-19	-1.022	1.214	54	61	54	108	99	73	58	78	63	144	73	31	0.057	262.316	0.014	0.071
96	0	0.85	8.85	268.8	4.66	241.09	1.011	-25	-19	-2.557	2.557	156	158	156	181	98	72	58	82	68	144	72	31	0.007	73.687	0.020	0.013
97	0	0.94	0.50	269.7	8.31	83.83	1.011	-25	-19	-0.498	0.265	92	102	95	158	99	72	57	79	72	144	72	36	0.019	301.125	0.008	0.022
98	0	0.55	7.51	270.5	3.98	68.35	1.007	-25	-19	-2.351	2.351	129	135	122	131	98	70	57	73	64	143	70	31	0.043	16.393	0.014	0.035
99	0	0.72	10.41	254.9	3.30	164.77	1.005	208	139	4.276	-2.615	-	-	-	-	97	70	56	83	63	142	70	29	0.058	277.899	0.013	0.056
100	0	0.75	8.85	254.9	3.30	164.77	1.005	208	139	4.276	-2.615	-	-	-	-	97	70	56	83	63	142	70	29	0.058	277.899	0.013	0.056
101	1	2.95	8.86	254.9	3.30	164.77	1.005	208	139	4.276	-2.615	-	-	-	-	97	70	56	83	63	142	70	29	0.058	277.899	0.013	0.056
102	1	2.51	8.15	254.9	3.30	164.77	1.005	208	139	4.276	-2.615	-	-	-	-	97	70	56	83	63	142	70	29	0.058	277.899	0.013	0.056
103	1	2.47	6.19	254.9	3.30	164.77	1.005	208	139	4.276	-2.615	-	-	-	-	97	70	56	83	63	142	70	29	0.058	277.899	0.013	0.056
104	0	0.36	6.31	254.1	10.08	132.44	1.024	208	139	4.935	-1.057	-	-	-	-	97	70	56	83	63	142	70	29	0.102	250.719	0.019	0.048
105	0	0.00	0.45	252.9	14.16	98.39	1.036	91	-19	0.822	-0.234	-	-	-	-	97	70	56	83	63	142	70	29	0.076	157.037	0.052	0.060
106	0	0.13	0.18	251.6	11.49	81.02	1.024	-25	-19	-2.723	2.111	-	-	-	-	97	70	56	83	63	142	70	29	0.031	125.932	0.044	0.152
107	0	2.17	10.18	251.2	7.04	54.83	1.008	-25	-19	-0.810	0.229	-	-	-	-	97	73	57	86	65	143	73	30	0.032	231.685	0.066	0.130
108	0	1.13	0.27	250.8	6.74	52.12	1.007	-25	-19	-0.128	0.182	-	-	-	-	97	72	56	84	66	142	72	31	0.107	134.204	0.008	0.049
109	1	2.83	10.27	253.6	4.79	98.68	1.004	-25	-19	0.751	-1.029	-	-	-	-	96	70	57	85	65	143	70	27	0.033	124.555	0.008	0.122
110	0	0.87	10.18	254.4	6.52	56.81	1.009	-25	-19	2.552	-2.070	-	-	-	-	96	68	54	82	64	143	68	29	0.063	53.866	0.019	0.090
111	0	0.54	9.29	256.1	3.16	344.95	1.003	91	-19	1.714	-1.798	-	-	-	-	95	69	54	81	63	142	69	30	0.042	323.724	0.014	0.026
112	0	0.33	8.67	250.2	10.63	138.06	1.023	91	139	5.242	-3.383	-	-	-	-	93	69	55	82	65	143	69	31	0.032	296.274	0.007	0.010
113	1	3.64	0.30	240.1	0.00	-1.00	1.000	-25	-19	0.000	0.000	-	-	-	-	98	71	56	81	69	142	71	29	0.044	352.184	0.015	0.049
114	0	0.36	8.77	245.9	20.95	56.19	1.074	-25	-19	-5.595	3.703	-	-	-	-	102	75	60	84	70	142	75	33	0.133	305.362	0.013	0.031
115	0	0.17	5.06	241.7	17.30	94.87	1.049	-143	-19	-3.080	1.884	-	-	-	-	101	74	60	82	67	142	74	30	0.090	121.866	0.017	0.016
116	1	3.30	0.20	236.9	0.00	-1.00	1.000	-25	-19	0.000	0.000	-	-	-	-	102	74	58	85	66	142	74	30	0.071	306.208	0.009	0.057
117	1	7.77	0.31	236.3	17.59	178.27	1.051	91	139	3.070	-1.954	-	-	-	-	104	75	61	80	66	142	75	31	0.086	109.487	0.048	0.043
118	1	8.43	0.09	232.0	0.00	-1.00	1.000	-25	-19	0.000	0.000	-	-	-	-	103	75	60	85	68	142	75	32	0.082	103.897	0.025	0.079
119	0	1.46	7.27	236.4	19.60	115.18	1.063	91	139	2.389	-1.302	-	-	-	-	102	75	61	83	65	142	75	30	0.042	209.659	0.008	0.035
120	0	0.41	9.94	239.7	17.59	137.43	1.051	91	139	0.767	-0.412	-	-	-	-	100	75	59	83	65	141	75	30	0.102	165.361	0.009	0.125
121	1	2.97	0.08	231.7	1.58	105.31	1.001	-25	-19	0.244	-0.678	-	-	-	-	101	75	64	82	67	142	75	31	0.160	78.495	0.009	0.022
122	0	1.53	4.46	238.1	6.01	305.22	1.006	-25	-19	-0.521	0.174	-	-	-	-	102	74	61	77	70	143	74	35	0.074	292.889	0.015	0.060
123	0	1.68	3.61	238.6	3.21	256.27	1.002	91	-19	1.181	-1.299	-	-	-	-	102	75	61	78	67	143	75	31	0.081	331.758	0.019	0.032
124	1	4.89	0.39	233.5	0.00	-1.00	1.000	-25	-19	0.000	0.000	-	-	-	-	102	74	61	78	69	143	74	32	0.084	297.264	0.006	0.060
125	1	4.47	0.69	234.4	9.14	334.15	1.016	-25	-19	2.309	-0.628	-	-	-	-	100	73	62	76	71	142	73	35	0.134	87.733	0.013	0.026
126	1	5.65	0.42	233.5	0.38	234.99	1.000	-25	-19	-0.131	0.131	-	-	-	-	101	74	61	79	72	143	74	34	0.061	113.811	0.013	0.030

Appendix Table. The response variables and remotely sensed predictors used in the NPMR models.

Profile	Response variables: Binomial	Response variables: Change in		Predictors																							
							Ruggedness	Topo postion index		Slope direction		Ikonos Bands				Landsat Bands March 2003								AIRSAR polarized p-Band			
Number	^{13}C enrich	$\delta^{13}C$	$CO_3^{=}$-C	Elevation	Slope	Aspect	Index	Broad	Fine	Curvature	Curvature	R	G	B	NDVI	B1	B2	B3	B4	B5	B61	B62	B7	phh	phhvv	phv	pvv
		‰	%	m (msl)	%	degrees																					
127	1	5.65	0.53	233.5	0.00	-1.00	1.000	-25	-19	0.000	0.000	-	-	-	-	101	74	58	81	72	143	74	35	0.073	155.817	0.029	0.025
128	1	5.90	0.66	233.5	0.00	-1.00	1.000	-25	-19	0.000	0.000	-	-	-	-	100	73	61	83	72	142	73	33	0.076	333.942	0.017	0.027
129	1	6.18	3.90	240.5	11.47	298.34	1.021	-25	-19	-1.360	1.327	-	-	-	-	102	75	60	81	68	142	75	31	0.047	273.448	0.007	0.152
130	0	0.52	7.17	246.7	7.34	256.69	1.014	-25	-19	2.715	-3.323	-	-	-	-	100	73	60	85	68	142	73	32	0.098	133.331	0.012	0.063
131	0	0.69	3.74	239.1	3.39	114.00	1.003	-25	-19	-1.479	0.821	-	-	-	-	101	74	60	83	65	141	74	32	0.087	250.494	0.010	0.145
132	0	1.92	2.61	228.7	0.20	135.00	1.000	-25	-19	0.000	0.000	-	-	-	-	101	74	59	80	65	142	74	31	0.009	300.222	0.006	0.015
133	1	5.25	2.37	228.7	0.00	-1.00	1.000	-25	-19	0.000	0.000	-	-	-	-	101	74	60	82	67	142	74	31	0.013	301.204	0.014	0.017
134	0	0.59	7.93	238.2	8.66	168.81	1.013	-25	-19	0.009	0.990	-	-	-	-	101	74	58	85	63	142	74	29	0.174	319.690	0.019	0.029
135	0	0.28	7.63	240.1	7.35	174.36	1.012	-25	-19	-2.588	0.451	-	-	-	-	102	75	60	86	66	141	75	30	0.071	153.026	0.001	0.096
136	0	1.15	8.04	242.3	7.90	83.32	1.011	91	-19	2.900	-1.812	-	-	-	-	99	74	60	88	69	142	74	31	0.024	191.154	0.014	0.021
137	0	0.46	6.54	239.0	3.54	290.67	1.003	-25	-19	0.384	-0.248	-	-	-	-	101	74	58	84	66	142	74	28	0.094	250.032	0.012	0.005
138	0	0.72	8.61	236.7	4.09	324.00	1.004	-25	-19	1.827	-0.691	-	-	-	-	101	72	59	84	66	142	72	31	0.029	203.618	0.007	0.020
139	0	0.66	8.78	229.1	7.60	289.33	1.014	91	139	3.078	-3.382	-	-	-	-	102	74	58	81	61	141	74	27	0.036	39.075	0.013	0.012
140	0	2.37	2.74	225.0	9.43	277.62	1.020	-25	-19	0.728	-2.860	-	-	-	-	100	73	57	78	62	141	73	28	0.028	128.297	0.005	0.031
141	0	0.45	7.63	222.5	4.77	270.49	1.008	-25	-19	-1.953	0.897	-	-	-	-	102	75	59	80	63	141	75	28	0.185	235.552	0.004	0.011
142	0	2.15	0.18	251.8	5.38	136.58	1.007	-25	-19	-3.575	2.613	-	-	-	-	91	67	52	81	67	145	67	32	0.092	29.424	0.017	0.032
143	0	0.14	2.04	256.0	3.25	212.35	1.004	-25	-19	-2.486	1.774	-	-	-	-	91	66	53	80	66	145	66	31	0.266	267.296	0.024	0.039
144	0	0.99	0.59	261.9	2.97	67.64	1.003	91	139	1.899	0.193	-	-	-	-	90	66	53	81	67	144	66	31	0.094	291.285	0.032	0.042
145	0	0.12	6.57	264.5	1.65	226.15	1.001	-25	-19	-1.256	0.778	-	-	-	-	92	67	54	79	72	144	67	33	0.062	336.497	0.010	0.070
146	0	0.12	5.82	265.9	8.45	27.97	1.012	-25	-19	-0.157	-0.070	-	-	-	-	90	66	54	77	71	145	66	35	0.051	260.485	0.004	0.048
147	0	0.00	9.64	269.5	7.24	39.02	1.016	208	139	6.103	-2.183	-	-	-	-	91	66	53	76	70	146	66	33	0.141	20.361	0.037	0.104
148	0	0.49	3.52	254.3	5.12	297.78	1.009	-143	-19	-3.779	3.366	-	-	-	-	91	66	55	77	70	145	66	35	0.065	55.973	0.008	0.084
149	1	2.99	0.23	250.2	6.83	325.37	1.008	-25	-19	-0.003	0.307	-	-	-	-	91	67	54	76	68	145	67	32	0.004	134.029	0.040	0.079
150	1	3.46	0.19	242.1	0.72	134.02	1.001	-25	-19	-0.024	0.024	-	-	-	-	90	67	53	75	70	146	67	34	0.074	180.686	0.014	0.022
151	0	0.00	7.67	246.7	5.61	205.45	1.005	-25	-19	0.434	0.388	-	-	-	-	90	65	53	79	68	146	65	32	0.048	241.829	0.010	0.048
152	0	0.39	5.85	247.2	10.79	329.15	1.018	91	139	1.293	-0.331	-	-	-	-	90	68	56	75	67	145	68	33	0.016	232.225	0.004	0.015
153	0	0.21	7.29	240.4	2.38	296.63	1.001	-25	-19	-1.353	0.441	-	-	-	-	93	65	53	76	65	145	65	31	0.174	115.899	0.027	0.060
154	1	3.35	0.02	230.2	2.19	70.45	1.002	-25	-19	-0.928	1.291	-	-	-	-	91	65	52	75	75	146	65	35	0.024	286.185	0.022	0.145
155	0	0.00	7.56	255.9	2.20	7.28	1.003	91	-19	0.606	-1.672	-	-	-	-	97	70	54	79	63	141	70	29	0.086	290.034	0.010	0.056
156	0	1.54	1.29	249.6	2.60	7.38	1.001	91	-19	1.124	-0.940	-	-	-	-	96	70	56	76	64	142	70	31	0.051	124.547	0.012	0.009
157	0	0.85	0.22	247.6	0.00	-1.00	1.000	-25	-19	0.000	0.000	-	-	-	-	96	72	55	81	71	141	72	35	0.052	28.271	0.011	0.071
158	1	8.08	0.22	252.4	18.59	219.86	1.064	91	139	1.236	-2.409	-	-	-	-	101	70	56	80	71	142	70	34	0.033	143.976	0.003	0.014
159	0	0.32	3.53	273.4	30.42	82.95	1.200	-260	-338	-15.306	12.013	-	-	-	-	99	72	59	87	76	143	72	36	0.020	16.359	0.005	0.055
160	0	0.00	7.74	256.3	0.00	-1.00	1.000	-25	-19	0.000	0.000	-	-	-	-	97	72	56	81	62	141	72	30	0.055	41.942	0.015	0.025
161	0	0.98	2.88	257.5	5.08	249.11	1.005	91	-19	1.164	0.413	-	-	-	-	100	71	56	82	67	141	71	30	0.055	116.710	0.012	0.058
162	0	0.08	3.30	254.9	8.92	234.84	1.016	-25	-19	-1.658	1.051	-	-	-	-	99	72	57	82	64	141	72	29	0.057	329.540	0.008	0.025
163	0	0.56	6.27	252.7	7.46	185.99	1.012	-25	-19	-1.679	-0.768	-	-	-	-	100	74	60	83	67	142	74	32	0.104	70.715	0.033	0.049
164	0	0.45	7.29	256.3	0.00	-1.00	1.000	-25	-19	0.000	0.000	-	-	-	-	99	71	58	81	62	141	71	27	0.020	113.134	0.011	0.030
165	0	0.00	6.89	258.3	6.03	309.83	1.006	-25	-19	2.172	-0.966	-	-	-	-	97	71	57	81	64	141	71	29	0.023	81.799	0.031	0.060
166	0	1.62	3.51	255.6	9.97	148.58	1.018	-25	-19	1.768	0.329	-	-	-	-	102	72	55	83	67	141	72	30	0.034	276.553	0.007	0.061
167	0	0.14	7.20	253.7	8.18	286.31	1.012	-25	-19	-1.677	0.674	-	-	-	-	99	72	58	80	65	142	72	29	0.081	216.488	0.004	0.020
168	0	0.00	2.37	254.7	14.46	105.99	1.037	91	139	4.576	-3.926	-	-	-	-	99	72	59	82	67	142	72	30	0.043	140.730	0.025	0.043
169	0	1.55	1.05	251.1	3.26	340.12	1.003	-25	-19	1.127	0.476	-	-	-	-	100	75	60	84	67	142	75	31	0.097	197.328	0.048	0.024